

## Characterization of Root System Architectures from Field Root Sampling Methods

Shehan Morandage

Energie & Umwelt / Energy & Environment

Band / Volume 520

ISBN 978-3-95806-511-6





Forschungszentrum Jülich GmbH  
Institut für Bio- und Geowissenschaften  
Agrosphäre (IBG-3)

# **Characterization of Root System Architectures from Field Root Sampling Methods**

Shehan Morandage

Schriften des Forschungszentrums Jülich  
Reihe Energie & Umwelt / Energy & Environment

Band / Volume 520

---

ISSN 1866-1793

ISBN 978-3-95806-511-6

Bibliografische Information der Deutschen Nationalbibliothek.  
Die Deutsche Nationalbibliothek verzeichnet diese Publikation in der  
Deutschen Nationalbibliografie; detaillierte Bibliografische Daten  
sind im Internet über <http://dnb.d-nb.de> abrufbar.

Herausgeber und Vertrieb: Forschungszentrum Jülich GmbH  
Zentralbibliothek, Verlag  
52425 Jülich  
Tel.: +49 2461 61-5368  
Fax: +49 2461 61-6103  
[zb-publikation@fz-juelich.de](mailto:zb-publikation@fz-juelich.de)  
[www.fz-juelich.de/zb](http://www.fz-juelich.de/zb)

Umschlaggestaltung: Grafische Medien, Forschungszentrum Jülich GmbH

Druck: Grafische Medien, Forschungszentrum Jülich GmbH

Copyright: Forschungszentrum Jülich 2020

Schriften des Forschungszentrums Jülich  
Reihe Energie & Umwelt / Energy & Environment, Band / Volume 520

D 5 (Diss. Bonn, Univ., 2020)

ISSN 1866-1793  
ISBN 978-3-95806-511-6

Vollständig frei verfügbar über das Publikationsportal des Forschungszentrums Jülich (JuSER)  
unter [www.fz-juelich.de/zb/openaccess](http://www.fz-juelich.de/zb/openaccess).



This is an Open Access publication distributed under the terms of the [Creative Commons Attribution License 4.0](https://creativecommons.org/licenses/by/4.0/), which permits unrestricted use, distribution, and reproduction in any medium, provided the original work is properly cited.

# Abstract

**Background and objectives:** The root system architecture (RSA) of a plant determines the plant's ability to capture resources efficiently from the soil and directly linked to plant performance. The development and distribution of plant's root systems are determined by the soil and surrounding environmental conditions. With the emerging methods of phenotyping techniques and the necessity of improving crop yield with limited resources, root phenotyping for developing new genotypes is given increasing attention to fulfill the increasing food demand of the world. Therefore, characterizing the behavior of root system with its surrounding environment and identifying beneficial traits are of attention in the agricultural industry. However, obtaining the information about root systems and their interaction with soil of all stages of root systems of field-grown crops is a challenging task because of the hidden nature of roots. Traditionally, the root information is extracted from field root sampling methods, which provide limited information about root growth and distribution. Therefore, obtaining a wide range of information such as the entire root system architecture can be identified as one of the main challenges in this regard. Moreover, the influence of soil and climatic factors on root growth has not been studied extensively. Thus, estimating distribution and functions of root systems that grow in different soil and climatic conditions are poorly understood. Root architecture models are becoming increasingly popular to study root growth and its functions successfully to understand and explain the mechanisms of root growth functions and to be used as a tool for exposing "hidden" root systems. Therefore, in this study, we demonstrate the use a RSA model to characterize root system traits from classical field root sampling schemes based on synthetic experiments and evaluate the differences in simulated root growth patterns and measured dynamic root development data in terms of different crops, soil, and environmental conditions.

**Materials and Methods:** The quantification of parameter sensitivities was conducted based on a synthetic experiment that mimics the root growth and root sampling procedure in the real field. The root system architecture (RSA) model CRootBox was used along with root architecture parameters to simulate winter wheat and maize root systems in a virtual

---

field plot, similar to real field practices and subsequently used sampling methods; soil coring, root counting in trenches and weekly observation of roots through rhizotubes from a camera to sample roots virtually. Then, the sampling data was converted to root system measures to investigate the parameters of RSA that are sensitive to root system measures. Moreover, the principal component analysis (PCA) was carried out to understand the parameter correlations. The selected most sensitive parameters of RSA of winter wheat from core sampling method were estimated with the Markov chain Monte Carlo DREAM<sub>(ZS)</sub> sampler. Since the stochasticity of forward model leads to unstable log-likelihood estimates, we averaged the log-likelihood of 32 forward model runs and modified the MCMC acceptance mechanism. Furthermore, the log-likelihood was inflated to account the unknown data dependencies that cause the overfitting problem. After 15000 iterations, we compared the differences between true parameter values and posterior distribution of estimated parameters. To evaluate the influence of soil and climatic factors on root growth of winter wheat and maize crops, we carried out field experiments to measure root growth in two different soil types and collected data from the rhizotron facility in Selhausen, Germany. The collected data were used to simulate root growth based on functions implemented in CRootBox RSA model to compare the differences between measured and simulated data, and to investigate whether root simulation is representative of real field measurements.

**Results:** The sensitivity analysis results indicate that most of the parameters of zero-order roots are the most sensitive; especially number ( $NB$ ), maximum length ( $maxl0$ ), inter-branch distance ( $ln0$ ), and elongation rate ( $r0$ ) of zero-order roots and the higher-order roots are less sensitive to characteristic root system measures. The PCA analysis results indicate parameter pairs, such as number ( $NB$ )- inter-branch distance ( $ln0$ ), gravitropism ( $tr0$ )-insertion angle ( $theta0$ ) of zero-order roots, are highly correlated. Bayesian sampling for posterior took a long inversion run time (3 weeks for three chains run in 32 parallel processors). The approximate posterior distributions of  $NB$ ,  $maxl0$ ,  $ln0$ ,  $r0$ ,  $theta0$  parameters are narrowly centered and the other parameters show large parameter uncertainty. A few of the estimated parameters of zero-order roots show approximate posterior distributions that are narrowly centered around true parameter values. Yet the other zero-order and higher-order root parameters are not well resolved and show a large posterior uncertainty. The field measurements indicate significant differences in root length density (RLD) between the root growth in silty loam and stony soil. A higher root length density values were reported in root growth in silty loam soil than the stony soil of both wheat and maize crops and higher development of roots in depth below 60 cm and lower amounts of roots within the first 40 cm in silty loam soil was reported. The simulation results are not representative of measured data and the differences observed in measured data are not

---

successfully reproduced by the model.

**Conclusions:** The root growth of the same type of crop could alter significantly with the growth medium and surrounding environmental conditions. However, these differences are not well incorporated into root growth models. Moreover, root length density measurements that are obtained from minirhizotron methods require reviewing thoroughly for use in simulation studies due to lack of calibration for converting root density to root length density values and the influence of tubes, soil conditions that alter root growth patterns of rhizotron methods should be investigated properly. The classical field sampling methods contain enough information about the root system traits, or root architectures parameters of zero-order roots such as  $NB$ ,  $maxl0$ ,  $ln0$ ,  $r0$  and Bayesian inference of core sampling data could be used to characterize some of the zero-order roots of wheat crop.

# Zusammenfassung

**Hintergrund und Zielsetzung:** Die Wurzelsystem-Architektur (engl.: root system architecture, RSA) einer Pflanze bestimmt ihre Fähigkeit, Ressourcen effizient aus dem Boden zu gewinnen; dies ist direkt mit ihrer Leistungsfähigkeit verbunden. Wachstum und Entwicklung von Wurzelsystemen wird durch den Boden und die Umgebungsbedingungen bestimmt. Durch neue Methoden der Phänotypisierung und der Notwendigkeit, erhöhten Ernteertrag bei begrenzten Ressourcen zu erzielen, wird der Phänotypisierung von Wurzeln für die Entwicklung neuer Genotypen zunehmende Aufmerksamkeit geschenkt. Daher ist die Charakterisierung der Wurzelsysteme in Abhängigkeit mit ihrer Umgebung und die Identifizierung nützlicher Eigenschaften in der Agrarindustrie von Bedeutung. Die Gewinnung von Informationen über Wurzelsysteme und deren Wechselwirkung mit dem Boden in allen ihren Stadien von Feldkulturen ist jedoch aufgrund des unterirdischen Wachstums der Wurzeln eine Herausforderung. Traditionell werden solche Informationen aus Probenahmen im Feld extrahiert, die nur begrenzte Informationen über das Wurzelwachstum liefern. Daher ist es wichtig, eine breite Palette von Informationen zu erhalten, wie z.B. das gesamte Wurzelsystem. Systemarchitektur kann als eine der größten Herausforderungen in diesem Zusammenhang identifiziert werden. Der Einfluss von Boden- und Klimafaktoren auf das Wachstum von Wurzeln wurde noch nicht umfassend genug untersucht. Daher wurde die Abschätzung der Verteilung und Funktionen von Wurzelsystemen, die in verschiedenen Boden- und Klimabedingungen wachsen, bisher nur wenig verstanden. Wurzelarchitekturmodelle werden immer beliebter, um das Wurzelwachstum zu untersuchen und um die Modelle als Werkzeug zur Identifizierung von Wurzelsystemen zu nutzen. Daher zeigen wir in dieser Studie die Verwendung eines RSA-Modells zur Charakterisierung von Wurzelsystemmerkmalen aus klassischen Feldprobenahmen, die auf synthetischen Experimenten basieren. Wir beurteilen die Unterschiede zwischen simulierten Wurzelwachstumsmustern und gemessenen dynamischen Wurzelentwicklungsdaten in Bezug auf verschiedene Kulturen, Böden und Umweltbedingungen.

**Materialien und Methoden:** Die Quantifizierung der Parameter-Sensitivitäten wurde

---

basierend auf einem synthetischen Experiment, welches das Wurzelwachstum und das Wurzelprobenverfahren im realen Feld nachahmt, durchgeführt. Das Wurzelsystem-Modell CRootBox wurde zusammen mit Parametern der Wurzel-Architektur verwendet, um Wurzelsysteme von Winterweizen und Mais in einem virtuellen Feldplot zu simulieren und anschließend wurden virtuelle Probenahmemethoden durchgeführt: Bohrkerne, Wurzelzählung in Ausgrabungen und die Monirhizotron-Technik. Die Daten aus diesen virtuellen Stichprobennahmen wurden in Messgrößen der Wurzelsysteme umgewandelt, um die Parameter der RSA zu untersuchen, die für diese Messgrößen sensitiv sind. Darüber hinaus wurde die Hauptkomponentenanalyse (engl.: principal component analysis, PCA) durchgeführt, um die Parameterzusammenhänge zu verstehen. Die ausgewählten sensitivsten Parameter der RSA von Winterweizen aus Bohrkern-Methode wurden mit dem Markov-Kette Monte Carlo DREAM<sub>(ZS)</sub> Probennehmer geschätzt. Da die Stochastik des Forward-Modells zu instabilen Log-Likelihood-Schätzungen führt, haben wir die Log-Likelihood von 32 Forward-Modellläufen gemittelt und den MCMC-Akzeptanzmechanismus modifiziert. Darüber hinaus wurde die Log-Likelihood erhöht, um die unbekanntes Datenabhängigkeiten zu berücksichtigen, die das Problem der Überanpassung verursachen. Nach 15000 Iterationen vergleichen wir die Unterschiede zwischen wahren Parameterwerten und der posterioren Verteilung der geschätzten Parameter. Um den Einfluss von Boden- und Klimafaktoren auf das Wurzelwachstum von Winterweizen- und Maiskulturen zu bewerten, haben wir Feldversuche zur Messung des Wurzelwachstums in zwei verschiedenen Bodentypen durchgeführt und Daten aus der Rhizotronanlage in Selhausen gesammelt. Die gesammelten Daten wurden verwendet, um das Wurzelwachstum basierend auf Funktionen des RSA-Modells in CRootBox zu simulieren, um die Unterschiede zwischen Mess- und Simulationsdaten zu vergleichen und um zu untersuchen, ob die Wurzelsimulation repräsentativ für reale Feldmessungen ist.

**Ergebnisse:** Die Ergebnisse der Sensitivitätsanalyse deuten darauf hin, dass die meisten Parameter der Wurzeln nullter Ordnung die sensitivsten sind; vor Allem die Zahl ( $NB$ ), die maximale Länge ( $maxl0$ ), die Abstände zwischen den Zweigen ( $ln0$ ) und die Rate der Längenausdehnung ( $r0$ ) von Wurzeln nullter Ordnung. Ferner sind die Wurzeln höherwertiger Ordnungen weniger empfindlich gegenüber charakteristischen Messungen des Wurzelsystems. Die Ergebnisse der PCA-Analyse zeigen, dass Parameterpaare wie die Anzahl ( $NB$ ) und die Abstände zwischen den Zweigen ( $ln0$ ) oder der Gravitropismus ( $tr0$ ) und der Einführwinkel ( $theta0$ ) von Wurzeln nullter Ordnung hoch korreliert sind. Die Bayes'sche Probenahme die A-posteriori-Wahrscheinlichkeit hatte eine lange Inversionslaufzeit (3 Wochen für drei Ketten, die in 32 parallelen Prozessoren liefen). Die ungefähren hinteren Verteilungen der  $NB$ ,  $maxl0$ ,  $ln0$ ,  $r0$ ,  $theta0$ -Parameter sind eng zentriert und die

---

anderen Parameter zeigen eine große Parameterunsicherheit. Einige der geschätzten Parameter von Wurzeln nullter Ordnung zeigen ungefähre posteriore Verteilungen, die eng um wahre Parameterwerte zentriert sind. Die anderen Wurzelparameter nullter und höherer Ordnung sind jedoch nicht gut aufgelöst und weisen eine große posteriore Unsicherheit auf. Die Feldmessungen zeigen signifikante Unterschiede in der Wurzellängendichte (RLD) zwischen dem Wurzelwachstum in schluffigen Lehmböden und steinigten Böden. Es wurden höhere Wurzellängendichtewerte für das Wurzelwachstum in schluffigen Lehmböden als in steinigten Böden sowohl für Weizen- als auch für Maiskulturen gefunden und ferner eine höhere Wurzelentwicklung in einer Bodentiefe unterhalb von 60 cm und geringere Wurzelmenngen innerhalb der ersten 40 cm in schluffigen Lehmböden. Die Simulationsergebnisse sind nicht repräsentativ für Messdaten und die beobachteten Unterschiede in den Messdaten werden vom Modell nicht erfolgreich reproduziert.

**Schlussfolgerungen:** Das Wurzelwachstum der gleichen Kulturpflanze kann sich signifikant verändern bedingt durch die Bodenstruktur und die Umgebungsbedingungen. Diese Unterschiede sind jedoch nicht gut in Wurzelwachstumsmodelle integriert. Es wurden Messungen der Wurzellängendichte durchgeführt, die mit der Minirhizotron-Methoden gewonnen wurden; solche Daten müssen, bevor sie ins Simulationen verwendet werden, gründlich überprüft werden auf Grund fehlender Kalibrierung zur Umwandlung der Wurzelndichte in die Wurzellängendichte. Ferner muss der Einfluss von Minirizothron-Rohren und von den Bodenverhältnissen, die das Wurzelwachstumsmuster beeinflussen, genau untersucht werden. Die klassischen Feldstichprobenverfahren enthalten genügend Informationen über die Eigenschaften des Wurzelsystems oder über die Parameter der Architekturen von Wurzeln nullter Ordnung, wie z.B.  $NB$ ,  $maxl0$ ,  $ln0$ ,  $r0$ . Die Bayes'sche Inferenz der Bohrkern-Probenahme-Daten könnten verwendet werden, um einige der Wurzeln der Weizenkultur nullter Ordnung zu charakterisieren.

# Contents

<b>Abstract</b>	<b>i</b>
<b>Zusammenfassung</b>	<b>iv</b>
<b>Contents</b>	<b>vii</b>
<b>List of Abbreviations</b>	<b>xii</b>
<b>List of Figures</b>	<b>xiii</b>
<b>List of Tables</b>	<b>xxi</b>
<b>1 General Introduction</b>	<b>1</b>
1.1 Importance of architectural root traits in plant phenotyping . . . . .	2
1.2 Field root sampling methods . . . . .	3
1.3 Influence of soil and environmental factors on root growth . . . . .	6
1.4 RSA models and their parameterization . . . . .	8
1.5 Aims and Objectives . . . . .	10
1.6 Outline of the thesis . . . . .	11

---

<b>2</b>	<b>Parameter sensitivity analysis of a root system architecture model based on virtual field sampling</b>	<b>13</b>
2.1	Introduction . . . . .	14
2.2	Materials and Methods . . . . .	16
2.2.1	Simulation of root systems . . . . .	16
2.2.2	Sensitivity analysis . . . . .	25
2.2.3	Principal component analysis of sensitivities . . . . .	30
2.3	Results . . . . .	32
2.3.1	Root systems simulations . . . . .	32
2.3.2	Root sampling . . . . .	33
2.3.3	Sensitivity Analysis . . . . .	39
2.3.4	Principal Component Analysis . . . . .	43
2.4	Discussion . . . . .	46
2.5	Summary and Conclusions . . . . .	50
2.6	Outlook . . . . .	51
<b>3</b>	<b>Bayesian Inference of Root Architectural Model Parameters from Synthetic Field Data</b>	<b>53</b>
3.1	Introduction . . . . .	54
3.2	Materials and Methods . . . . .	57
3.2.1	Forward model and virtual root sampling data . . . . .	57
3.2.2	Selection of the most sensitive parameters of root system architecture and their prior distribution . . . . .	60
3.2.3	Selection of the synthetic measurements . . . . .	63

3.2.4	Bayesian approach . . . . .	63
3.2.5	Markov chain Monte Carlo sampling . . . . .	64
3.2.6	Dealing with model stochasticity and non-independent data errors . . . . .	65
3.3	Results . . . . .	71
3.3.1	MCMC sampling and convergence . . . . .	71
3.3.2	Parameter correlations . . . . .	74
3.3.3	Validation of inferred RSA parameters . . . . .	78
3.4	Discussion . . . . .	79
3.4.1	MCMC inversion run time for RSA parameter estimation . . . . .	79
3.4.2	Fixing problematic and highly correlated parameters from field observations . . . . .	79
3.4.3	Possibility of application on real field root sampling data . . . . .	80
3.5	Conclusions . . . . .	80
<b>4</b>	<b>To which extent can explicit consideration of soil information explain observed differences in root growth? A simulation study.</b>	<b>82</b>
4.1	Introduction . . . . .	83
4.2	Materials and methods . . . . .	87
4.2.1	The root architecture model CRootBox . . . . .	87
4.2.2	Parameterization of the root architecture model for winter wheat and maize . . . . .	88
4.2.3	Field experiments . . . . .	89
4.2.4	Influence of static soil physical properties on simulated root growth patterns . . . . .	92

4.2.5	Influence of dynamic soil conditions on root growth patterns . . . .	95
4.3	Results . . . . .	98
4.3.1	Comparison between measured root arrival curves of winter wheat and maize in stony and silty loam soil . . . . .	98
4.3.2	Simulated and measured root length density (RLD) distributions of winter wheat and maize plants in soils with high and no stone content	100
4.3.3	Root growth in macropores . . . . .	101
4.3.4	Root obstacle avoidance . . . . .	102
4.3.5	Root growth in loose and compacted topsoil . . . . .	103
4.3.6	Sensitivity analysis of static soil properties on rooting depth . . . .	104
4.3.7	Soil temperature . . . . .	105
4.3.8	Root growth in soils with soil strength as dependent on measured soil water content . . . . .	106
4.3.9	Comparison between field sampling data and simulation results that include all measured soil information and its effect on root growth .	107
4.4	Discussion . . . . .	110
4.4.1	Similarities between simulated and literature root length density profiles . . . . .	110
4.4.2	Differences in RLD's in simulations, literature data, rhizotube observations, and trench profile data . . . . .	110
4.4.3	How differences in stone contents affect the other soil properties . .	112
4.4.4	Simulations of root systems based on soil type and root distribution patterns and the potential role of macropores as a governing factor of deep root systems . . . . .	113
4.4.5	The alteration of root traits and root system architecture . . . . .	115

---

4.4.6	Relationship between shoot development and root distribution as a function of properties . . . . .	118
4.4.7	Suggestions for model improvements . . . . .	119
4.5	Conclusions and outlook . . . . .	119
<b>5</b>	<b>Synthesis</b>	<b>121</b>
5.1	General Conclusions . . . . .	121
5.1.1	Parameter sensitivities and correlations of RSA model . . . . .	122
5.1.2	Inference of RSA parameters . . . . .	123
5.1.3	Differences in measured and simulated root distribution of soils with different stone contents . . . . .	124
5.2	Outlook . . . . .	125
	<b>Appendix A</b>	<b>126</b>
	<b>Appendix B</b>	<b>132</b>
	<b>Appendix C</b>	<b>133</b>
	<b>Acknowledgement</b>	<b>139</b>
	<b>Bibliography</b>	<b>157</b>

# List of Abbreviations

AR	Acceptance Ratio
ABC	Approximate Bayesian Computation
CRIM	Complex Refraction Index Model
IR	Infrared
ISRR	International Society for Root Research
LAI	Leaf Area Index
MCMC	Markov Chain Monte Carlo
MPS	Matrix Water Potential Sensor
MR	Minirhizotron
NHST	Null Hypothesis Significance Testing
PCA	Principal Component Analysis
RSA	Root System Architecture
RSE	Relative Standard Error
RAC	Root Arrival Curves
RID	Root Intersection Density
RLD	Root length Density
TDR	Time-domain Reflectometry

# List of Figures

2.1	Nomenclature of root architectural parameters used in CRootBox model to simulate root systems of wheat and maize crops. Zero order roots include all crown roots, seminal roots, brace roots and primary roots (adapted from ISRR nomenclature). . . . .	17
2.2	Winter wheat plant positions, plant configuration, plot size and sampling schemes of virtual cores, trench profile and minirhizotron methods (maize sampling methods are similar to wheat except the sampling positions and the sampling size). 3D view of the wheat sampling schemes (A), aerial view of coring and trench profiles (B), vertical profile of a grid of trench root counting method (C). . . . .	21
2.3	Setup of the vertical trench profiles and the grid cells in which root intersections were counted for wheat (left) and maize (right). . . . .	24
2.4	Schematic cross section of a rhizotube installed in Selhausen test site and tube locations of the images used in the simulation study. . . . .	25
2.5	Flow chart showing the main steps used in the methodological approach. . . . .	32
2.6	Simulated maize root systems in a virtual field plot until 180 days after sowing (color scale represents the appearance time of the root segments). Vertical transparent cylinders represent the soil cores, horizontal cylinders the rhizotubes, and vertical planes the trenches. Winter wheat simulations followed a similar simulation procedure with different plant density and sampling locations. . . . .	33

- 
- 2.7 Root length density profiles obtained from 15 soil cores in a field plot with wheat (left), and maize (right) at 30-day time intervals. The lines represent the average of the profiles that are simulated in 100 realizations of the plots. The grey shaded areas represent the standard deviation of the obtained profiles from 15 soil cores in the different realizations. Red shaded area represents the standard deviation of the root length densities in the 1500 soil cores at the end of the growing season. . . . . 34
- 2.8 Range of root length density profiles obtained from 15 soil cores in a field plot with wheat (left), and maize (right) at 240 and 180 days respectively, based on the full set of parameter variations used in sensitivity analysis. . . 34
- 2.9 Relative standard error of the estimated mean root length density of wheat (left) and maize (right) at different depths obtained from soil cores as a function of the sample size: lines represent the theoretical relation between the standard error of the mean and the sample size and symbols are standard errors of sets of means. . . . . 36
- 2.10 Spatial distribution of wheat and maize grid-based root counts in virtual trench profiles. Dots represent the standard deviation of the mean root counts (winter wheat at 240 days after sowing (left) and maize at 180 days after sowing (right)). . . . . 37
- 2.11 Mean root arrival curves (RAC) in horizontal rhizotubes at different depths (T1-10 cm, T2-20 cm, T3-40 cm, T4-60 cm, T5-80 cm, T6-120 cm) for winter wheat (left) and maize (right). Lines are means of root length densities obtained from 2000 images per observation time (20 locations in 100 tubes in different realizations of the field plots) and shaded areas represent standard deviations of means estimated from 20 images in one realization of the field plot (shaded areas) . . . . . 38
- 2.12 Summary of the sensitivities of the characteristic root system measures, which are derived from virtual field observations (see Table 2.4), to parameters of the root system architecture model (Table 2.1) (W: winter wheat, M: maize)). Classes of parameter sensitivities and non-linearity effects; parameters are categorized into six zones based on the elementary effects and standard deviations. The continuous line represents 1:1 line and the dashed line represents  $= 2\sigma / \sqrt{r}$  with  $r=10$  is the number of parameter trajectories. 39

2.13	Normalized means of absolute elementary effects ( $\mu^*$ ) of the most sensitive RSA parameters on root length densities at different depths in soil cores (RLD, first row), on root impact densities at different depths in trench profiles (Rz, second row), and on the maximum amount of roots observed in rhizotubes at different depths (RMm, third row) for winter wheat (left) and maize (right) 240 days and 180 days after sowing, respectively. . . . .	42
2.14	Normalized means of absolute elementary effects ( $\mu^*$ ) and standard deviations of elementary effects ( $\sigma$ ) of the most sensitive RSA parameters on median root arrival times (At, top) and on the IQR of root arrival times (bottom) observed in rhizotubes at different depths (red, green, blue, black, cyan and magenta colors represent the depths 10, 20, 40, 60, 80, 120 cm respectively) for winter wheat (left) and maize (right). . . . .	42
2.15	Biplots of parameter loadings for the 1st and 2nd PCs (first row) and the 2nd and 3rd PCs (second row) using data from soil cores for the wheat crop (left column), and for the maize crop (right column). . . . .	45
2.16	Biplots of parameter loadings for the 1st and 2nd PCs (first row) and the 2nd and 3rd PCs (second row) using data from rhizotubes for the wheat crop (left row), and for the maize crop (right column). . . . .	46
3.1	Top(A): Simulated winter wheat root systems in a virtual field plot until 240 days after sowing (color scale indicates the appearance time of the root segments and the vertical transparent cylinders represent the soil cores). Bottom: RLD profiles of simulated core sampling data. Black dashed lines show the RLD of each core sample separately and the green line shows the mean RLD of 15 core samples (B), the blue line in (C) indicates the mean of 32 sets of 15 soil cores and the red line indicates the average of 15 cores that was chosen and used as measured data for inverse estimation of RSA parameters (C). . . . .	59
3.2	Evolution of the log-likelihood as a function of the number of repetitions, i.e sets of 15 soil cores, used to average the simulated data before calculating the log-likelihood. The red line indicates changes in the classical log-likelihood while the blue line denotes changes in the inflated log-likelihood. . . . .	67

---

3.3	Distributions I and II used to compute the used inflation factor (see main text for details). . . . .	68
3.4	The trajectory of Log-likelihood and the MCMC acceptance rate throughout the sampling. . . . .	72
3.5	Left: Sampling trajectory of the NB parameter in each of the 3 Markov chains. Each chain is coded with a different color (green, blue, red) and the true value is denoted by the horizontal black dashed line. Right: Corresponding marginal posterior density plot computed after discarding the first 2940 samples as burn-in. . . . .	72
3.6	Tracer plots of MCMC sampling trajectories of the three parallel Markov chains. Each chain is coded by one different color. The dashed black lines show the true parameter values, and the y-axis indicates the lower and upper bounds of the uniform prior parameter distributions. . . . .	73
3.7	Marginal posterior probability density functions of sixteen parameters. The horizontal x-axes indicates the prior range of parameter values, and the y-axes present the probability. Blue marker represents the true parameter value. . . . .	74
3.8	Biplot of principal component analysis of parameter loadings for the 1st and 2nd PCs of soil coring data (modified after (Morandage et al., 2019)). . . .	75
3.9	Scatter plot and corresponding marginal probability distributions and joint distribution of selected pairs of RSA parameters and respective with correlation factors. . . . .	78
3.10	Root length density profiles that are simulated from the posterior samples (black) and from the true parameter set (blue), and the measurement data (red). . . . .	78

4.1	Deflection of the root segments due to obstacle avoidance; root grows downward direction towards an obstacle, S1, and cannot be penetrated and change its direction to find a suitable direction while turn alpha degree left-hand side and prevented by another stone (S3); therefore it needs to change beta degrees right-hand side and find new growth direction (A). Packing of stones in different diameter classes to occupy the entire domain (160*100*100 cm soil block) based on compositions given in Table 4.2 to grow one root system (B). . . . .	93
4.2	The relationship between relative root elongation rates (wheat and maize) and the properties of growth medium; soil temperature (Clausnitzer and Hopmans, 1994), soil bulk density (wheat (Colombi et al., 2017) and maize (Popova et al., 2016)), and soil water potential and soil moisture content (Bengough et al., 1997; Dexter and Hewitt, 1978) of soils with 1.55 g cm <sup>-3</sup> of bulk density. . . . .	98
4.3	Root length density changes with days after sowing (root arrival curves) observed in rhizotubes, which are located at T1-10 cm, T2-20 cm, T3-40 cm, T4-60 cm, T5-80 cm, and T6-120 cm depths. . . . .	99
4.4	Root length density distribution of winter wheat and maize at the end of the growing seasons measured by the minirhizotron method (green) plotted against the simulated RLD curves (blue). The solid green lines indicate the measurements from the F1 facility, and the dashed green lines indicate the F2 facility MR measurements. The gray shaded areas indicate root length density profiles derived based on measured data from the literature of wheat (Palta et al., 2004; Wasson et al., 2014; Xu et al., 2016; Xiyang et al., 2009) and maize (Buczko et al., 2008; Gao et al., 2010; Mekonnen et al., 1997; Postma and Lynch, 2012; Zhan and P Lynch, 2015; Zhuang et al., 2001). . . . .	101
4.5	Comparison between simulated root growth patterns in homogeneous soil (black dashed line) and soils with the influence of crack densities, plotted as root length density profile at the end of the growing seasons of wheat (left) and maize (right). . . . .	102

4.6	The relationship between root length density destitution (left-wheat and right-maize) and packing density of stones that are higher than 5 mm in diameter. Particle compositions are defined as increasing packing density of different sizes of particles; P1-indicates the root growth without the influence of stones and S4 indicates the experimental grain size distribution of the upper rhizotron facility (F1), and S2, S3, and S5 consist of 25%, 50% and 125% of S4 fractions respectively . . . . .	103
4.7	Root length density distribution patterns observed with varying degrees of bulk densities between 1.3 g cm <sup>-3</sup> and 1.7 g cm <sup>-3</sup> of topsoil layer (<30 cm), which undergoes hardening and loosening of soil due to plowing and compaction. . . . .	104
4.8	Sensitivity analysis for the maximum rooting depths (D99) of wheat (solid lines) and maize (dashed lines) with varying degrees of soil bulk density of topsoil (red lines), crack intensity(green lines), and stone content (blue lines). 105	105
4.9	Simulated mean root arrival curves for winter wheat during the 2015-2016 growing season (left) and 2017 maize growing season (right) considering the influence of temperature on root growth in stony soil, F1 (dashed line) and silty loam soil, F2 (+ markers), plotted against the optimal temperature conditions (solid continuous line) at depths 10, 20, 40, 60, 80, and 120 cm. 106	106
4.10	Simulated mean root arrival curves for winter wheat during the 2015-2016 growing season (left) and 2017 maize growing season (right) considering the influence of soil strengths in the fine material of stony soil, F1 (dashed line) and silty loam soil, F2 (+ markers), plotted against the optimal soil conditions (solid continuous line) at depths 10, 20, 40, 60, 80, and 120 cm. . . . 107	107
4.11	Comparison between simulated and measured root length density profiles of wheat (left) and maize (right) considering the influence of physical properties of stony, F1 and silty loam soil, F2. . . . .	108
4.12	Leaf area index (LAI) and crop height of winter wheat (left) and maize (right) change with time in plants grow in stony soil, F1 (solid line) and silty loam soil, F2 (dashed line). . . . .	118

A.1	Normalized means of absolute elementary effects ( $\mu^*$ ) and standard deviations of elementary effects ( $\sigma$ ) of the most sensitive RSA parameters on the maximum root length density in vertical root length density profiles derived from soil cores (RMc, first row), on the total root length per surface area derived from soil core measurements (Tc, second row), and on the average root count density vertical profile walls (Tt, third row). Blue line: 1:1 line, red line: $\sigma^* = 2 \sigma/\text{sqrt}(r)$ line (winter wheat (A) and maize (B) after 240 days and 180 days of simulation time respectively). . . . .	128
A.2	Normalized means of absolute elementary effects ( $\mu^*$ ) and standard deviations of elementary effects ( $\sigma$ ) of the RSA parameters on the depth above which 99% of the total root length is observed (D99) for winter wheat (left) and maize (right) 240 days and 180 days after sowing, respectively. Blue line: 1:1 line, red line: $\sigma^* = 2 \sigma/\text{sqrt}(r)$ . . . . .	128
A.3	Normalized means of absolute elementary effects ( $\mu^*$ ) of the most sensitive RSA parameters on root impact densities in vertical transects of trench profiles (RX) at different distances from the stem for winter wheat (left) and maize (right) 240 days and 180 days after sowing, respectively. . . . .	129
A.4	Biplots of parameter loadings for different PCs when all data are combined for the wheat crop. . . . .	130
A.5	Biplots of parameter loadings for different PCs when all data are combined for the maize crop. . . . .	131
B.1	Correlation matrix of all the inferred parameters. The Heat map shows the variation of correlations from higher negative correlations (blue) to higher positive correlations (red). . . . .	132
C.1	Soil temperature changes during the study period of winter wheat growing season (Nov 2015-Jul 2016) measured by the MPS-2 sensors installed at the F1 facility (left) and the F2 facility (right). . . . .	133
C.2	Soil moisture content changes during the study period of winter wheat growing season (Nov 2015-Jul 2016) measured by the TDR sensors installed at the F1 facility (left) and the F2 facility (right). . . . .	134

C.3	Soil water potential changes during the study period of winter wheat growing season (Nov 2015-Jul 2016) measured by the MPS-2 sensors installed at the F1 facility (left) and the F2 facility (right). . . . .	134
C.4	Soil temperature changes during the study period of maize growing season (May 2017-Sep 2017) measured by the MPS-2 sensors installed at the F1 facility (left) and the F2 facility (right). . . . .	135
C.5	Soil moisture content changes during the study period of maize growing season (May 2017-Sep 2017) measured by the TDR sensors installed at the F1 facility (left) and the F2 facility (right). . . . .	135
C.6	Soil water potential changes during the study period of maize growing season (May 2017-Sep 2017) measured by the MPS-2 sensors installed at the F1 facility (left) and the F2 facility (right). . . . .	136
C.7	Root intersection density distribution of maize at the end of the growing season measured by the trenching method. The solid red line indicate the measurements from the F1 facility, and the dashed red line indicate the F2 facility measurements. . . . .	136
C.8	Simulated mean root arrival curves for winter wheat during the 2015-2016 growing season (left) and 2017 maize growing season (right) based on measured soil properties of F1 facility. . . . .	137
C.9	Simulated mean root arrival curves for winter wheat during the 2015-2016 growing season (left) and 2017 maize growing season (right) based on measured soil properties of F2 facility. . . . .	137
C.10	Photographs showing macroscopic soil structures and rooting patterns of maize observed in the upper rhizotron facility (top) and the lower rhizotron facility (bottom). F1A, F1B, and F1C represent how the roots grow around large stones to find suitable paths. F2A demonstrates the root growth in a deep vertical crack. F2B shows the root growth on a vertical crack surface. F2C shows root growth inside a biopore and dead roots from the previous growing seasons . . . . .	138

# List of Tables

2.1 List of root architectural parameters of wheat and maize used in root system simulations and sensitivity analyses (Schnepf et al., 2018). Except the number of zero-order roots NB, each parameter is a stochastic parameter with a mean and a standard deviation (values inside the brackets indicate the standard deviations of the parameters). . . . . 18

2.2 Virtual field simulation setup: plant seeding positions, plot size and plant density configuration of wheat and maize. . . . . 20

2.3 Description of sampling methods: number and sizes of cores, trenches and rhizotubes, used in virtual sampling schemes. . . . . 22

2.4 Description of characteristic root system measures used in sensitivity analysis along with respective sampling methods. . . . . 27

2.5 Percentage of variance explained by the first 5 principle components of the sensitivities when only data from coring (cores), rhizotube measurements (rhizotubes) are used and when rhizotube, core and impact data are combined (All) The parameter names with the highest PC loading are given in parenthesis. . . . . 44

3.1 List of root architectural parameters of wheat used in root system simulations and the prior range of inferred parameters. Except for the number of zero-order roots NB, each parameter is a stochastic parameter with a mean and a standard deviation (values inside the brackets indicate the standard deviations of the parameters). Numbers in the parameter names refer to the root orders. Underlined values are the parameters used for inference and the others are fixed to true parameter values. . . . . 62

---

3.2	Mean of log-likelihoods $\ell$ of the true parameter set that are obtained from a combination of 20 different observations and 15 sets of forward simulations (each consisting of 15 realizations), standard deviation of the loglikelihoods due to observation dataset noise $stdev\ell_{\mathbf{y}}$ , and due to stochastic simulation noise $stdev\ell_{\boldsymbol{\varepsilon}}$ for 9 different parameter sets. See the main text for the calculation details of $stdev\ell_{\mathbf{y}}$ and $stdev\ell_{\boldsymbol{\varepsilon}}$ . . . . .	70
4.1	Grain size distribution Selhausen test site according to ISO 14688-1:2002 (2002) modified after (Weihermüller et al., 2007) and (Stadler et al., 2015). The values with * sign indicate volume fractions and the other values indicate the weight fractions. . . . .	90
4.2	Distribution of particle sizes and respective percentages of stony soils used to simulate root growth under different scenarios. . . . .	94
4.3	Root elongation rates of winter wheat (Colombi et al., 2017) and maize (Popova et al., 2016) observed in the soils with different bulk densities. . .	95
4.4	Differences in F1 facility in comparison to F2 facility between simulated and measured root growth patterns of wheat and maize crops concerning the $D_{max}$ , $T_c$ , $RM_m$ , and $A_t$ root system measures. . . . .	109

# Chapter 1

## General Introduction

Since the beginning of the nineteenth century, the world population has increased exponentially due to increasing food and resource availability, increasing birth and decreasing death rates as a result of improving healthcare facilities. Although the population growth rate is declining since the 1960s, the total population of the world is still rising (Roser et al., 2019). An increasing population will likely need more natural resources that are vital to human life. Therefore, to ensure the food supply to feed the entire population is considered as one of the main challenges in the world (Gilland, 2002; Kc et al., 2018; Taiz, 2013; Nations, 2019), because the increased demand for food should be supplied with limited resources. In addition to population growth, other challenges are associated with extreme climatic conditions, such as flash flooding and drought conditions decrease food production, as well as land degradation, desertification, diseases, and pest control (Power, 2010; Taiz, 2013). On the contrary, due to emerging methods and technological development from 1950 through 1960, lead to significant improvements in the agricultural industry. This period is commonly referred to as “The Green Revolution”, which introduced the use of excessive amounts of chemical fertilizers, weed, and pest control chemicals, heavy use of machinery, stress-resistant varieties with higher yields (Pingali, 2012). Next, the second green revolution focused on sustainable crop production, taking into account the surrounding soil environmental conditions (Leong and Savage, 2013; Lynch, 2007). Thus, more attention was given to increase food production, especially in developing countries through crop breeding programs.

In order to meet the requirements of increasing food production, new crop genotypes are currently developed, which are better equipped to resist biotic and abiotic stresses such as drought or pests. Phenotyping is commonly referred to as measuring and analyzing

the characteristic features of an organism, which is an essential step in breeding programs. The main challenge in this regard is to identify the beneficial traits that result in this stress-resistance. Therefore, large amounts of experimental data obtained from different agricultural fields are required to assess the functions of those beneficial traits. Although traditionally agricultural programs give higher priority to above-ground variables and shoot part of crops, the current challenges give rise to an increased focus on plant roots and below-ground processes.

In order to predict and explain the real-world behavior of root systems, root growth models are been successfully used (Dupuy et al., 2010). These models are particularly useful in evaluating the performance of specific architectural root traits to certain environmental conditions because the use of increasing computational power can be used to include more variables that can be tested with different scenarios. Moreover, models can use synthetic data to evaluate the methodological approaches in the field conditions with minimum costs and to understand the functional mechanisms of root systems. Therefore, the combination of simulations and field experiments could be used to identify the behavior and significance of architectural root traits in phenotyping programs. Furthermore, the responses of root system changes to changing soil environments can be quantified by combining field data with a simulation model.

## **1.1 Importance of architectural root traits in plant phenotyping**

The root system architecture of a plant indicates the spatial distribution of its roots that determines the plants' ability to capture water, nutrients, and other functions that support plant growth. The supply of these resources direly affects plant productivity (Lynch, 2007). RSA further describes the length, angle, growth rate, diameter, number of laterals, of primary roots, and laterals of root systems. The root distributions of plants are unique in terms of genotype, species, climate, soil, and environmental conditions (Comas et al., 2013; de Moraes et al., 2018; Fan et al., 2016; Gorim and Vandenberg, 2017; Voss-Fels et al., 2018). Some plants have a particular affinity to adapt resource-limited environments, and the soil environmental conditions prevent plants from growing at its maximum stages. Therefore, soil information is also critical in this manner. The adaptation of plants, depending on soil environmental conditions, lead to optimize crop performance, e.g., deep root system genotypes, helps plants to capture water from deep soil layers, while shallow root systems

are efficient for capturing water from rainfall or irrigation (Bodner et al., 2015; Wasson et al., 2014). A similar adaptation can be seen in nutrient capturing efficiency from roots to reduce competition for nutrients (Del Bianco and Kepinski, 2018; Gregory, 2006; Lynch, 1995, 2013). This affinity of plants leads scientists to identify the beneficial traits and the performance of each trait contribution for phenotyping programs (Figuroa-Bustos et al., 2018). Therefore, obtaining information about root traits is becoming increasingly prevalent, and the lack of phenotypic information and methods to access and evaluate the functional behavior is one of the main challenges in root phenotyping community (Kuijken et al., 2015). Although plant breeders traditionally focus on the above-ground processes of plants, plant-breeding programs that focus on root system traits for developing new genotypes for improving crop production is becoming increasingly popular (Bardgett et al., 2014). Therefore, obtaining dynamic information of root traits are in high demand (Ndour et al., 2017).

## 1.2 Field root sampling methods

Direct observation of root systems in field-grown plants is a challenging task since it is hidden in the soil. Since the end of the 19th century, several root sampling methods have been developed. Soil coring, excavation methods, shovelomics, root intersection counting and root observation of minirhizotron methods are amongst the most popular approaches (Maeght et al., 2013). These field-sampling methods generally require long processing time and are labor-intensive. Traditionally, root sampling methods are used to measure the root distribution with depth (as root length density) from soil cores (Wasson et al., 2014), root intersection counting in trench profiles (Vansteenkiste et al., 2014), root arrival curves (root length density varies with time in continuous measurement) using minirhizotron methods (Cai et al., 2016; Majdi et al., 1992; Rewald and Ephrath, 2013) and excavation methods (Böhm, 1979a) to determine the total root mass distribution of plants. Those methods have advantages and drawbacks depending on the data quality and the costs associated with processing and analyzing steps (Judd et al., 2015). The soil coring and monolith methods provide root length density as root length per unit volume of soil (RLD), while trench counting, core break counting, and rhizotube observation methods calculate the root intersections (RID) and thus require a conversion from RID to RLD (Kücke et al., 1995). In general, all these field sampling methods provide aggregated information with minimal information about root traits (Wasson et al., 2012).

**Excavation methods:**

In order to study the entire root system or a specific part of a root system in detail, excavation methods are used (Böhm, 1979a; Kutschera, 1960). Excavation of a whole root system requires a considerable amount of time and effort, and a large portion of soil is excavated from shovels or inserting large diameter cores to shallow depths at the plant base to obtain information about crown roots (Chen et al., 2017). Excavation methods are particularly useful in determining the RSA traits of nodal or crown roots such as numbers and insertion angles for phenotyping studies (Slack et al., 2018). For root sampling of row crops and obtaining the 3D distribution of root length density, large size monolith sampling needs to be carried out (Kuchenbuch et al., 2009).

**Soil coring:**

Soil coring is one of the most widely used methods for root studies (Majdi et al., 1992), which provides root length density at specific depths, total root length, maximum rooting depths. The selection of core positions, sample size, sampling depth, number of samples, sampling volume, and sampling intervals are important for representative estimates of RLDs (Buczko et al., 2008; Frasier et al., 2016; Kumar et al., 1993) because of the selection of the sampling size is crucial since the variability of core sampling data could be exceptionally higher due to spatial variability of the soil and the differences in the distribution of roots in highly heterogeneous soil. Therefore, the data should be processed carefully to distinguish between genotypic variability and random error of field sampling data (Wasson et al., 2017). The main steps of standard operating procedures for soil coring is as follows: inserting cores to specific depths manually or hydraulically; extracting cores from the soil; cutting long cores into short segments with specific lengths; removing soil and separate roots; separating death and live roots based on color; and finally counting roots manually or using a scanner. The WinRhizo scanning system is widely used to scan and estimate the root lengths, root counts and root diameters automatically (Bouma et al., 2000; Wasson et al., 2014). Alternatively, core-break counting approach, which considers the intersection counting of core segments is adapted to standard core sampling methods to minimize the processing time significantly (Hodgkinson et al., 2017).

**Trench profiles:**

Trench profile method is highly useful for obtaining information on the lateral spreading of root systems of row crops. The location of the trench profile is frequently selected

perpendicular to rows, and the trenches are dug either by hands or excavators. Then, the profile wall is prepared to expose roots from soil using a brush and water sprayer to distinguish roots from surroundings easily, and the root intersections are counted in a mesh grid (Böhm, 1979b). Since soil cores provide one-dimensional information about root length density, and the locations of cores have an impact on average root distribution over the field plot, but in contrast, trench counting provides two-dimensional distribution of root system such as the root counts changes with the plant base. However, trench methods do not provide information about root mass, and it is challenging to recognize live roots among dead roots. Consequently, existing roots from previous crops could be accounted to the current root counting data (Azevedo et al., 2011). The main advantage of the trench root counting method is that the root counting is a fast and less laborious method than the core sampling procedure and the conversion from RID to RLD could be identified as another drawback since it requires calibration for volume-based conversion (Azevedo et al., 2011).

### **Minirhizotron methods:**

Observation of root growth using the minirhizotron technique (MR) differs from other field methods since the MR uses a direct minimally invasive technique to monitor root systems on the plot scale. This method includes the installation of transparent tubes and capturing root growth data through specially design cameras as video recordings or images. The images are processed manually or by using a semi-automatic image processing software such as RootFly (Zeng et al., 2008) and calculate the root lengths or roots counts within the area of the image. The MR tubes are installed horizontally, vertically, or inclined to the soil surface. The main advantage of the MR method is that the ability to measure and capture root growth at different time steps during all stages of crop growth (Smit et al., 2000), and besides root decay can be observed. Although MR methods have many advantages over the other field sampling methods, there are few limitations such as maximum rooting depth can be not detected by horizontally placed tubes (Cai et al., 2016; Garré et al., 2012; Majdi, 1996; Postic et al., 2019; Svane et al., 2019). Although MR is less laborious, the initial cost for installation and long image analysis and processing time can be considered as significant drawbacks. There are few MR facilities operated in the world. It is found that the MR method underestimates the total root counts of the first 30 cm and overestimates the deeper layers (Samson and Sinclair, 1994), due to the influence of tubes (De Ruijter et al., 1996). The MR methods do not directly provide the information about root length densities and total root lengths in a unit volume of soil. Instead, it provides the root counts in image windows or root length densities of the image windows. Moreover, the lack

of correlation with other field root sampling methods is one of the main drawbacks in MR methods (Majdi et al., 1992).

### 1.3 Influence of soil and environmental factors on root growth

The root distribution of a plant is highly affected by environmental factors, climatic conditions, and properties of the growth medium (soil). Since plant performance strongly depends on the distribution of the root system that contributes to supply water, nutrients, and anchor to the soil for plant growth, it is critical to identify the factors that affect the root growth patterns. The composition of soil such as texture, organic content, and stone content determines the soil physical properties, i.e., water retention capacity, temperature, and bulk density. These conditions affect the overall development of root systems (Bengough et al., 2005; Dexter and Hewitt, 1978; Donald et al., 1987; Laboski et al., 1998; Passioura, 2002; Pierret et al., 2007; White and Kirkegaard, 2010). The main environmental factors that affect the growth of root system are considered as temperature and soil moisture dynamics. These two factors affect the soils' ability to supply water demand for the plant and the cell extension, cell division, and metabolism. However, the main challenge is to quantify the effects caused by soil, environmental and climatic conditions, and how plants respond to these changes and to find ways to optimize the crop yield.

The ability of roots to penetrate and extend through the soil, responds to root-zone soil temperature because chemical and biological activities in roots and surrounding soil environment are affected by temperature changes (Creber et al., 1993). Temperature affects root length density, maximum rooting depth, root elongation rates, branching intensity, surface area, growth direction, and lateral branch angles of the root system (Kaspar and Bland, 1992; Macduff et al., 1986; Nagel et al., 2009; Onderdonk and Ketcheson, 1973; Vincent and Gregory, 1989). Root growth models generally include the effect of temperature on root elongation (Clausnitzer and Hopmans, 1994).

Soil moisture content fluctuates due to irrigation, precipitation, drought conditions, or evapotranspiration with time and depth. Water stress has an adverse effect on root development since C supply from shoots to roots is disturbed as a result of a reduction in water and nutrient transport and reductions in plant cell functions. On the other hand, moisture condition in soil contribute also for changes in root-soil penetration resistant or soil

strength, which determines the root distribution of a plant (Kirby and Bengough, 2002), because roots need to overcome the mechanical resistance that applies by soil for root extension (Buttery et al., 1998; Haling et al., 2011). On the other hand, the excess amount of water in the soil causes anoxic conditions and reduces the root growth. Moreover, roots have the affinity to grow towards the directions of higher moisture conditions, and this mechanism is referred to as hydrotropism (Dietrich, 2018).

The bulk density of soil is expressed as the weight of dry soil per unit volume. Bulk density increases with increasing soil compaction and increasing bulk density of soil increases the penetration resistance. Since root extension in the soil is linked to soil penetration resistance, bulk density determines the penetration resistance of soil in combination with moisture content. Soil's bulk density typically varies between  $1.3\text{-}1.7\text{ g cm}^{-3}$ , and bulk densities higher than  $1.7\text{ g cm}^{-3}$  are not favorable for root growth. When roots penetrate through hard soil, roots tend to increase the diameter, reduce the elongation rate and reduce the maximum root lengths (Bengough et al., 1997, 2005; Gao et al., 2016; Houlbrooke et al., 1997; Taylor and Brar, 1991; Tracy et al., 2012). Therefore, root water uptake capacity of plants and nutrient absorption efficiency is reduced and has an overall influence on crop performance (Masle and Passioura, 1987; Pardo et al., 2000; Tardieu, 1994; Unger and Kaspar, 1994; Valentine et al., 2012). Moreover, roots buckle when penetrating hard soil and reduce the maximum rooting depths (Bizet et al., 2016).

Soil macropores may form in soil due to physical (cracks) or biological (biopores) processes. Cracks are formed mainly in soils with higher clay-silt content because when soils undergo several cycles of wetting and drying process, and especially clay minerals tend to expand and shrink. Consequently, it forms several cracks in the soil. These cracks provide a favorable growth medium for roots because of the lower penetration resistance and pore spaces contain filled materials with higher amounts of nutrients. Similar to cracks, except the shape and genesis, earthworms or existing roots create biopores that are enriched with nutrients and highly favorable for plant growth. When undisturbed, these zones preserve the original structure for a long period of time and alter root distribution patterns. Especially, plants grow in soils with low water contents in the upper horizons tend to show higher rooting depths and extract water from deeper soil and optimize crop performance due to the presence of biopores in soil.

Soil is composed of water, air and a large portion of minerals and organic matter as the solid component. The solid phase contains materials with different sizes of particles. Although soils with large particles or stones are not very productive due to low water retention capacity, low nutrient content and lack of good contact between roots and soil, some non-

optimal soils are used in agricultural purposes because of limited availability of arable soils. In addition to resource capturing, when roots extend through coarse-grained soil, roots change growth directions to avoid the granular materials that cannot be penetrated by roots and grow through fine less resistant material (Whiteley and Dexter, 1984). Therefore, the presence of large consolidated particles or granules significantly affect the rooting patterns and exhibit significant changes in RSA in comparison to root growth in fine-grained soil (Fakih et al., 2017; Popova et al., 2013, 2016). The mechanism of root growth in granular soil is explained as if a root tip meets an obstacle that cannot be penetrated by root, root tend to deform and find a new direction for root extension (Bizet et al., 2016; Popova et al., 2013). The ability of roots to buckle or penetrate through soil depends on root type, length, diameter, and soil depth, in addition to the physical nature of the obstacle (Whiteley and Dexter, 1984), and the force applied by the root tip on soil particles (Kolb et al., 2017). If the soil consists of a large number of granules, roots need to buckle numerous times and thus considerably change the entire structure of the root system, rooting depth and lateral extent. Therefore, the amount of soil volume that is explored by the soil and the resources captured by the root system can be reduced significantly.

## 1.4 RSA models and their parameterization

Root architecture models require root architecture parameters, which consist of information about architectural root traits as the input, to reconstruct root systems of a specific plant that grow in certain soil environmental conditions (Dunbabin et al., 2013). Several models of root architecture and functions that simulate root systems and their functional and structural relationships are used in root modelling community such as OpenSimRoot (Postma et al., 2017), R-SWMS (Javaux et al., 2008), CRootBox (Schnepf et al., 2018), SPACSYS (Wu et al., 2007), RootTyp (Pagés et al., 2004), and etc. There are similarities and also differences in those models and are described in (Dunbabin et al., 2013). These RSA models can be used to interpret the data obtained from cost-intensive field experiments and to simulate water and nutrient uptake efficiency of specific genotypes and thus identify the genotypes with beneficial traits. The required number of parameters of RSA for simulations varies with the type of the crop, growth stage, and model complexity associated with the objectives of the research. Therefore, the parameterization of RSA models is helpful to find the trait information and ultimately use for modeling and simulation studies. The RSA parameters consist of both static and dynamic parameters that include root elongation rates of primary and branching roots. Therefore, dynamic root growth data is

required to estimate these parameters (Pagés and Picon-Cochard, 2014; Pagés et al., 2013).

Lab-based methods are widely used to characterize the RSA traits, especially for the early stages of plants (Atkinson et al., 2019; Hamada et al., 2012; Kalogiros et al., 2016; Leitner et al., 2014; Meister et al., 2014; Voss-Fels et al., 2018). RSA parameters can be derived directly from plants growing in germination papers, transparent materials or plant growth in soil using MRI/X-rays scanning, or direct observation of rhizotron images, based on image processing methods (Lobet et al., 2015; Bodner et al., 2017, 2018; Bucksch et al., 2014; Chen et al., 2017; Clark et al., 2011; Landl et al., 2018; Topp et al., 2013; van Dusschoten et al., 2016), and RSA parameters can be extrapolate from early stages of plants to mature plants (Zhao et al., 2017) or can be combined with root growth models (Kalogiros et al., 2016).

Although lab-based or greenhouse methods are widely used in root phenotyping, the main disadvantage in lab-based methods is that the lack the interaction between plant and surrounding field environmental conditions such as precipitation, solar radiation, wind condition, and real soil conditions (Gregory, 2009; Paez-Garcia et al., 2015). The other major drawback is that laboratory tests do not always account for the data from mature plants and are limited to the early stages of plants because of practical reasons. The trait information may vary with the growth stages, and therefore, the traits of young plants are not representative of plants with matures stages (de Dorlodot et al., 2007). Since the trait data obtained from laboratory methods are not well represented to field-based mature root systems that have a stronger influence from soil environmental conditions, it is necessary to obtain trait data from field-grown root systems. Therefore, the importance of field-based RSA characterization is given higher importance (Araus and Cairns, 2014; Meister et al., 2014).

Some field-based sampling methods such as excavation methods provide measurements of RSA parameters from carefully excavated root systems (Kutschera, 1960; Weaver et al., 1924), or direct sampling schemes are used to estimate root elongation rates and root angles using large cylindrical cores (Chen et al., 2017). The main limitation of excavation methods is that the entire process takes an enormous amount of time for analyzing root systems carefully, and thus parameterization of a large number of genotypes requires an enormous amount of labor costs. To overcome this challenge, plant scientists focus on developing methods on improving classical field sampling methods to obtain hidden trait information in sampling data. Such as trench profiles, minirhizotron, and excavations. Since field root sampling data contains aggregated information, some studies show that the parameters can be retrieved with the aid of detailed RSA model calibration and inference methods (Garré

et al., 2012; Pagés et al., 2012; Vansteenkiste et al., 2014).

Furthermore, parameterization of RSA models considering the influence of growth medium is even more challenging as RSA parameters and traits differ due to adaptation with soil and environmental conditions (Rich and Watt, 2013). The generalized functions and modeling approaches for quantifying the effects of RSA traits with environmental conditions, i.e., temperature (Clausnitzer and Hopmans, 1994), soil bulk density (Colombi et al., 2017; Popova et al., 2016), moisture conditions (Bengough et al., 1997; Dexter and Hewitt, 1978; Tardieu, 1994), influence of obstacles in soil (Fakih et al., 2017), macropores (Landl et al., 2017), are introduced by several authors.

Different types of roots behave in different ways to the changes in surrounding environments, and literature data are limited to specific crops, growth stages, and certain conditions. Thus, simulation results that consider those approaches could associate with higher uncertainty because the functions that were derived for a specific crop type for certain environmental effects are not applicable in a similar manner to other crop types or environments. However, in general, these approaches that consider the environmental effects provide a satisfactory overview for the future research directions for field-based root phenotyping research, which still requires significant improvements in methodological approaches such as account whole RSA parameters, and to reduce the error associated with model stochasticity and parameter uncertainty.

## 1.5 Aims and Objectives

While laboratory methods provide useful information about detailed RSA of young plants that grow in control environments, field-grown crops have limited methods to acquire the RSA information about mature roots systems and the information content is limited only to aggregated sampling data. Therefore, field root sampling data should be evaluated with the perspective of quantifying RSA parameters, which could be sensitive to specific root system measures or sampling methods. However, in this regard, the main obstacle is the lack of a direct relationship between parameters and respective root system measures in real field sampling data. In order to overcome this challenge, a modeling approach that mimics root growth in real field conditions and root sampling procedures can be used as a synthetic experiment for resembling real field sampling data with the information of respective RSA parameters.

Since the simulations of root system development and sampling data do not account for the soil and environmental effects on sensitivity analysis results and inverse parameter estimation, the certainty of applications in those approaches could highly depend on the soil-environmental factors that depend on growth medium and location. Therefore, investigation of root system dynamics should be carried out in different soils and different water regimes to evaluate the underlying mechanisms. Moreover, dynamic field root sampling data is required to estimate the RSA parameters during the different growth stages of plants and to study the distribution of root systems with dynamic soil and climatic conditions. For this purpose, minirhizotron facilities for root observation can be identified as the most suitable approach because the effect of different soil types on root growth dynamics could be quantified along with soil hydraulic properties and climatic data.

The main objective of the research work presented in this thesis is to improve classical field sampling techniques for obtaining the information of RSA of plants that grow in different soil and environmental conditions. The main research objective was divided into three sections as follows:

- i) To investigate how sensitive field sampling method results (root length densities from coring, root intersection counts from trenching, root arrival curves from rhizotubes) are to the different root architectural parameters using 3D dynamic simulations of wheat and maize root architectures in a field and virtual field sampling.
- ii) To assess a Bayesian inference method to inversely estimate root architectural parameters using a synthetic data set of wheat root length densities from coring with known ground-truth and to quantify the uncertainty of the estimated parameters;
- iii) To assess and quantify the effect of stone content and related changes in soil physical properties (temperature, soil water content and matric potential) on root architecture development based on measurements and simulations for winter wheat and maize.

## 1.6 Outline of the thesis

The thesis is divided into five chapters:

**Chapter 1** presents the current state of the art and the problem formulation: In this chapter, we highlight the importance of root phenotyping to enhance the crop yield and the current challenges in field root phenotyping community. Furthermore, we briefly explain

the main field root sampling methods: excavation, soil coring, trench root counting, and minirhizotron methods and discuss the advantages and drawbacks of each method. Moreover, we summarize the methods that use for parameterization of RSA and their limitations, and the dependency of RSA of plants on soil environmental conditions.

**Chapter 2** describes the parameter sensitivity of the root system architecture model based on field sampling methods and corresponding root system measures of each root sampling method. It further describes the effect of sampling size, sampling locations, and the sensitivity dependency of the most sensitive parameters on the other parameters.

**Chapter 3** presents the Bayesian inversion approach that used to inversely estimate the root architecture parameters of winter wheat crop based on soil coring sampling method. Then, we discuss the uncertainty associated with the inversely estimated parameters due to model stochasticity and correlated parameters.

**Chapter 4** studies the effect of stone content and related soil conditions on simulated root architecture developments. In this chapter, we compare the simulated root data with measured dynamic root growth data of wheat and maize crops and soil information that were obtained from minirhizotron facilities to evaluate the soil and climatic effects on root growth patterns.

Finally, **Chapter 5** summarizes our main research findings of this work and recommendations for future research directions for improving field sampling schemes to obtain detailed information about the root system architectures, and how the soil and environmental conditions affect the RSA of a plant and overall root distribution.

## Chapter 2

# Parameter sensitivity analysis of a root system architecture model based on virtual field sampling

Adapted from: Morandage S, Schnepf A, Leitner D, Javaux M, Vereecken H, Vanderborght J (2019), Parameter sensitivity analysis of a root system architecture model based on virtual field sampling. *Plant and Soil* 438: 101-126. doi: 10.1007/s11104-019-03993-3.

## 2.1 Introduction

Agriculture faces the challenge of sustaining an increasing global food demand under increasingly limited resources such as water and nutrients. Since roots are the organs that plants use to acquire these resources, understanding plant root architectures and their interaction with the soil is particularly important.

Depending on the environmental conditions, different types of root systems are beneficial for the uptake of resources from soil. Regarding water uptake, shallow root systems are proposed to be beneficial in environments where water uptake is driven by rainfall supply while deep root systems are beneficial in environments where plants rely on water stored in deeper soil layers (Bodner et al., 2015; Wasson et al., 2014). Knowing the role of root traits or root architectural parameters for water and nutrient uptake is important for selecting optimal varieties in water and nutrient limited environments (Gregory, 2006; Lynch, 1995). Yet, the lack of phenotypic data of different genotypes is the main challenge in plant breeding programs (Kuijken et al., 2015). Furthermore, until recent years, most breeding programs have focused on the shoot of plants, whereas the root system has been given less attention (Bardgett et al., 2014).

Root architectural models reconstruct representations of the root system of a plant based on its pre-defined root architectural parameters (Dunbabin et al., 2013). The root system architecture (RSA) represents the arrangement of primary, secondary and higher order root segments and how they are connected to each other. RSA varies from plant to plant and species to species depending on the genotype and soil environmental conditions (Comas et al., 2013). The parameters of these models can be considered to represent root traits or characteristics of the RSA of a certain plant in a certain soil environment. Lab based methods are widely used for determining root architectural parameters (Hamada et al., 2012; Kalogiros et al., 2016; Leitner et al., 2014) but also examples exist that used root systems that were carefully excavated from the soil (Kutschera, 1960; Weaver et al., 1924). Using manual or automatized image processing, digitized root systems are obtained (Lobet et al., 2015), from which root system parameters can be derived directly (Bodner et al., 2017; Bucksch et al., 2014; Chen et al., 2017; Clark et al., 2011; Landl et al., 2018).

Next to ‘static’ structural parameters, RSA models also describe the dynamic root development and use parameters that represent root elongation rates. To estimate these parameters, dynamic root data are required (Pagés and Picon-Cochard, 2014; Pagés et al., 2013). However, conditions in labs or greenhouses that have an important impact on plant

and root growth may differ considerably from real field conditions such as precipitation, radiation, wind patterns, soil structure and soil depth (Gregory, 2009; Leitner et al., 2010). Moreover, plant and root growth in small pots is not representative of root systems of large and/or mature plants. Traits of root systems at mature stage may differ considerably from traits observed during the early stages of plant development and are therefore difficult to predict from the early stage traits (de Dorlodot et al., 2007). The variables observed with different methods in the lab or greenhouse and the RSA parameters that are derived from these observations are therefore not directly transferable to plants grown under field conditions.

Studying root systems in the field is a difficult task due to a lack of direct access to the root system. It is impossible to get information about an entire root system without disturbing its original morphology because it is completely hidden beneath the soil surface. Several root sampling methods were developed to gain information about root system dynamics in the field. These methods are generally time consuming and labor intensive. Classical field methods are root intersection counting in vertical profile walls of a trench, soil coring, and non-destructive minirhizotron methods (Leitner et al., 2010). Soil coring is a widely used field sampling method to obtain the distribution of root length density with depth (Schroth and Kolbe, 1994). The trench profile method is suitable for studying root distributions in 2-D. The main disadvantage of the trench profile method over core sampling is that the root biomass cannot be measured. The trench profile method has some difficulties when counting roots in deep layers and it may be difficult to distinguish between dead and living roots (Azevedo et al., 2011). Soil coring or trench profile methods do not provide direct information about the branching of a root system, but provide only the observed RLD or intersection counts. Although root counts and root length densities are correlated with each other, their relation depends on the orientation of the roots with respect to the intersection surface. The orientation of the roots may change with depth and depends on the plant/crop type. Using RSA models, depth and plant specific calibrations could be derived that relate the two types of observation (Grabarnik et al., 1998; Vansteenkiste et al., 2014). Minirhizotron methods are useful to study the root growth at different times and depths at the same position without destroying the root system (Smit et al., 2000). Although minirhizotrons provide root arrival curves at specific depths in the soil profile, rhizotubes could act as obstacles to root growth and the observations can be altered slightly due to influence of rhizotubes installations (Garré et al., 2012).

However, those sampling techniques do not provide direct information about the RSA model parameters or of specific root traits of different phenotypes (Wasson et al., 2012).

Root architectural models can be helpful to interpret data obtained from cost intensive field experiments. Techniques like parameter fitting or inverse modeling could be applied to derive RSA model parameters from field observations (Garré et al., 2012). In order to reconstruct realistic RSA, RSA models typically rely on a large number of parameters. The inverse estimation of a large number of parameters from indirect information may be hampered by equifinality, i.e., when several sets of parameter combinations lead to the same or very similar predictions of the observed variables. Equifinality may occur when model predictions of the data that are collected are not sensitive to changes of a certain parameter, or when changes in model predictions due to a change in one parameter can be compensated by changes of other parameters.

The main objective of this work is to define the sensitivity of different types of observations, which can be derived from field observations of root systems, to RSA parameters of the CRootBox model. This analysis identifies sensitive parameters for different observation types and gives insight in which observation types provide information about which parameters. This is important to design field sampling methods. Maize and wheat root systems will be considered as example crops. Root length densities (RLD) derived from soil cores, root impact counts (RIC) derived from vertical profile walls, and temporal distributions of root counts in horizontal rhizotubes that represent root arrival curves (RAC) will be considered as field observations.

In the material and methods part of the paper, we present the RSA model, how ‘virtual’ observations were derived from simulations with the RSA model, how the sensitivity analyses were carried out and how we interpret the sensitivities using principal component analysis (PCA). In the results section, we first present the simulated or ‘virtual’ observations and analyze the impact of the sample size on the uncertainty about the observations. Secondly, we present and discuss the sensitivity of different observations to the RSA parameters including PCA results.

## 2.2 Materials and Methods

### 2.2.1 Simulation of root systems

Despite the fact that virtual experiments are not limited to a certain crop type, we selected winter wheat and maize as crop types for virtual simulations and sampling due to their importance as agricultural crops and the availability of root architectural parameters for



due to gravity) have to be defined. Root diameters were not considered for simulations. For zero order and first order roots, the growth rate is a function of the root length and becomes zero when the root reaches a maximal length (*maxl*) ( see (Schnepf et al., 2018) for the implementation of gravitropism and growth rates as a function of root length). In order to reproduce the random nature of the root system, RSA parameters are stochastic parameters with a mean and a standard deviation (see (Leitner et al., 2010; Schnepf et al., 2018) for the implementation of the random RSA development). A complete list of CRootBox root architectural parameters is given in Table 2.1.

**Table 2.1:** List of root architectural parameters of wheat and maize used in root system simulations and sensitivity analyses (Schnepf et al., 2018). Except the number of zero-order roots NB, each parameter is a stochastic parameter with a mean and a standard deviation (values inside the brackets indicate the standard deviations of the parameters).

No	Code	Root order	Parameter name	Unit	Values	
					Wheat	Maize
1	lb0 (std)	0	length of basal zone	cm	0.8 (1.2)	0.1 (0.1)
2	la0 (std)	0	length of apical zone	cm	4.2 (6.4)	18 (1.8)
3	ln0 (std)	0	branch spacing	cm	1.2 (0.5)	0.6 (0.06)
4	maxl0 (std)	0	maximum length	cm	130 (30)	110 (30)
5	r0 (std)	0	initial growth rate	cm day <sup>-1</sup>	1.2 (0.6)	2.6(0.6)
6	tr0 (std)	0	tropism		1.2 (0.2)	1.0(0.6)
7	theta0 (std)	0	branching angle	rad	1.4 (0.2)	1.0 (0.5)
8	lb1 (std)	1	length of basal zone	cm	0.8 (1.0)	0.2 (0.4)
9	la1 (std)	1	length of apical zone	cm	1.8 (2.4)	0.4 (0.04)
10	ln1 (std)	1	branch spacing	cm	1.0 (1.5)	0.4 (0.3)
11	maxl1 (std)	1	maximum length	cm	2.0 (1.0)	2.6 (1.6)
12	r1 (std)	1	initial growth rate	cm day <sup>-1</sup>	0.4 (0.12)	2.0 (0.2)
13	tr1 (std)	1	tropism		1.0 (0.4)	1.0 (0.3)
14	theta1 (std)	1	branching angle	rad	1.2 (0.4)	1.2 (0.25)
15	la2 (std)	2	length of apical zone	cm	2.2 (0.4)	0.5 (0.2)
16	r2 (std)	2	initial growth rate	cm day <sup>-1</sup>	1.0 (0.2)	2.0 (0.2)
17	tr2 (std)	2	tropism		0.1 (0.6)	1.5 (0.35)
18	theta2 (std)	2	branching angle	rad	1.12 (0.4)	1.2 (0.2)
19	NB	0	number of zero order roots	nos	20	30

We defined primary roots, seminal roots and crown roots as zero order roots in the simulations. First order roots emerge from the zero order roots and second order roots emerge from the first order roots. We assumed that zero order roots emerge all together, next to the seed at the beginning of the growing season. Lateral roots emerge from their parent branch only after the apical zone has reached a defined length.

A winter wheat (*Triticum aestivum*) root system typically consists of 10-30 zero order roots and a secondary fibrous root system with three orders of branching (Wasson et al., 2012). The root density of wheat is relatively homogeneous in the horizontal direction due to the high planting density (Couvreur et al., 2014). For some varieties of wheat and depending on the soil and weather conditions, roots can reach up to 170 cm. The root elongation rate is typically in the order of 1-1.5 cm day<sup>-1</sup> (Colombi et al., 2017). The highest number of wheat roots are observed within the first 40 cm depth (Hoad et al., 2004). Maize (*Zea mays*) is a row crop and thus field-measured root length density of maize varies in the horizontal direction perpendicular to the rows. The root system of maize consists of primary, lateral and shoot-borne roots and the elongation rates vary from 1-4 cm day<sup>-1</sup>. Maize roots can reach up to 150 cm depth with lateral spreading of 120 cm, depending on soil texture (Feldman, 1994; Hochholdinger and Tuberosa, 2009). Root architecture parameters were generally derived from experimental data during the early stages of plants grown in laboratories under controlled environments but are not necessarily representative for older plants or for field conditions. Therefore, we followed a trial and error approach to derive parameters that are representative for plants grown under field conditions. We systematically changed some parameters (elongation rate ( $r\theta$ ), maximum length ( $maxl\theta$ ) and numbers ( $NB$ ) of zero order roots) such that resulting field-scale values of root length densities were realistic compared to known literature values. Table 2.1 shows the values of root architectural parameters of wheat and maize, used as input parameters in the root growth model. The parameter bounds for the sensitivity analysis were selected as 50% and 150% of the parameter value as the lower and the upper bounds, respectively.

Two different plant configurations were considered for the two crops. Plant density was determined according to common practices applied in Europe (Kolb et al., 2017). The inter row distance for wheat was 12 cm with 3 cm plant spacing within a row. 224 wheat plant root systems were simulated in a plot of 96 cm by 84 cm consisting of 8 rows with 28 plants in a row. Sowing density of maize is lower than that of wheat. The distance between the maize rows was 75 cm and the plant spacing in a row was 13 cm. 108 maize plants were simulated in a plot of 450 cm by 234 cm consisting of 6 rows with 18 maize plants in each row. The depth of the soil domains was 160 cm. Seeding depths were chosen as 3 cm and 5

cm for wheat and maize, respectively. The total life spans of wheat and maize plants were set to 240 and 180 days respectively. Table 2.2 shows the plant configurations and plot sizes of each crop type. Simulation results were saved as VTK files and Paraview (Ayachit, 2015) was used to visualize the results.

**Table 2.2:** *Virtual field simulation setup: plant seeding positions, plot size and plant density configuration of wheat and maize.*

Plant configuration	Wheat	Maize
Plot size (width*length*depth)	96 cm*84 cm*160 cm	450 cm*234 cm*160 cm
Number of rows	8	6
Number of plants in a row	28	18
Plant distance in a row	3 cm	13 cm
Distance between two rows	12 cm	75 cm
Total number of plants	224	108

### Virtual field sampling:

Classical field sampling schemes; soil coring, trench profiles and minirhizotron observations were implemented in the virtual field plots to obtain the information about root distributions (Figure 2.1). We used signed distance functions to represent the geometries of rhizotubes, soil cores and trenches, and made use of the CRootBox feature that allows to explicitly represent obstacles for root growth (rhizotubes). Table 2.3 shows the sampling methods, sampling size and sampling locations of virtual wheat and maize plots.

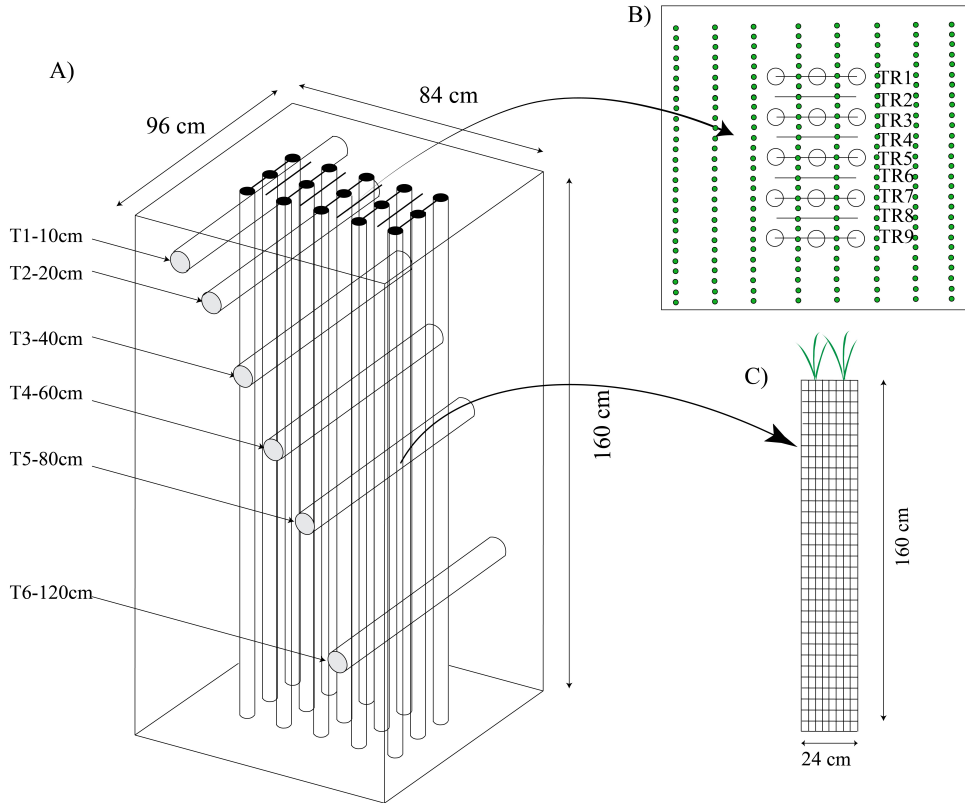


**Figure 2.2:** Winter wheat plant positions, plant configuration, plot size and sampling schemes of virtual cores, trench profile and minirhizotron methods (maize sampling methods are similar to wheat except the sampling positions and the sampling size). 3D view of the wheat sampling schemes (A), aerial view of coring and trench profiles (B), vertical profile of a grid of trench root counting method (C).

**Table 2.3:** Description of sampling methods: number and sizes of cores, trenches and rhizotubes, used in virtual sampling schemes.

Sampling method	Wheat	Maize
<b>Coring<sup>a</sup></b>	15(radius=2.1 cm,depth=160 cm)	16(radius=2.1 cm,depth=160 cm)
<b>Trenches<sup>b</sup></b>	9 (width=24 cm, depth=160 cm) grid size= 3*5 cm	9 (width=150 cm, depth=160 cm) grid size= 5*5 cm
<b>Minirhizotron<sup>c</sup></b>	6 tubes (radius = 3.2 cm) depths 10, 20, 40, 60, 80, 120 cm 20 images per tube image size=1.65*2.35 cm	6 tubes (radius = 3.2 cm) depths 10, 20, 40, 60, 80, 120 cm 20 images per tube image size=1.65*2.35 cm

<sup>a</sup> soil core sampling based on (Wasson et al., 2014).

<sup>b</sup> trench root counting method based on (Vansteenkiste et al., 2014).

<sup>c</sup> rhizotube setup according to Selhausen minirhizotron facility (Cai et al., 2016)

### Virtual soil coring:

Cylindrical cores of 4.2 cm diameter and 160 cm length were sampled and subsequently sliced horizontally in 5 cm intervals to determine the RLD of each sampling volume (69.72 cm<sup>3</sup>). We adjusted the sampling size similar to real field sampling schemes. For wheat we chose 3 locations in-between rows for 5 different rows, and for maize, we took 16 virtual cores with core positions in-between two plants within a row (Figure 2.2). To avoid boundary effects, zones of 20 cm from the borders of the plot for wheat and 75 cm for maize were not considered for sampling. Core sampling was performed with monthly time intervals for 8 months for wheat and 6 months for maize. In order to account for the stochasticity of the model, this sampling procedure was repeated in 100 simulated field plots for each crop type, resulting in a total number of 1500 soil cores for wheat and 1600 for maize.

### Estimation of sample size for root studies:

In order to study the effect of sample size on the mean root length distribution with depth and to select a representative sample size for the root studies, we calculated the mean and standard deviation of RLD profiles that are based on a sample size of 1500 cores. With this

sampling scheme for virtual coring, we are already at the upper limit of what is possible in real field experiments in terms of number of cores sampled per plot. As a measure of how good the sample mean root length density is compared to the “true” mean root length density, we use the relative standard error (RSE) for different sample sizes  $n$  with the sample size. We chose 10% of relative standard error (RSE) of the mean as the criterion to determine the number of required cores. The RSE was calculated in two ways. The first method, RSE1, used the theoretical relation between the standard error of the estimate of the mean, the number samples  $n$ , and the standard deviation of the samples,  $std$ . The second method, RSE2, calculated the standard deviations of sets of means,  $std\_mean$ , that were obtained using different sample numbers.

$$RSE1 = \left( \frac{\left( \frac{std}{mean} \right) 100}{\sqrt{n}} \right) \quad \& \quad RSE2 = \left( \frac{std\_mean}{mean} \right) 100 \quad (2.1)$$

A smaller RSE requires a larger number of samples. Under field conditions, it may be necessary to find a compromise between the required precision and the number of samples that are economically feasible in practice.

### Virtual trenching:

Nine trenches 24 cm wide and 160 cm deep for wheat, and 150 cm wide and 160 cm deep for maize (TR1-9) were virtually constructed perpendicular to the rows (Figure 2.3) and in each trench two profiles of root intersections below a single plant row were obtained. Similar to core sampling, trenches were positioned in the center of the plots to avoid boundary effects. For the wheat profiles, root intersections were counted in 3 by 5 cm grid cells and in the maize profiles in 5 cm by 5 cm grid cells (see Figure 2.3 for the spatial arrangement of the grid cells with respect to the plant rows). The root system simulations and corresponding virtual samplings were repeated for 100 simulated field plots so that for each grid cell in a profile, a dataset of 1800 root intersection counts (all orders of roots intersections) was obtained from which a mean and standard deviation was calculated. Finally, maps of the mean intersection counts in the grid cells that illustrate the spatial root distribution in the profiles were made at the end of the growing period.

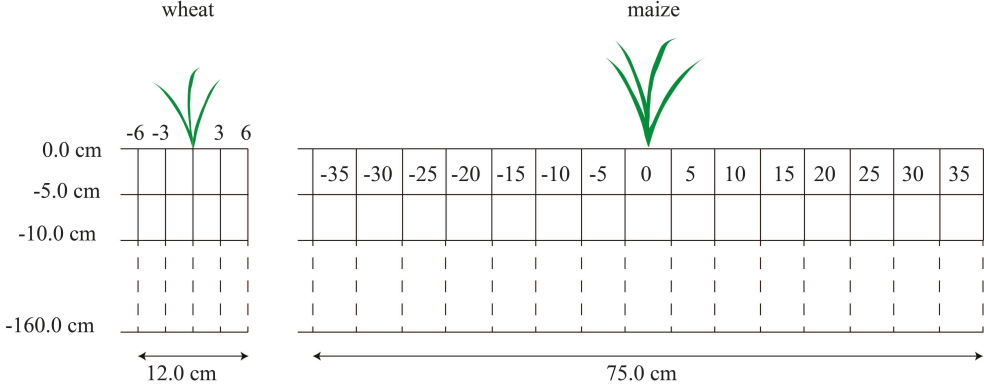


**Figure 2.3:** Setup of the vertical trench profiles and the grid cells in which root intersections were counted for wheat (left) and maize (right).

### Virtual minirhizotron:

To account for the influence of rhizotubes, which act as obstacles to root growth, on the root distributions, root growth simulations were repeated for a setup with horizontally installed rhizotubes. To simulate the growth of roots around the rhizotubes or other obstacles, CRootBox uses signed distance functions to divert the growth direction of a root tip when it meets an obstacle (Schnepf et al., 2018). The arrangement of the plants in minirhizotron simulations was identical to the one for the soil coring or trench profile methods.

The configuration of the rhizotube locations and the observations in the rhizotubes were similar to those at the minirhizotron facility in Selhausen (Germany) (see (Cai et al., 2016) for detailed information). At the Selhausen test site, rhizotubes of 6.4 cm outer diameter were installed horizontally at depths of 10, 20, 40, 60, 80 and 120 cm (Cai et al., 2016) and perpendicular to the plant rows. In order to avoid an impact of overlying rhizotubes on root observations in deeper rhizotubes, rhizotubes at different depths were 10 cm shifted horizontally with respect to each other (Figure 2.2). Root observations in a rhizotube were made by a camera that was positioned at 10 different locations in the tube where 2 images were taken from both sides of the tube by turning the camera 80° clockwise and 80° counterclockwise with respect to the vertical. The size of the minirhizotron image was set according to the camera configuration of the Bartz system (VSI /Bartz Technology Corporation), which is 1.65 cm wide and 2.35 cm long along the arc circle of the rhizotube (Figure 2.4) for the considered rhizotubes.

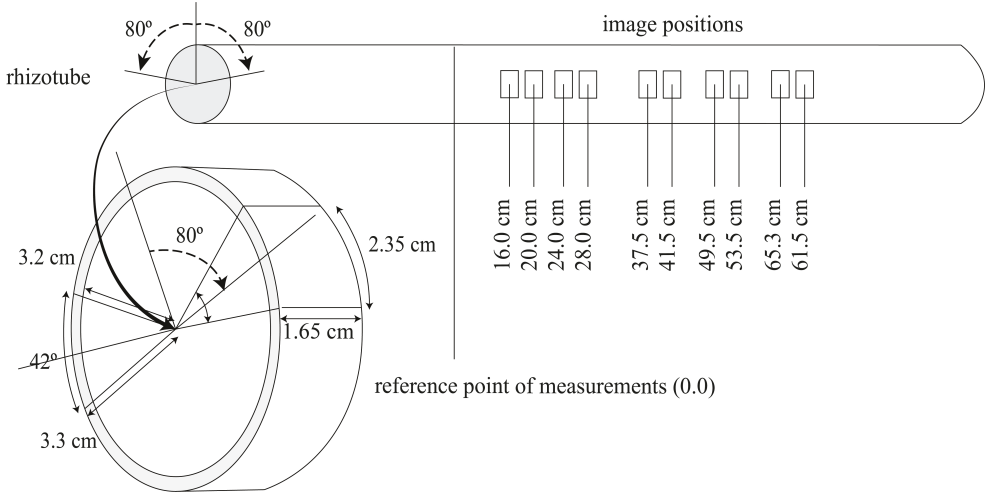


**Figure 2.4:** Schematic cross section of a rhizotube installed in Selhausen test site and tube locations of the images used in the simulation study.

For the wheat and maize plots, images were taken from respectively a 50 cm and a 100 cm long stretch. Sampling positions were chosen within four inner rows of a plot to minimize the boundary effects. Images were taken weekly over a period of 240 and 180 days for wheat and maize respectively. Unlike coring or trench profile methods, roots are not directly sampled in the minirhizotron method. The camera can capture only the roots which are close to the rhizotubes but it is a challenging task to determine the viewing depth of the camera which varies with soil type and texture. According to our experience, we assumed that roots within 1 mm from the tube were seen in the images and the length of the root segments in the image was divided by the area of the image to derive the RLD (note that the RLD obtained from rhizotube images has a different unit ( $\text{cm cm}^{-2}$ ) than the RLDs derived from soil coring ( $\text{cm cm}^{-3}$ ) and can therefore not be compared directly). For each observation time and tube depth, a RLD was calculated from 2000 images (20 images in a tube for 100 field plots) and the time series of RLDs at a given depth represents the root arrival curve (RAC) at that depth.

### 2.2.2 Sensitivity analysis

As in (Schnepf et al., 2018), we explicitly distinguish between the “model input parameters,” from which we compute the 3D root architecture using CRootBox, and “characteristic

root system measures”, which we compute from the resulting 3D root architecture. The former corresponds to individual root traits which could be of interest in e.g. phenotyping. The latter corresponds to the aggregated information as it can be obtained from root field measurements. From the simulated observations, a number of characteristics were derived. How these characteristics change with the parameters of the RSA model was evaluated in a sensitivity analysis. The characteristics that we considered for the sensitivity analysis are listed in Table 2.4. Since coring and trenching methods are destructive in real field sampling, we selected the results of last time step (240 and 180 days for wheat and maize respectively) for the sensitivity analysis. However, weekly time steps (total 32 measurements for wheat and 24 measurements for maize) were taken for the minirhizotron method.

Virtual soil coring provided us with the RLD profiles. From those profiles, we derived the following additional characteristic root system measures: D99, RMc, and Tc in the sensitivity analyses. The RLDs were calculated by averaging the root length densities in the 1500 (1600 for Maize) simulated soil cores for each of the 32, 5 cm core segments. D99 represents the depth above which 99% of the total root length was observed. RMc is the maximum of the average RLD profile. Tc is the total root length per surface area and was obtained by integrating the RLD over depth (see Table 2.4 for the descriptions and units of the root system measures).

**Table 2.4:** Description of characteristic root system measures used in sensitivity analysis along with respective sampling methods.

Sampling method	Function	units	Description
<b>Coring</b>	RLD	$\text{cm cm}^{-3}$	vertical profiles of mean root length densities in 5cm thick slices of soil cores up to 160 cm depth
	D99	cm	the depth above which 99% of the total root length is observed
	RMc	$\text{cm cm}^{-3}$	maximum root length density in the RLD profiles.
	Tc	$\text{cm cm}^{-2}$	total root length per surface area
<b>Trench</b>	RX	counts $\text{cm}^{-2}$	root count density in 5 cm wide vertical transects of the trench profiles
	Rz	counts $\text{cm}^{-2}$	root count density in 5 cm thick horizontal transects of the trench profiles
	Tt	counts $\text{cm}^{-2}$	average root count density in the trench profiles
<b>Minirhizotron</b>	At	$\text{d}^{-1}$	reciprocal of the median root arrival times at 10, 20, 40, 60, 80, and 120 cm depth
	IQR	d	interquartile range of root arrival times at 10, 20, 40, 60, 80, and 120 cm depth
	RMm	$\text{cm cm}^{-2}$	maximum root length density in a root arrival curve.

From the trench profile data, we derived three characteristic root system measures: Tt which is the total number of intersections in the profile, RX which represents the lateral root distribution in the direction perpendicular to the rows and Rz which represents root distribution with depth. RX was calculated for each vertical column of grid cells by summing up the root intersections in that column. Making use of the symmetric behavior of the root growth with respect to the vertical axis below the seed, we averaged the values of the columns at the same distance left and right of the plant row.

From rhizotube observations of the root arrival curves (RAC), we derived the reciprocal of the median arrival time of the roots at a certain depth, At. The median arrival time was defined as the time at which the root length density in the RAC reached 50% of the maximal root density, RMm, of the RAC at that depth. The reciprocal was taken to avoid

numerical complications for tubes that were below the maximal rooting depth for which At was equal to zero. The difference between the times at which the densities in the RAC reached 75% and 25% of the RMm represents the interquartile range of the root arrival times, IQR, which is inverse proportional to the slope of the RAC. For tubes below the maximum root depth, IQR was zero.

The Morris one-at-a-time sensitivity analysis method was performed to quantify the sensitivity of different characteristic root system measures to each parameter of the root architecture model (Morris, 1991). Morris one-at-a-time sensitivity analysis method has been applied previously to perform sensitivity analysis of root architectural models (Garré et al., 2012; Pagés et al., 2012). The method calculates elementary effects,  $EE_i$  of a certain parameter  $p_i$  on a characteristic root system measure  $Y(\mathbf{p})$ , as:

$$EE_i = \frac{Y(\mathbf{p} + range_i \mathbf{e}_i \Delta_i) - Y(\mathbf{p})}{\Delta_i} \quad (2.2)$$

where  $\mathbf{p}$  represents the model parameter vector with dimension  $k$ ,  $range_i$  is the range of parameter  $i$ ,  $\mathbf{e}_i$  is a unit vector with dimension  $k$  that points in the  $i^{th}$  direction and  $\Delta_i$  is a perturbation factor of the  $i^{th}$  parameter. To account for non-linearities and interactions between different parameters, the elementary effects of a certain parameter was evaluated for  $r$  different parameter sets  $\mathbf{p}$ . The mean of the elementary effects,  $m_i$  and of the absolute values of elementary effects,  $m_i^*$  represent the overall influence of the parameter when it varies within its range on the considered characteristic root system measure:

$$m_i = \frac{\sum_{j=1}^r EE_i^j}{r} = \frac{\sum_{j=1}^r Y(\mathbf{p}^{(j)} + range_i \mathbf{e}_i \Delta_i) - Y(\mathbf{p}^{(j)})}{\Delta_i} \quad (2.3)$$

$$m_i^* = \frac{\sum_{j=1}^r |EE_i^j|}{r} \quad (2.4)$$

To evaluate the non-linearity of the relation between  $Y$  and the parameter  $p_i$  and its interaction with other parameters, the standard deviation of the elementary effects,  $s_i$ , is calculated:

$$s_i = \sqrt{\frac{\sum_{j=1}^r (EE_i^j - m_i)^2}{r}} \quad (2.5)$$

In order to obtain accurate and precise estimates of the sensitivity parameters  $m_i$ ,  $m_i^*$  and  $s_i$ , it is important to use a representative sample of the parameter space. However, for models with many parameters that require a long computation time, the number of parameter sets that can be used to calculate the parameter sensitivity is limited. We used the Method of Modified Optimized Trajectories that was proposed by (Ruano et al., 2012) and that is based on the methods of (Morris, 1991) and (Campolongo et al., 2007). First, 500 parameter trajectories, which are sets of  $k+1$  parameter vectors  $\mathbf{p}$  ( $k$  is the number of parameters in the parameter vector, in our case 37), were generated according to the method proposed by (Morris, 1991). Each parameter could take values on a fixed and uniform grid that was chosen to have  $m = 4$  levels with the lowest and highest value that are, respectively, 50% lower and 50% higher than the mean parameter value given in Table 2.1. Each parameter trajectory was generated starting from a randomly chosen initial parameter vector on the  $m$ -level grid. In the parameter trajectory, only one parameter is changed between two consecutive parameter vectors and every parameter is changed once in the trajectory. The parameter change factor  $\Delta_i$  in the trajectory was set according to (Morris, 1991) to  $m/(2^*(m-1))$  or  $2/3$ . To calculate the elementary effects, only 10 trajectories ( $r = 10$ ) were selected from 500 generated parameter trajectories so that CRootBox was run for 380 parameter sets. The 10 sets were selected based on the distances between the parameter vectors of the different trajectories. The largest distances were chosen so that the selected parameter vectors spanned the parameter space.

Finally, sensitivity indices or normalized mean absolute elementary effects and normalized standard deviations were calculated as a percentage of the overall effect of all parameters:

$$\mu^*_i = 100 \frac{m_i^*}{\sum_{i=1}^k m_i^*} \quad (2.6)$$

$$\sigma_i = 100 \frac{s_i}{\sum_{i=1}^k m_i^*} \quad (2.7)$$

If the parameter sensitivity is equally distributed among all 37 parameters, each parameter should contribute 2.7% ( $100/37$ ) to the overall effect. Therefore, we selected 5%, which is approximately double the equal parameter sensitivity, as the margin to determine the sensitivity levels. We defined parameters with sensitivity indices ( $\mu^*$ ) greater than 10, between 5 and 10, and below 5 as the most sensitive, moderately sensitive and non-sensitive parameters, respectively. Parameters with a sensitivity index  $\mu^* > \sigma$  and  $\mu^* > 2\sigma/\text{sqrt}(r)$  were defined as parameters with respectively high and severe non-linear effects (Morris,

1991).

The parameter sensitivities,  $\mu^*$ , were presented as the percentage of the total variation of the observed output variable (root system characteristic measure) due to variation in all the input parameters (RSA) that can be attributed to the variation in parameter  $i$ . To evaluate the parameter sensitivity against the uncertainty of an observed variable due to sampling uncertainty, the standard deviation of the observed variable was normalized by the overall effect of all parameters:

$$R^* = 100 \frac{stdev}{\sum_{i=1}^k m_i^*} \quad (2.8)$$

where  $stdev$  is the standard deviation of the observed variable or characteristic root system measure (averages of RLD, of Rz, or of RMm). When  $R^* < \mu^*_i$ , the effect of parameter  $i$  on the observed variable can be distinguished from the uncertainty of the observation.

### 2.2.3 Principal component analysis of sensitivities

The sensitivity analyses reveal parameters that have a strong influence on certain aggregated root system characteristics that are derived from field sampling. But, the effects of different parameters on these characteristic root system measures may be strongly correlated. This implies that a change that is induced by one parameter may be compensated by another parameter. Parameters with strongly correlated effects cannot be derived independently by inverse modelling. In order to assess which parameters could be derived from the observed characteristic root system measures, we carried out a principal component analysis of the sensitivities.

The relation between model parameters  $\mathbf{p}$  and model output  $\mathbf{Y}$  can be represented using a linear approximation of the model as:

$$Y(p) = \Delta p^T J + Y(p_0) \quad (2.9)$$

Where  $\mathbf{p}_0$  is a reference parameter set and  $\mathbf{J}$  is the Jacobian of the model that corresponds with the sensitivity of the model output  $\mathbf{Y}$  to the parameters  $\mathbf{p}$ . This linear approximation is for instance used to estimate parameters using non-linear regression. In analogy to linear regression, the Jacobian corresponds with the independent variable matrix  $\mathbf{X}$ . When

the independent variables (columns of  $\mathbf{X}$ ) are strongly correlated with each other, the estimates of the parameters become very uncertain (multicollinearity). This implies that not all parameters of the model can be inferred from the regression and that the model is overdetermined. In order to avoid multicollinearity, new independent variables that are linear combinations of the original variables and that are not correlated with each other can be derived using a principal component analysis (PCA). The principle components (PC) explain a certain part of the variability of the independent variable dataset and because of their mutual independence, the total variability in the dataset is the sum of the variabilities explained by each of the PC's. The PC's are ranked in function of the variability that they explain with the first PC explaining the most. By selecting only the first PC's as independent variables for the regression, the dimension of the problem and hence the number of parameters that are estimated can be reduced. Turning the problem around, the principal component analysis (PCA) provides information about how many and which parameters of the model can be estimated from the observed dependent variables  $Y$  and its sensitivities to the parameters  $\mathbf{p}$ . The coefficients that relate the different independent variables (sensitivities to the parameters  $\mathbf{p}$ ) to the PC's, i.e. the loadings, can be plotted for two PC's in biplots. The vectors shown in a biplot for different independent variables (sensitivities to the parameters  $\mathbf{p}$ ) indicate how much of the variability of the two PC's is linked to the variability of the independent variables (length of the vector) and how strongly independent variables are correlated among each other.

As an estimate of the Jacobian, we used the average value of the sensitivities,  $m_i$ . When different observation types with different dimensions (e.g. root length in soil cores vs root counts in a profile or in a rhizotube) are combined, the sensitivities have different dimensions as well. In order to evaluate the impact of combining different observation types on the amount of parameters that can be estimated independently, the sensitivities were normalized by the average length of the sensitivity vectors for a certain observation type. In other words, we calculated the length of the vectors in each row of  $\mathbf{X}$  for a certain observation type  $Y$  and took the average of these lengths. Then the values in the  $\mathbf{X}$  matrix for that observation type were divided by this average length. We considered as observation types: root lengths in soil cores; average arrival times, IQRs of arrival time distributions, and maximum root counts derived from root counts in rhizotubes; and the amount of roots counted in vertical transects at different distances from the rows. In order to account for the different number of observations for the different observation types, weights were assigned to the sensitivities corresponding with different observations. For the cores, 45 observations were available, for the rhizotube observations 18 (3 types and 6 depths) and for the counts in vertical transects 2 for wheat and 8 for maize.

A flowchart with the simulations of the root system architectures, sampling methods, derivation of characteristic root system measures, the sensitivity and PCA analyses is given in Figure 2.5.

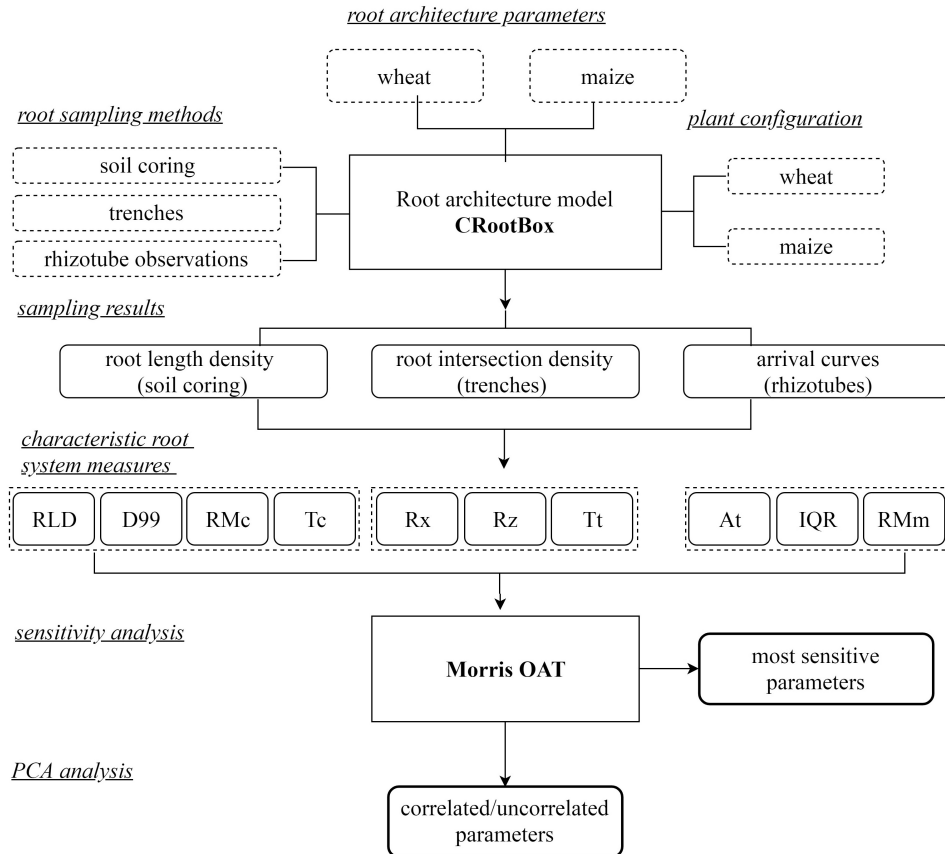


**Figure 2.5:** Flow chart showing the main steps used in the methodological approach.

## 2.3 Results

### 2.3.1 Root systems simulations

Figure 2.6 presents a 3D visualization of the root systems of maize plants at 180 days after sowing that were simulated using CRootBox in a field plot. Similar simulations were

done for wheat. Sampling methods and the locations of sampling are also shown in the figure. Computation time for the virtual field simulations significantly varied with the RSA parameters and number of root systems that were simulated in the virtual field plots. Simulation of root growth and sampling in one field plot took 177 seconds for wheat and 878 seconds for maize on a desktop computer with Intel(R) core (TM) i3-4150 cpu @ 3.50GHz processor and 8.00 Gb RAM.

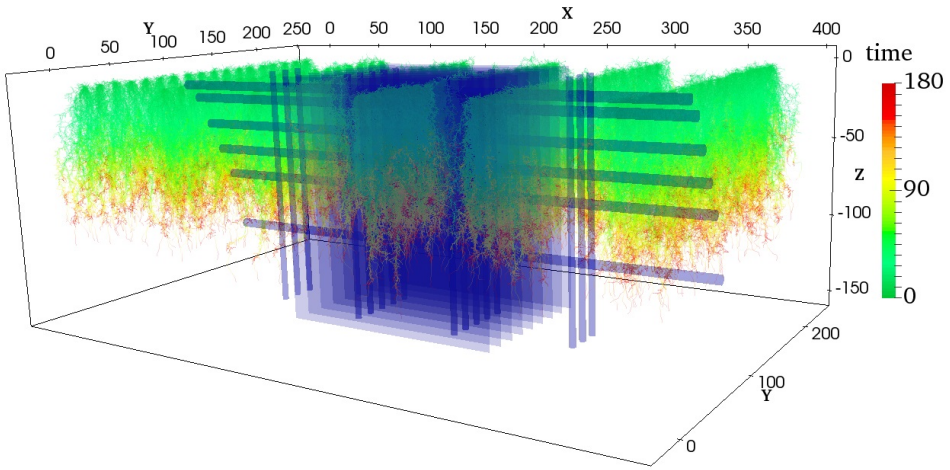


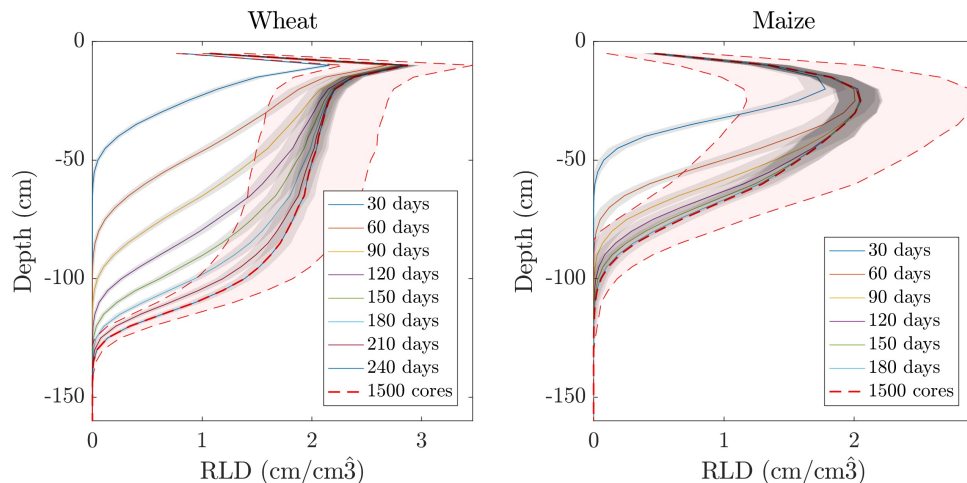
**Figure 2.6:** Simulated maize root systems in a virtual field plot until 180 days after sowing (color scale represents the appearance time of the root segments). Vertical transparent cylinders represent the soil cores, horizontal cylinders the rhizotubes, and vertical planes the trenches. Winter wheat simulations followed a similar simulation procedure with different plant density and sampling locations.

### 2.3.2 Root sampling

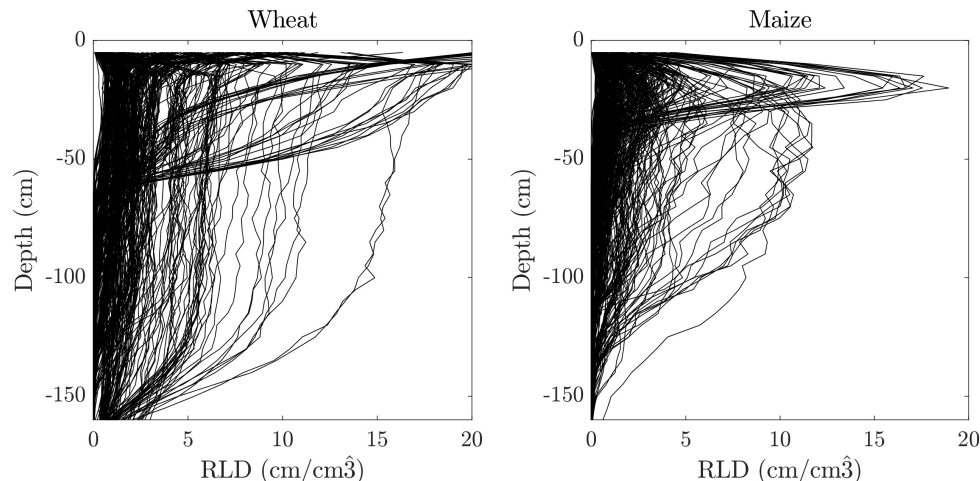
#### Coring:

Figure 2.7 shows the core sampling results at one-month intervals for maize and wheat, respectively. Each line of the graph represents the mean root length density and the gray shaded bands represent the standard deviation of the estimate of the mean root length density that is based on 15 cores in one realization of a field plot. The standard deviation of root length densities in the individual soil cores is represented by the red shaded band. The results of the two plant types, maize and wheat, show different patterns. The maximum

simulated rooting depth of wheat is 10-20 cm deeper than that of maize whereas the highest root length density for maize is reached about 10 cm deeper than for wheat.



**Figure 2.7:** Root length density profiles obtained from 15 soil cores in a field plot with wheat (left), and maize (right) at 30-day time intervals. The lines represent the average of the profiles that are simulated in 100 realizations of the plots. The grey shaded areas represent the standard deviation of the obtained profiles from 15 soil cores in the different realizations. Red shaded area represents the standard deviation of the root length densities in the 1500 soil cores at the end of the growing season.

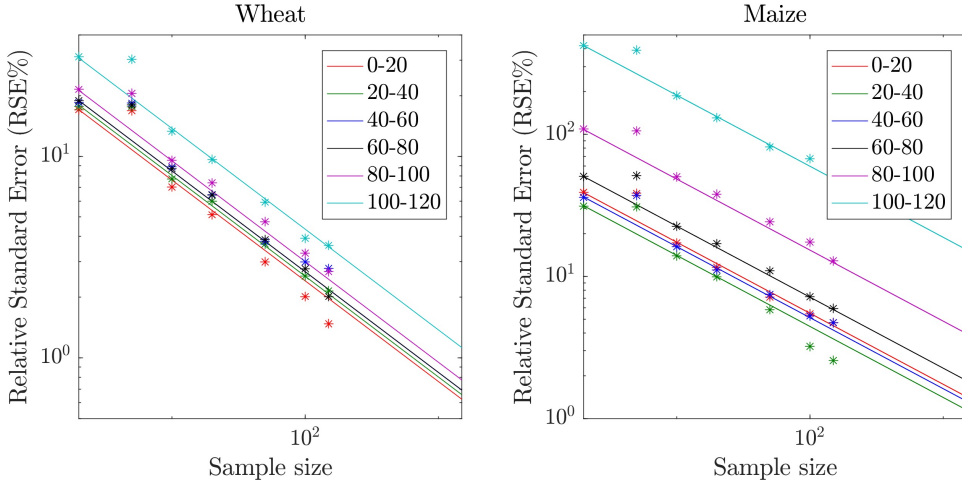


**Figure 2.8:** Range of root length density profiles obtained from 15 soil cores in a field plot with wheat (left), and maize (right) at 240 and 180 days respectively, based on the full set of parameter variations used in sensitivity analysis.

The individual root length density profiles that are shown in Figure 2.8 represent the distributions that were simulated for the reference RSA parameter set in Table 2.1. In order to demonstrate the variability of the root distributions in the sensitivity analysis, we plotted in Figure 2.8 root length density profiles for the 380 considered parameter sets. This plot illustrates the flexibility of the RSA model to simulate different root length density distributions by changing its parameters between 50% and 150% of the standard parameters set. Depending on the parameters, different shapes of root density distributions: bell shaped, sigmoid, nearly uniform and exponential; different maximal root depths ranging from 30 cm to over 160 cm depth; and different maximal root densities:  $20 \text{ cm cm}^{-3}$  compared to approximately  $2 \text{ cm cm}^{-3}$  for the standard parameter set are obtained.

### **Estimation of representative sample size:**

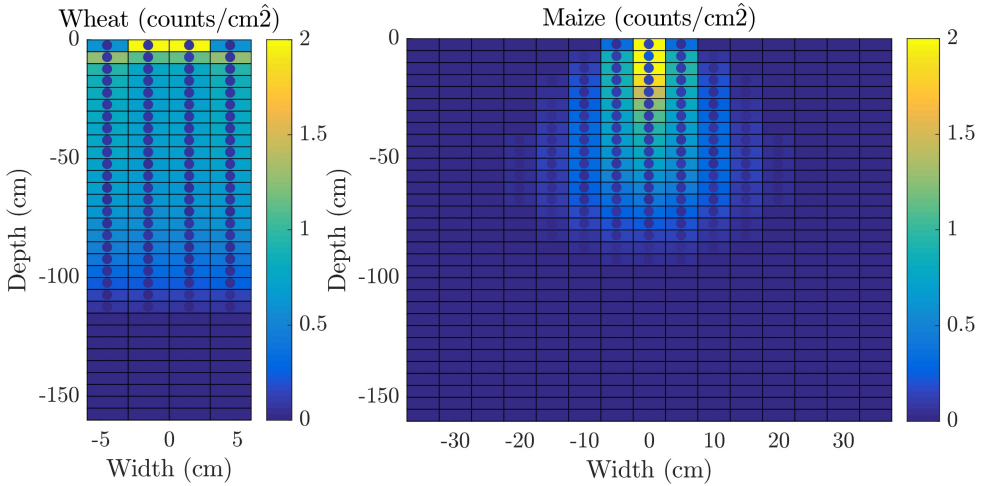
Figure 2.9 shows the relative standard error of the mean root length density, RSE, versus the number of cores that was used to calculate the mean. To reach a RSE smaller than 10%, 10 cores are sufficient for wheat except for the deeper soil horizons where root densities are smaller. This is in agreement with results of wheat field core samples (Hang Lai Thi Thu, 2011). For maize, around 50 cores would be required to reach the 10% RSE threshold in the upper soil layers, whereas an even higher number of cores would be required for the layers below 60 cm. RSE may increase due to selection of sampling position such as positions just below the seed or in between two rows in maize sampling because higher number of roots are observed close to the seed position and root density decrease with increasing distance from the plant base. It is important to note that the sample volume also contributes to the precision of the root length density measurements which increases with the volume of selected sampling size (larger diameter cores increase the precision of the selected number of cores, and vice versa).



**Figure 2.9:** Relative standard error of the estimated mean root length density of wheat (left) and maize (right) at different depths obtained from soil cores as a function of the sample size: lines represent the theoretical relation between the standard error of the mean and the sample size and symbols are standard errors of sets of means.

### Trenching:

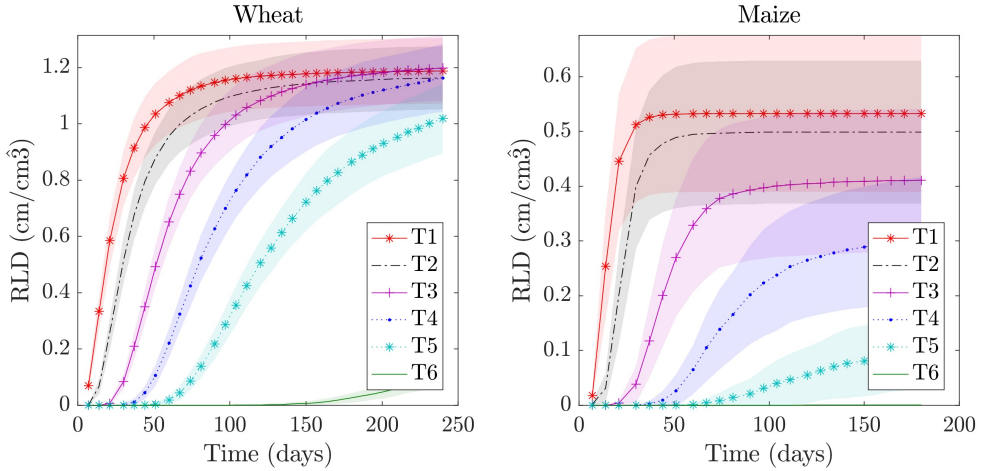
Root counting in trenches of the two considered crops shows relatively diverse results for wheat and maize (Figure 2.10). The winter wheat root distribution is laterally homogeneous below 10 cm depth, whereas maize shows higher lateral heterogeneity of root counts; root counts decrease with the increasing distance from the seed position. The highest root count density was observed close to the seed position.



**Figure 2.10:** Spatial distribution of wheat and maize grid-based root counts in virtual trench profiles. Dots represent the standard deviation of the mean root counts (winter wheat at 240 days after sowing (left) and maize at 180 days after sowing (right)).

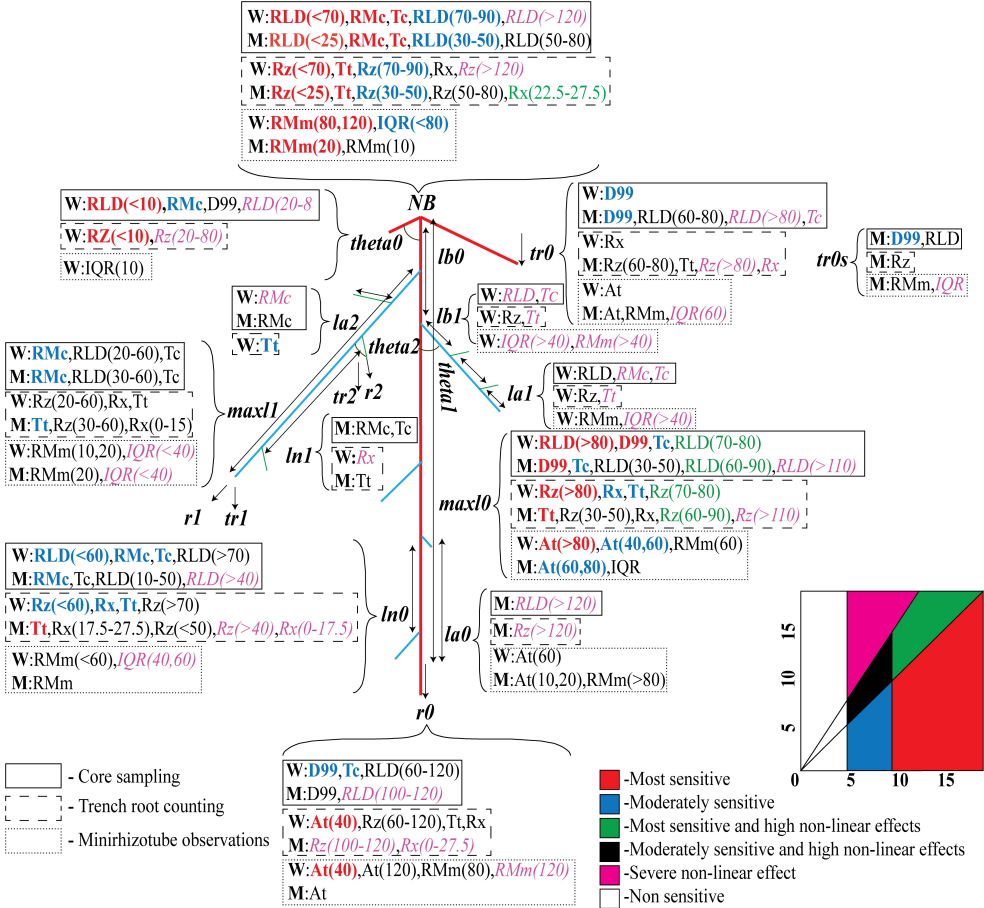
### Minirhizotrons:

Simulated root arrival curves to the rhizotubes at different depths represent the variation of root distribution and density with time (Figure 2.11). Depth profiles of root length densities derived from rhizotubes had a different shape than those derived from soil cores. For instance, for wheat at 240 days there is almost no variation of root densities between 10 and 60 cm depth observed in the rhizotubes whereas the profiles derived from soil cores show a considerable variation with depth. In maize, the rhizotubes indicate the highest root density at 10 cm depth, whereas the profiles derived from soil cores show the highest root length density at 20 cm depth. The reason for these differences can be due to the different locations below the plant rows that are sampled by the rhizotubes and the soil cores and the impact of the root orientation on the root densities that are observed in the rhizotubes.



**Figure 2.11:** Mean root arrival curves (RAC) in horizontal rhizotubes at different depths (T1-10 cm, T2-20 cm, T3-40 cm, T4-60 cm, T5-80 cm, T6-120 cm) for winter wheat (left) and maize (right). Lines are means of root length densities obtained from 2000 images per observation time (20 locations in 100 tubes in different realizations of the field plots) and shaded areas represent standard deviations of means estimated from 20 images in one realization of the field plot (shaded areas)

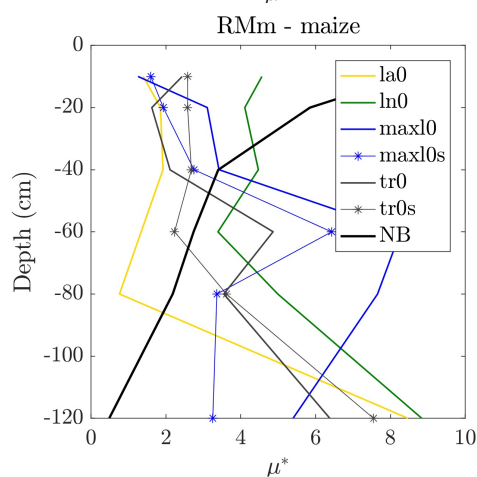
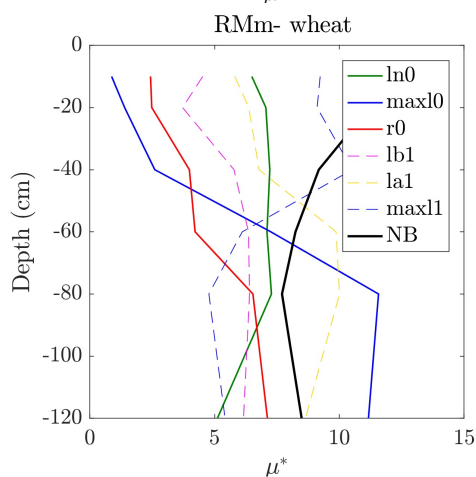
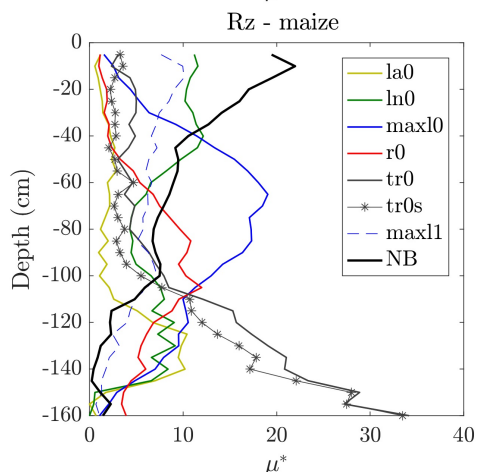
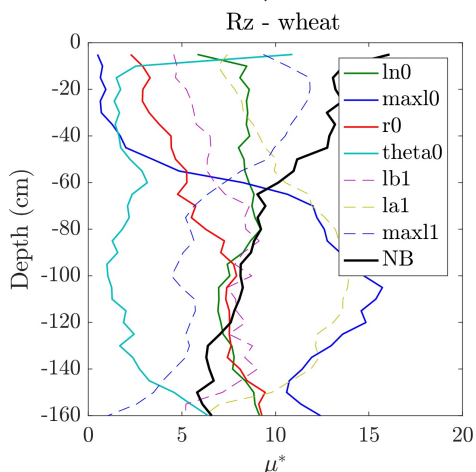
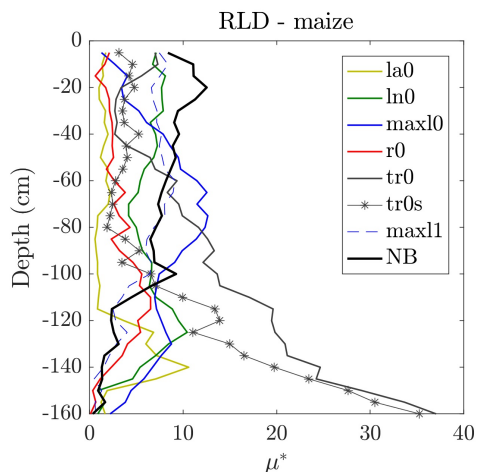
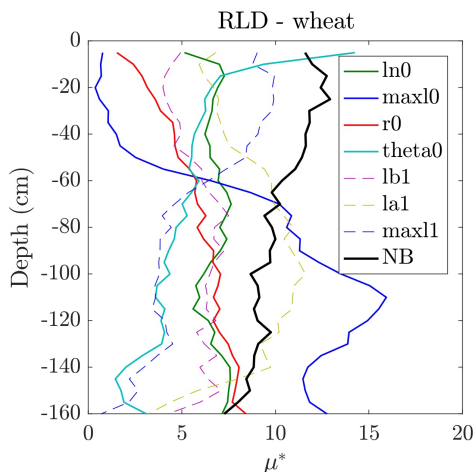
### 2.3.3 Sensitivity Analysis



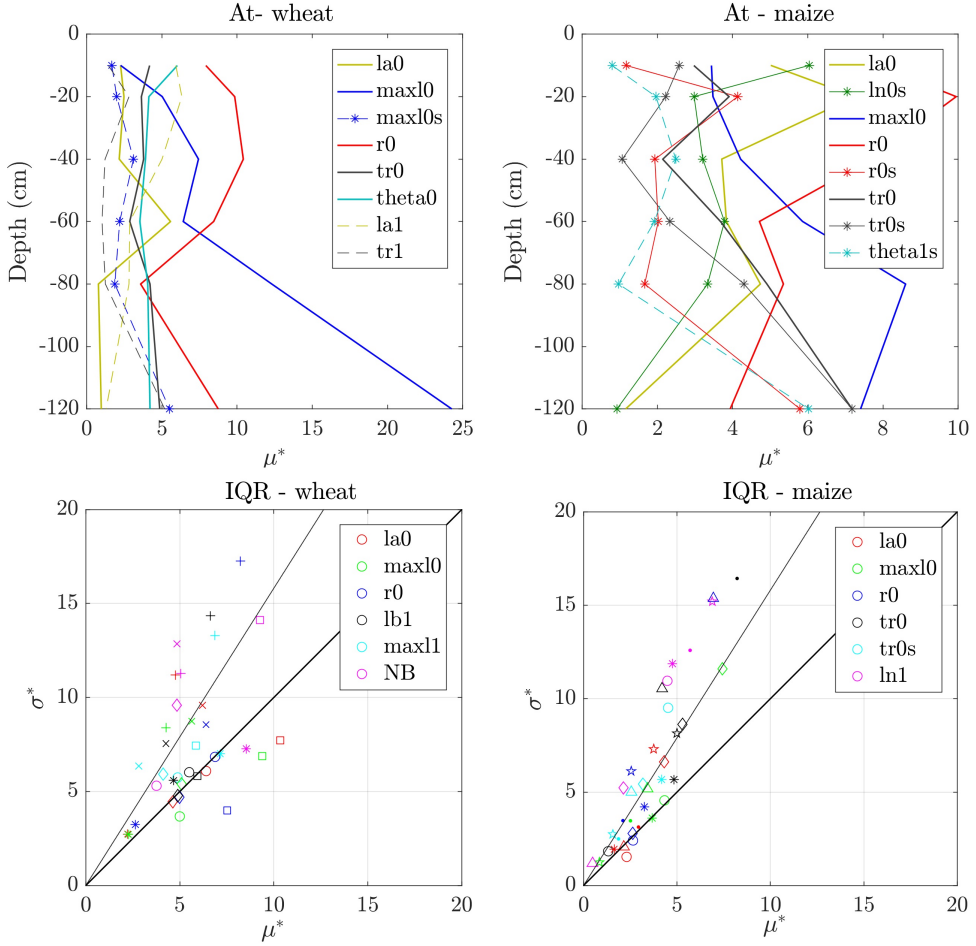
**Figure 2.12:** Summary of the sensitivities of the characteristic root system measures, which are derived from virtual field observations (see Table 2.4), to parameters of the root system architecture model (Table 2.1) (W: winter wheat, M: maize)). Classes of parameter sensitivities and non-linearity effects; parameters are categorized into six zones based on the elementary effects and standard deviations. The continuous line represents 1:1 line and the dashed line represents  $= 2\sigma/\sqrt{r}$  with  $r=10$  is the number of parameter trajectories.

Figure 2.12 shows which characteristic root system measures are influenced by the RSA parameters. Each parameter is characterized by its normalized mean of absolute elementary effects and normalized standard deviation and illustrated by the color-code and font type shown in Figure 2.12. Parameter sensitivities of root system measures that vary with depth and that are obtained from all three sampling methods; coring (RLD), trenching

(Rz) and minirhizotron methods (RMm, At) also vary with depth and the change of the parameter sensitivity with depth differs between different parameters and between the two crops (Figure 2.13). For instance, for wheat and maize, the sensitivities of RLD, Rz and RMm to  $NB$  (number of zero order roots) decrease with depth whereas their sensitivities to  $maxl0$  (maximal length of zero order roots) increase with depth. The latter is consistent with the maximum rooting depth (D99) that shows the highest sensitivity to  $maxl0$  (Figure A.2). RLD and Rz in maize are sensitive at greater depths to  $tr0$  (gravitropism of zero order roots) whereas RLD and Rz in wheat close to the soil surface are sensitive to  $theta0$  (insertion angle of zero order roots) (see Figure 2.13). The sampling uncertainty in one realization of the field plot (i.e. 15(16) cores, 9 trenches, 1m long rhizotubes) relative to the total effect of all parameters,  $R^*$ , was for RLD, Rz and RMm always lower than 2% so that the parameter sensitivities,  $\mu_i^*$  shown in Figure 2.13 could be distinguished from sampling uncertainty.



**Figure 2.13:** Normalized means of absolute elementary effects ( $\mu^*$ ) of the most sensitive RSA parameters on root length densities at different depths in soil cores (RLD, first row), on root impact densities at different depths in trench profiles (Rz, second row), and on the maximum amount of roots observed in rhizotubes at different depths (RMM, third row) for winter wheat (left) and maize (right) 240 days and 180 days after sowing, respectively.



**Figure 2.14:** Normalized means of absolute elementary effects ( $\mu^*$ ) and standard deviations of elementary effects ( $\sigma$ ) of the most sensitive RSA parameters on median root arrival times (At, top) and on the IQR of root arrival times (bottom) observed in rhizotubes at different depths (red, green, blue, black, cyan and magenta colors represent the depths 10, 20, 40, 60, 80, 120 cm respectively) for winter wheat (left) and maize (right).

The sensitivities of root system measures that quantify the total amount of roots such as

the total root length,  $Tc$ , the total number of root impacts in a trench,  $Tt$ , or the maximal root length density,  $RMc$  are shown in Figure A.1. These measures show in general largest sensitivities to  $NB$ ,  $ln0$  (branching distance on zero order roots),  $maxl1$  (maximal length of first order roots), and  $maxl0$  ( $Tt$  and  $Tc$ ). From the trench observations, a characteristic that represents the lateral variations in root impacts,  $RX$ , and that is related to the lateral extent of the root system was derived. For maize, the sensitivity of  $Rx$  to  $NB$ ,  $tr0$  and  $maxl0$  varies with the lateral distance from the plant row whereas for wheat  $RX$  and the sensitivity of  $RX$  to the RSA parameters do not vary with lateral distance (see Figure A.3). Finally, root characteristics that represent the dynamics of the root system development such as the reciprocal of the median root arrival time,  $At$ , and the interquartile range of arrival times,  $IQR$ , at different depths were derived. The sensitivities of  $At$  and  $IQR$  to RSA parameters are shown in Figure 2.14. In contrast to the other root system characteristic measures that were derived from measurements at the end of the simulated root growth period, these dynamic root characteristics are sensitive to the growth rate of the zero order roots,  $r0$ . The difference between uncertainty of the observed variable to the total sensitivities of the parameters  $R^*$ , which is lower than the detectable parameter sensitivities, except  $Rz$  measure of maize trench root counting method (results are not shown).

### 2.3.4 Principal Component Analysis

The variability of the sensitivities of the core data to the different RSA parameters can be explained for the largest part by the first two PC's whereas the third PC explains less than 5% of the variability (Table 2.5). When rhizotube data are used or when all data are combined, the variability of sensitivities is spread more over the different PCs. This indicates that the impact of certain parameters on certain observation can less be compensated by changing other parameters. The parameter with the highest PC loading for the first PC is the number of zero-order roots ( $NB$ ). For the other PCs, the parameters with the highest loadings differ between the crop and between the type of data that are considered. However, for the rhizotube data, the growth rate of the zero-order roots,  $r0$ , has the highest loading for the second PC for both wheat and maize. Figure 2.15 and Figure 2.16 show biplots of parameter loadings for the 1st and 2nd PCs and the 2nd and 3rd PCs using data from respectively soil cores (see Figure 2.15) and rhizotubes (Figure 2.16) for wheat and maize. The alignment of the loading vectors of  $NB$  and  $ln0$  with the first PC axis in the biplots indicates that the first PC is correlated with the  $NB$  and  $ln0$  sensitivities whereas the opposite orientation of the vectors shows that  $ln0$  has the opposite effect compared to the effects of  $NB$ . A larger distance between branches leads to a lower root length density whereas a larger number of zero order roots leads to a higher

root density. The close alignment of loading vectors to the second PC (e.g. *maxl0* and *tr0* for the core data from respectively wheat and maize and *r0* for the rhizotube data) identifies parameters that have an effect on the observations that is independent of the parameters that are related to the first PC and that cannot be compensated by changing these parameters.

**Table 2.5:** Percentage of variance explained by the first 5 principle components of the sensitivities when only data from coring (cores), rhizotube measurements (rhizotubes) are used and when rhizotube, core and impact data are combined (All) The parameter names with the highest PC loading are given in parenthesis.

PC	Cores	Rhizotubes	All
<b>Wheat</b>			
1	73.3 (NB)	51.9 (NB)	55.6 (NB)
2	18.9 ( <i>maxl0</i> )	27.5 ( <i>r0</i> )	19.0 ( <i>r0</i> )
3	4.6 ( <i>theta0</i> )	6.5 ( <i>la1</i> )	9.4 ( <i>maxl0</i> )
4	1.0	3.7	4.9 ( <i>theta0</i> )
5	0.6	2.7	2.6
<b>Rest</b>	1.6	7.7	8.5
<b>Maize</b>			
1	70.5 (NB)	35.7 (NB)	57.2 (NB)
2	17.9 ( <i>tr0</i> )	28.4 ( <i>r0</i> )	15.3 ( <i>tr0</i> )
3	3.9 ( <i>maxl0</i> )	11.7 ( <i>la0</i> )	8.1 ( <i>r0</i> )
4	2.2	8.0	4.3 ( <i>la0</i> )
5	1.5	4.2	4.2
<b>Rest</b>	4	12	10.9



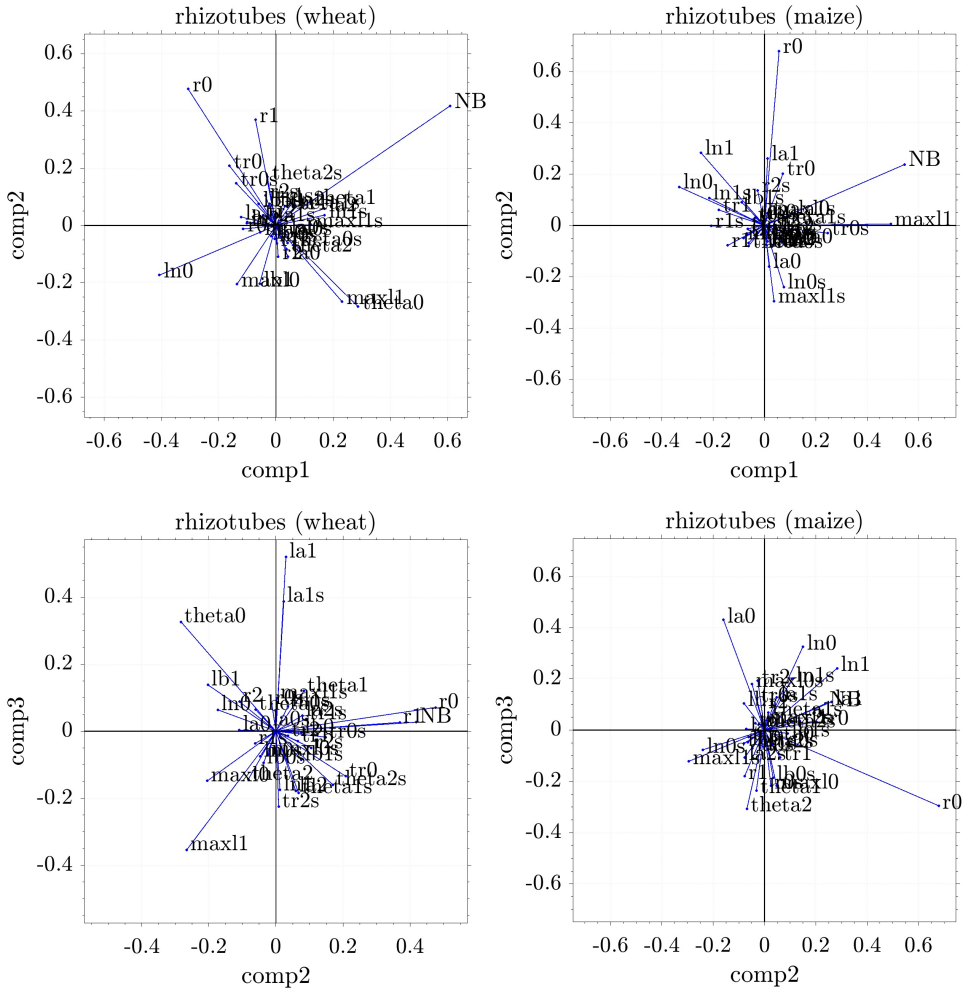


Figure 2.16: Biplots of parameter loadings for the 1st and 2nd PCs (first row) and the 2nd and 3rd PCs (second row) using data from rhizotubes for the wheat crop (left row), and for the maize crop (right column).

## 2.4 Discussion

Although the simulated root density distributions results with depth deviate in some cases from the often suggested exponentially decreasing root density with depth for agricultural crops (Fan et al., 2016), the main characteristics of root length density profiles obtained from soil coring such as maximal rooting depths at different times and average root length

densities show good agreements with experimental data (Wasson et al., 2014). One of the reasons for the difference in root density profile is that we did not select soil cores just below the shoot of the plant where simulated root densities are much higher. In comparison to the coring method, trenches provide detailed information about lateral distributions across plant rows. A clear lateral distribution of root densities in maize indicates that root density profiles obtained from root coring may depend on the location where the cores are taken. If the core sampling scheme does not cover the spatial variability of root densities, the obtained distribution may not be representative for the laterally averaged root length density distribution.

Root arrival curves (RAC) to rhizotubes show a remarkable feature in Figure 2.11: the large standard deviation of the mean root density that is calculated from 20 images in one tube for one realization of the field plot. The surface area or corresponding soil volume that is sampled by the images is relatively small so that a large number of images is required to obtain a precise estimate of the RAC. This can be achieved by taking more images using longer tubes and/or using more tubes at one depth. The standard error of the mean root density that was calculated from 120 images taken from three tubes at the same depth in a winter wheat plot was estimated to be 8% by (Cai et al., 2016). This would correspond with a standard error of 20% when the mean is estimated from 20 images, which is slightly larger than what we simulated for winter wheat. In our model simulations, we did not consider soil heterogeneity which may be an additional factor influencing the spatial variability of root densities that is observed in the field. The larger variability of RAC estimated from 20 images for maize can be attributed to the larger lateral variation of root densities of maize. Rhizotubes have often been installed with a certain insertion angle instead of horizontally. The large number of images that is required to obtain a precise estimate of the RAC at a certain depth would imply that a large number inserted rhizotubes to obtain a precise estimate of the RAC.

Sensitivity analyses of the characteristic root system measures that were obtained from the three different root sampling methods demonstrate that the parameter sensitivity varies not only with the sampling method, but also with each characteristic root system measure, which reflect properties such as rooting depth, root mass, and lateral spreading of the root system in soil. Also, of note are the differences in sensitivities for the two crops. This can be related on the one hand to different cropping density. On the other hand, the non-linearity of the model also leads to different sensitivities for root systems with a different architecture (or a different set of RSA parameters). The variance of the sensitivities is distributed more over the PCs of the rhizotube data (Table 2.5) which indicates that more

parameters can be derived from rhizotube data than from soil core data or trench profile observations. Rhizotube data also provided information about the dynamics of the root growth. This information could also be obtained when soil cores or trench profiles were taken at several times but parameter sensitivities were in our study only calculated for soil coring and trench profile data that were obtained at a single time. When all datasets were combined, additional information about root length densities from deeper soil layers (maize) or from closer to the soil surface (wheat) and information about the lateral root distributions (maize) in the soil core and root impact data, which was not present in the rhizotube data, gave extra loading to the RSA parameters  $tr0$  (maize) and  $theta0$  (wheat).

Regarding the rankings of sensitivities (Figure 2.15), the number and maximal length of the zero order roots,  $NB$  and  $maxl0$ , have a strong influence (red and green numbers) on a large number of characteristic root system measures. Next come the growth rate  $r0$  and the branching distance,  $ln0$ , of the zero order roots which have a moderate influence on a large number of characteristic root system measures; and the branching angle,  $theta0$ , and gravitropism,  $tr0$ , of the zero order roots and the maximal length of the first order roots,  $maxl1$ , with a moderate influence on a few characteristic root system measures. Of note is that the parameters that describe the first (except  $maxl1$ ) and second order roots have a less strong direct influence but their influence depends strongly on other parameters as indicated by the large normalized standard deviations,  $\sigma$  (Eq.(2.7)), of their effects. The higher order root parameters have a severely non-linear impact on some of the characteristic root system measures (magenta numbers).

Looking at the distribution of the influences of the parameters on the RLD with depth (Figure 2.13), it seems that the second PC reflects the sensitivity of the root densities deeper in the soil profile. For wheat, PC2 is strongly linked to the maximal length of zero order roots,  $maxl0$ , whereas for maize, especially the gravitropism of the zero order roots,  $tr0$ , is important. For both maize and wheat,  $maxl0$  and  $tr0$  have positive PC2 loadings which indicates that these parameters influence root densities at larger depths in the same way, i.e. higher root densities at greater depths can be obtained by longer primary roots or by roots that grow downwards more vertically due to a higher gravitropism. But the importance of both parameters for root densities at greater depths differs for the two crops.  $maxl0$  influences strongly the maximal rooting depth (D99) for both maize and wheat (Figure A.2).

The third PC is for wheat linked to the angle of the zero order roots,  $theta0$ , which influences the root densities close to the soil surface (see Figure 2.13). It should be noted that for both maize and wheat,  $theta0$  has negative PC2 loadings which indicates that an increase in

$theta0$  (more horizontal roots) leads to a lower root density at larger depths. For maize, the third PC is more strongly related to  $maxl0$  than to  $tr0$  and reflects the root distributions at intermediate depths, which are more sensitive to  $maxl0$  (see Figure 2.13).

The total root length  $Tc$ , which can be considered to be the product of the root depth and the root density, is sensitive to all the parameters that are related to PC1, PC2 and PC3. For wheat, these are  $NB$ ,  $ln0$ ,  $maxl0$ ,  $theta0$  and  $maxl1$ , whereas for maize these correspond to  $NB$ ,  $ln0$ ,  $maxl0$ ,  $tr0$  and  $maxl1$  (Figure A.1). The  $\sigma\text{-}\mu^*$  plot for  $Tc$  also shows a severe non-linear sensitivity of the total root length of wheat to the parameters that characterize higher order roots ( $maxl1$ ,  $la1$ ,  $lb1$ ). Since in the PCA the mean sensitivities  $m_i$  are considered, the non-linear effects are not expressed by the PCs.

Comparing the  $\sigma\text{-}\mu^*$  plot for  $Tc$  (total root length) with that for  $Tt$  (total number of intersections in a trench profile), (Figure A.1) the two plots look very similar. This indicates that  $Tc$  and  $Tt$  contain similar information about RSA parameters. Similar conclusions could be drawn when comparing sensitivity depth profiles for RLDs derived from soil cores (Figure 2.13), for RLDs derived from minirhizotube observations (RMm in Figure 2.13), and for RIDs derived from trenches (RZ in Figure 2.13). Although there are some differences in depth profiles of RLDs/RIDs that are derived from the different methods, these three types of aggregated information about root systems show a similar sensitivity to RSA parameters. This indicates that they contain similar information about RSA parameters. This suggests that adding root coring data to minirhizotube data for the same depth range will not lead to a lot of additional information that can be used to estimate RSA parameters.

Looking at the sensitivities of the lateral distribution of root impacts densities (RID) in trench profiles (Figure A.3), it is obvious that for wheat, with a uniform lateral distribution of root counts, the sensitivity of the RID averaged with depth,  $RX$ , to the RSA parameters does not vary a lot with lateral distance and is very similar to the sensitivity of the total number of root impacts  $Tt$ . However, for maize the sensitivity of  $RX$  varies considerably with lateral distance and  $RX$  is more sensitive to  $tr0$  than to  $NB$ , which is opposite to the sensitivity of  $Tt$  to  $tr0$  and  $NB$ . The  $tr0$  defines how strongly zero order roots are growing downward or can grow laterally, which explains the sensitivity of  $RX$  to  $tr0$ . Combining soil core with trench profile data provides extra information for estimating RSA parameters. The PCA of the combined dataset showed that the loadings of the parameters  $tr0$  and  $maxl0$  to PC2 and PC3 increased which means that  $tr0$  and  $maxl0$  could be better discriminated when trench profile data are combined with soil core data (results not shown).

The biplots of the parameter loadings of the PCs that were derived from the sensitivities

to the rhizotube data (RMC, At, and IQR at different depths) show that the first PC is related to the same parameters as the first PC of the soil cores (Figure 2.16). This PC is therefore also related to the average root densities in the soil profile. The second PC is related to the growth rate,  $r\theta$ , and corresponds with the median arrival time of the roots at different depths (Figure 2.15). The third PC is related to  $la1$  (the length of the apical zone of the first order roots) for wheat and to  $la\theta$  for maize. Since the median root arrival time near the surface is sensitive to  $la1$  (wheat) and  $la\theta$  (maize) (Figure 2.15), the third PC is related to the root arrival time near the soil surface. The influence of the parameters on the slope of the arrival curve is strongly or severely non-linear, which indicates that the effect of parameters on the slope of the arrival curve depends strongly on the values of the other parameters (Figure 2.15).

## 2.5 Summary and Conclusions

Root systems of a large number of plants in a field setting and different field sampling methods such as soil coring, root impacts on vertical soil trenches, and images taken from horizontal rhizotubes were simulated using the RSA model CRootbox. As an example, two crops with a different planting density and root architecture, maize and wheat were considered. Making use of the improved computational efficiency of CRootbox, it was possible to repeat the simulations for a large number of realizations of the field plots and a large set of RSA parameters. Based on these simulation data, the uncertainty or variability of root sampling data and the sensitivity of characteristic root system measures, which can be inferred from field data, to RSA parameters could be assessed. The most sensitive parameters were those of the zero order roots whereas the parameter of higher-order roots showed non-linear sensitivities, which means that their influence depended on the values of other parameters. Similar characteristic root system measures that were obtained with different methods, e.g. depth profiles of root density obtained from soil coring, from root impacts in vertical trenches, or from images taken in horizontal rhizotubes at different depths, showed similar sensitivity to the RSA parameters. However, the parameter sensitivity depended on the crop and the observation types, which implies that specific results cannot be generalized. Nevertheless, our results are consistent with an earlier sensitivity analysis of rhizotube observations to RSA parameters of spring barley (Garré et al., 2012). Although another RSA model was used, RootTyp (Pagés et al., 2004), the number of zero order roots ( $NB$ ) and the root growth rate of the zero order roots ( $r\theta$ ) were, as in our study, found to be the most sensitive parameters for, respectively, the root density observed in the rhizotubes

and the median arrival time of the roots. As also found in our study, the sensitivity of the slope of the root arrival time to RSA parameters was very non-linear.

Using principal component analyses of the parameter sensitivities, groups of parameters that had similar or counteracting effects on characteristic root system measures could be identified and linked to specific characteristic root system measures. The analyses demonstrated that the total number of zero order roots ( $NB$ ), the branching distance on the zero order roots ( $ln0$ ), and the maximal length of the zero order roots ( $maxl0$ ) influenced characteristic root system measures that are related to the overall root density (maximal root density, total amount root impacts) in a similar way. An increase in for instance  $NB$  could be compensated by a decrease in  $maxl0$  or an increase in  $ln0$ . This provided insight into which RSA parameters could be identified independently from specific characteristic root system measures by inverse modeling and which characteristic root system measures provide extra information to infer additional RSA parameters. Using information about root development over time, which can be obtained non-invasively from rhizotube images, is important to estimate root growth rates ( $r0$ ). Root density depth profiles obtained from horizontally installed rhizotubes can be extended with data from soil coring or from root impact counts in vertical trenches that provide a higher spatial resolution or give additional information about the lateral distribution of root densities. The PCA and sensitivity analyses showed the additional value of combining these datasets for the estimation of parameters like maximum length ( $maxl0$ ), insertion angle ( $theta0$ ) and gravitropism of zero order roots ( $tr0$ ) from field measurements.

## 2.6 Outlook

The development of the root system also depends strongly on environmental factors like soil temperature (Nagel et al., 2009), soil strength (Bingham and Bengough, 2003), shape and size of soil grains (Lipiec et al., 2016), and the presence of biopores (Perkons et al., 2014). Some studies showed that root architecture and characteristic root system measures of a certain plant genotype reflect its adaptation to environmental conditions (Hamada et al., 2012) such as the effect of tillage system on soil strength, the soil type and soil moisture condition (Cai et al., 2018; Muñoz Romero et al., 2010; Fan et al., 2017). Therefore, it is required to include soil information into RSA models. CRootBox does have the capability to simulate root growth affected by static soil condition as well as to dynamically changing soil conditions via coupling to soil models (see e.g. example 5 in (Schnepf et al., 2018)). At the cost of increasing the number of parameters, this shall be considered in future sensitivity

analyses. In this study, our sensitivity analysis results provide a broad insight about the sensitivities of classical field sampling data to different root architecture parameters. We highly recommend investigating the application of root architecture models to retrieve the specific root traits of different genotypes and their response to environmental conditions with the aid of an inverse modeling algorithm and to test the suitability of real sampling schemes to retrieve the root system architecture of a plant. This approach could further valorize field phenotyping data by linking them to individual root architecture parameters or root traits. These architectural traits could be plugged into functional structural models that predict the functional traits of root systems that could be of interest to breeders (Meunier et al., 2017; Passot et al., 2018).

## Chapter 3

# Bayesian Inference of Root Architectural Model Parameters from Synthetic Field Data

**Adapted from:** Morandage S, Laloy E, Schnepf A, Vereecken H, Vanderborght J (2019), Bayesian Inference of Root Architectural Model Parameters from Synthetic Field Data. *manuscript submitted for publication in Plant and Soil Journal*

## 3.1 Introduction

Plant root distribution in soil varies with the plant species (Fan et al., 2016), genotypes (Gorim and Vandenberg, 2017), and soil environmental conditions (de Moraes et al., 2018). The structure of the root system changes to adapt to soil-environmental conditions, e.g., in resource-limited environments (Morris et al., 2017).

Root system architecture describes the morphology and topology of a root system which is responsible for water and nutrient uptake. Plant functions, such as water and nutrient uptake, are strongly affected by root system architecture (RSA) (Hochholdinger, 2016). During the last few decades, plant-breeding programs have improved crop production significantly by introducing new varieties. (Del Bianco and Kepinski, 2018), showed the potential benefits of developing phenotypes such as crops with deep root systems to capture deep water and nutrients with high efficiency, and (Lynch, 2013) demonstrated the possibility of extracting deep water and N with the help of hypothetical maize ideotype by adapting architectural root traits.

Imaging methods have been used successfully to recover RSA parameters of plants grown in soil (Bodner et al., 2018; Topp et al., 2013; van Dusschoten et al., 2016) which were subsequently used in RSA models that extrapolate RSA from the seedling to mature plant stage (Zhao et al., 2017). Methods for root sampling and for characterizing RSA traits, and their limitations are summarized in (Fang et al., 2012; Judd et al., 2015). In comparison to field phenotyping, lab-based methods are widely used in root phenotyping due to a lack of accessibility and reliable methods to characterize the RSA of plants grown in field conditions (Atkinson et al., 2019; Meister et al., 2014). However, the root traits of young plants that were grown in the controlled lab environment are not sufficient to determine traits of mature plants that grow in field soils subject to the real field soil and environmental conditions (Paez-Garcia et al., 2015). Therefore, field phenotyping methods are becoming increasingly popular to characterize RSA in real field conditions (Araus and Cairns, 2014; Meister et al., 2014).

Traditionally, root sampling methods are used to measure the root distribution with depth (as root length density) from soil cores (Wasson et al., 2014), root intersection counting in trench profiles (Vansteenkiste et al., 2014), root arrival curves (root length density varies with time in continuous measurement) using minirhizotron methods (Majdi, 1996), and excavation methods (Böhm, 1979a), to determine the total root mass distribution of plants. All these methods have traditionally been used to obtain some limited information about

the root distribution in the soil. Nevertheless, the data may contain information about the detailed root system architecture or architectural root traits, i.e., number of primary roots, the distance between lateral roots, branching angles. However, obtaining RSA parameters from field data remains a challenge as they represent more aggregated information about the root system. In addition to classical methods, innovative field sampling methods have been introduced to obtain more detailed information about the root system (Bucksch et al., 2014; Wu and Guo, 2014). Although field sampling methods provide limited information, it is of utter interest to study the possibility of retrieving the hidden information (3-D RSA) in field sampling data.

Root architecture models consist of dozens of parameters that determine the structure and the morphology of the root system. Root sampling data contains information about several root system architectures as an aggregate. Even though simulated RSA architectures differ for different parameter sets, these differences may be averaged out in the aggregated sampling data so that different sets of RSA parameters may produce the same aggregated output. Therefore, when doing parameter estimation care must be taken to prevent overfitting which is associated with parameter uncertainty. In previous work (Morandage et al., 2019) we identified the most sensitive parameters of root systems of wheat and maize with respect to aggregated data or root system measures that were derived from soil coring, trenching and minirhizotron root sampling methods. In that same study, we showed how the sensitivity of the model output to the different root architectural parameters varies with the sampling method and considered “root system measures” (such as root length density at different depths in the soil profile, maximal rooting depth, etc.). We indicated that the most sensitive parameters could be retrieved potentially by inverse estimation. Moreover, using a principal component analysis of parameter sensitivities, we identified parameter groups of which the effect of their changes on the simulated root system measures could be compensated by changes of other parameters in that group.

In order to represent the fact that root systems of two plants of the same variety or even with the same genotype differ, random factors or stochasticity are built in RSA models. This randomness or stochasticity is averaged out in sampling data that aggregate information from different plants. But since sampling data contain information of a finite number of plants, the stochasticity or randomness of these individual plants is not averaged out completely but remains to some extent in the sampling data. This stochasticity or uncertainty in the sampling data is another source of parameter estimates uncertainty. Therefore, it is important to assess the uncertainty of the RSA parameters that are obtained from aggregated sampling data.

Bayesian inference can be identified as a potential approach for estimating RSA parameters from aggregated field sampling data and their uncertainty, encoded within the so-called parameter posterior probability density function (pdf). Although RSAs of plants derived from lab experiments differ due to differences in plant development stage and growing conditions from RSA of the sampled plants in the field, (Paez-Garcia et al., 2015), RSA parameters derived from the lab may provide a good approximation about the prior range of the parameters or their prior pdf.

The application of Bayesian methods has tested successfully in many fields of studies (Hines, 2015; Vrugt et al., 2009) and has been shown to be a robust approach to estimate parameters and their uncertainty, especially when the model outcome depends non-linearly on the parameters and non-linear parameter interactions exist. Previous sensitivity analyses (Garré et al., 2012; Pagés et al., 2012; Morandage et al., 2019) showed that this is the case for RSA models. In comparison to local and/or non-probabilistic optimization algorithms, the main disadvantage of Bayesian methods is that sampling the posterior distribution typically requires a large number of forward models runs. In addition, simulation of many root systems in the field and their sampling incurs large computational costs. Therefore, Bayesian inversion can take a considerable amount of time. Nevertheless, we show herein that the use of distributed computing together with a parallel Bayesian inversion algorithm, e.g., a multi-chain Markov chain Monte Carlo (MCMC) sampler, makes it possible to infer important RSA parameters from field sampling data. Markov chain Monte Carlo sampling with a symmetric proposal distribution makes us of the prior density and likelihood function of current and proposed parameter sets to create transitions in the chain. The value of the likelihood function classically depends on the errors between the simulated and observed data and the standard deviations of these errors. These standard deviations reflect the required fitting precision which in ideal conditions of no model errors should be equal to the uncertainty level(s) of the observed data. The problem that arises for RSA models that have a stochastic component is that the simulated observations themselves are stochastic. As mentioned before, this stochasticity can be reduced by increasing the number of plants that are simulated and used to calculate the aggregated root distribution. Unfortunately, this can incur prohibitively large computational costs. Therefore, approaches must be found to deal with this model stochasticity in a Bayesian inversion method.

Few studies were conducted to estimate the parameters inversely; a density-based model of root image data of individual root systems was investigated to determine the root growth parameters (Kalogiros et al., 2016). Although this study showed reasonable estimates with the measured root growth parameters, experiments were limited to short-lived root growth

in filter papers that do not resemble real field conditions. (Garré et al., 2012) used dynamic root growth data measured using minirhizotrons to calibrate the RSA model. The main limitation of the above approach was that a limited number of parameters of the model were estimated inversely, and the posterior distribution of the parameter estimates was not derived. Trench profiles and soil core data were used by (Vansteenkiste et al., 2014) to estimate the trait information such as total root length and root distribution successfully from measured and simulated data, and this study did not consider the RSA parameters extensively. A study was conducted by (Pagés et al., 2012) to show the possibility of retrieving some RSA parameters of a plant using field sampling methods. ‘CPU and memory consumption, especially for big root systems, as well as algorithmic and numerical problems due to the stochastic characteristics of the RSA model during inversion’ (Pagés et al., 2012) motivated them to develop a metamodel that was based on a global sensitivity analysis of the RSA model and that considered main parameter effects as well as parameter interactions. Furthermore, a recent study presented the use of the approximate Bayesian computation (ABC) framework to characterize root growth parameters from synthetic and experimental data that are limited only to early stages of root systems and that use directly observed RSA instead of aggregated field sampling data (Ziegler et al., 2019).

In this work, we present an approach to inversely estimate root architecture model parameters from field sampling data using Bayesian inference. Furthermore, we investigate the reliability of information about detailed root system architecture provided by our proposed inverse estimation approach. The rest of this paper is organized as follows. In section 2, we present our proposed inference method and how its performance is evaluated using plot-scale simulation of root density. In section 3, we study which RSA parameters can be successfully retrieved from the inversion of soil coring data. This is followed by section 4 which discusses the feasibility and remaining challenges associated with the application of our approach to real field conditions.

## 3.2 Materials and Methods

### 3.2.1 Forward model and virtual root sampling data

The synthetic soil coring root sampling data that are analogous to real field sampling data, were obtained from simulated root systems in a virtual field plot using known root architecture parameters. By using data from a virtual experiment instead of using real data,

we can evaluate how closely the inversely estimated RSA parameters match the known ‘true’ parameters. Based on this comparison, we can conclude which RSA parameters could be derived by inverse modeling.

We selected the stochastic root architecture model CRootBox (Schnepf et al., 2018) for root system simulations and root sampling. Please refer to (Schnepf et al., 2018) for detailed information about the root architecture model CRootBox. The detailed root system simulation, sampling and the sensitivities of root system measures to parameters of each sampling scheme are discussed in (Morandage et al., 2019).

For the inversion, we selected the core sampling data obtained from winter wheat root sampling. Wheat plant root systems were simulated in a 72 cm\*45 cm size plot that consists of seven rows with 16 plants in a row. The inter-row distance was 12 cm with 3 cm plant spacing within a row. Core sampling was performed with monthly time intervals for eight months. We adjusted the sampling size similar to real field sampling schemes. We chose 3 locations in-between rows for five different rows (15 core samples in a plot in total). To avoid boundary effects, zones of 20 cm from the borders of the plot were not considered for sampling (Figure 3.1(A)). Cylindrical cores of 4.2 cm diameter and 160 cm long were sampled and subsequently sliced horizontally in 5 cm intervals to determine the *RLD* of each sampling volume (69.72 cm<sup>3</sup>). Thus, core root sampling data are written to a text file which consists of 15\*8\*32 values of root length densities (see below) as the output of the forward model. Figure 3.1(B) indicates the *RLD*’s of 15 cores separately (black-dashed lines) and the mean *RLD* of those 15 cores (solid green line), while Figure 3.1(C) shows the mean of 32 repetitions (solid blue line) of mean *RLD* of 15 core samples to understand the stochastic nature of sampling data of simulated root systems.

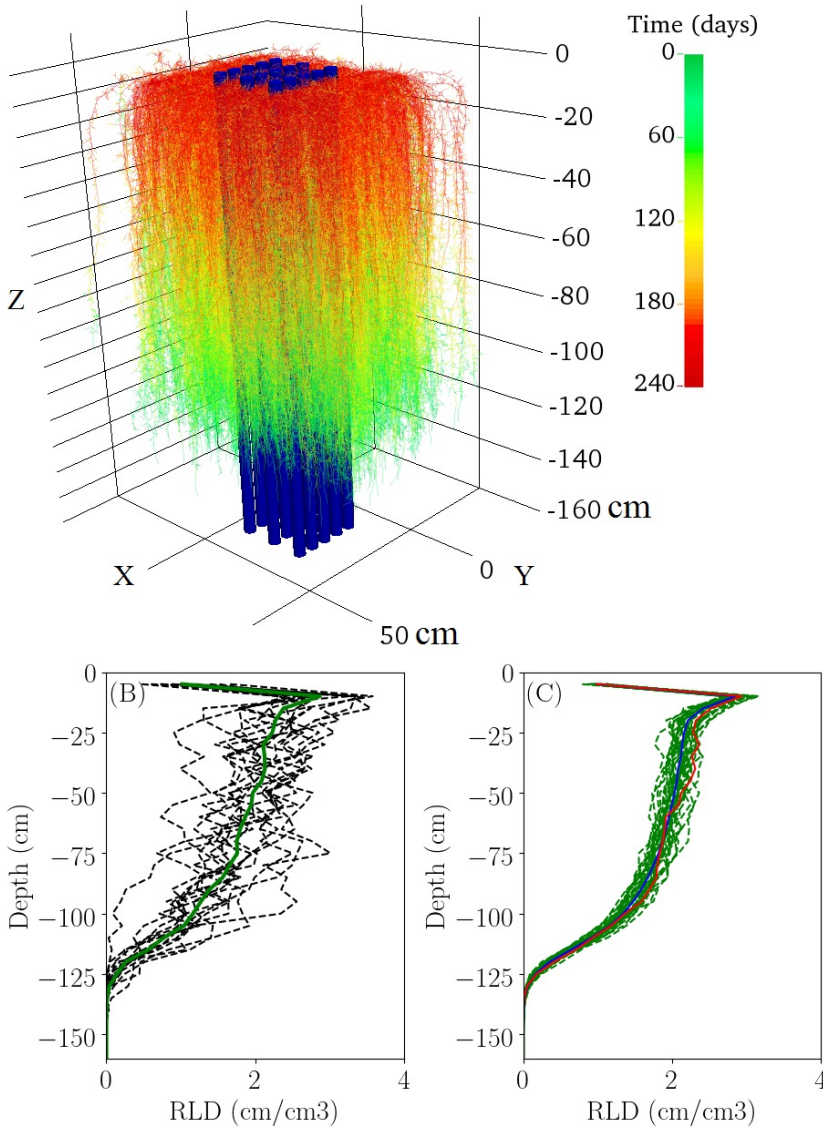


**Figure 3.1:** Top(A): Simulated winter wheat root systems in a virtual field plot until 240 days after sowing (color scale indicates the appearance time of the root segments and the vertical transparent cylinders represent the soil cores). Bottom: RLD profiles of simulated core sampling data. Black dashed lines show the RLD of each core sample separately and the green line shows the mean RLD of 15 core samples (B), the blue line in (C) indicates the mean of 32 sets of 15 soil cores and the red line indicates the average of 15 cores that was chosen and used as measured data for inverse estimation of RSA parameters (C).

Root length density of 5 cm segments of 160 cm long core samples were taken at monthly time intervals up to 8 months (8-time step information for 32, 5 cm depth intervals). We sampled 15 cores from the plot and calculated the mean and standard deviations of those 15 core samples. Therefore,  $RLD$  root sampling data consists of 256 mean root length density values  $M_{RLD}$  ( $cm\ cm^{-3}$ ) Eq.(3.1).

$$M_{RLD_{i,j}} = \frac{1}{n} \sum_{k=1}^n RLD_{i,j,k} \quad (3.1)$$

where  $n$  is the number of samples per depth (15),  $i$  is sampling depth index,  $j$  the sampling time index, and  $k$  is the sampling number index.  $RLD_{i,j,k}$  is a 3d matrix, which stores root length density ( $RLD$ ) values obtained from 32 depth intervals ( $i$ ), and 8 monthly intervals ( $j$ ) in 15 core samples ( $k$ ),  $n=15$  (number of cores taken from the plot). Since the variability of the root length densities between the 15 soil samples that were collected at a certain depth and time also contains information about the root system architecture, we also calculated standard deviation values for each of the 256 time and depth observations  $S_{RLD}$  ( $cm\ cm^{-3}$ ) Eq.(3.2).

$$S_{RLD_{i,j}} = \sqrt{\frac{\sum_{k=1}^n (RLD_{i,j,k} - M_{RLD_{i,j}})^2}{n}} \quad (3.2)$$

### 3.2.2 Selection of the most sensitive parameters of root system architecture and their prior distribution

We conducted a detailed analysis of sensitivities of 37 root architecture parameters in a previous study and found that the parameters of zeroth-order roots have higher sensitivities on root length densities obtained from soil cores (Morandage et al., 2019). Therefore, we selected numbers ( $NB$ ), internodal distance ( $ln0$  &  $ln0s$ ) maximum length ( $maxl0$  &  $maxl0s$ ) elongation rate ( $r0$  &  $r0s$ ), tropism strength ( $tr0$  &  $tr0s$ ), insertion angle ( $theta0$  &  $theta0s$ ) of zero-order roots and internodal distance ( $ln1$  &  $ln1s$ ), maximum length ( $maxl1$  &  $maxl1s$ ) first-order laterals, and length of apical zone ( $la2$  &  $la2s$ ) of second-order laterals as inferred parameters. All these parameters (except  $NB$ ) are stochastic in the model and parameter names ending with  $s$  refer to the standard deviation of the parameter. The stochastic parameter distribution was assumed to be a Gaussian distribution. Since the literature data does not provide a proper estimation for desired limits and distribution of

the field derived RSA parameters, we defined the 50% and 150% of true parameter values as the upper and lower bounds of the 17 inferred parameters and assumed that the priors are uniformly distributed within these limits. The list of all RSA parameters of winter wheat and their bounds used in this study are listed in Table 3.1.

**Table 3.1:** List of root architectural parameters of wheat used in root system simulations and the prior range of inferred parameters. Except for the number of zero-order roots *NB*, each parameter is a stochastic parameter with a mean and a standard deviation (values inside the brackets indicate the standard deviations of the parameters). Numbers in the parameter names refer to the root orders. Underlined values are the parameters used for inference and the others are fixed to true parameter values.

No	Code	Root order	Parameter name	Unit	Parameter values	Prior range
1	lb0 (std)	0	length of basal zone	cm	0.8 (1.2)	
2	la0 (std)	0	length of apical zone	cm	4.2 (6.4)	
3	ln0 (std)	0	branch spacing	cm	<u>1.2</u> (0.5)	0.6-1.8 (0.3-0.9)
4	maxl0 (std)	0	maximum length	cm	<u>130</u> (30)	65-195 (15-45)
5	r0 (std)	0	initial growth rate	cm day <sup>-1</sup>	<u>1.2</u> (0.6)	0.6-1.8 (0.3-0.9)
6	tr0 (std)	0	tropism		<u>1.2</u> (0.2)	0.6-1.8 (0.1-0.3)
7	theta0 (std)	0	branching angle	rad	<u>1.4</u> (0.2)	0.7-2.1 (0.1-0.3)
8	lb1 (std)	1	length of basal zone	cm	0.8 (1.0)	
9	la1 (std)	1	length of apical zone	cm	1.8 (2.4)	
10	ln1 (std)	1	branch spacing	cm	<u>1.0</u> (1.5)	0.55-1.65 (0.75-2.25)
11	maxl1 (std)	1	maximum length	cm	<u>2.0</u> (1.0)	1.0-3.0 (0.5-1.5)
12	r1 (std)	1	initial growth rate	cm day <sup>-1</sup>	0.4 (0.12)	
13	tr1 (std)	1	tropism		1.0 (0.4)	
14	theta1 (std)	1	branching angle	rad	1.2 (0.4)	
15	la2 (std)	2	length of apical zone	cm	<u>2.2</u> (0.4)	1.1-3.3 (0.2-0.6)
16	r3 (std)	2	initial growth rate	cm day <sup>-1</sup>	1.0 (0.2)	
17	tr2 (std)	2	tropism		0.1 (0.6)	
18	theta2 (std)	2	branching angle	rad	1.12 (0.4)	
19	NB	0	number of zero order roots	nos	<u>20</u>	10-30

### 3.2.3 Selection of the synthetic measurements

To create the used synthetic measurements, we ran the CRootBox model once using the reference or “true” parameters presented in Table 3.1. Since the CRootBox model is stochastic (see section 3.2.1), this creates just one realization of 256  $M_{RLD}$  and 256  $S_{RLD}$  values (see Eq.(3.1), and Eq.(3.2)) associated with the true parameters. However, such a single synthetic dataset would represent repeated root sampling data of the same plants and at the same locations. Since core sampling is a destructive method, in real field experiments cores taken at different times come from different locations and sample roots of different plants. Therefore, the synthetic dataset was constructed from 8 realizations that were each sampled at a different time. To derive the corresponding  $256 + 256 = 512$  standard deviations of the data errors,  $\sigma_i$ , that are required by our likelihood function Eq.(3.6), we generated 100 additional forward realizations using the true model parameters and computed the standard deviation of each of the  $i=1, \dots, 512$  simulated data points ( $i=1, \dots, 256$ :  $M_{RLD}$ ;  $i=257, \dots, 512$ :  $S_{RLD}$ ) across these 100 realizations.

### 3.2.4 Bayesian approach

In general, the output of a model  $F(\mathbf{x})$ , where  $\mathbf{x} = (x_1, x_2, \dots, x_d)$  is a  $d$ - dimensional parameter vector, is compared with observations  $\mathbf{y}$  to estimate the model parameters:

$$\mathbf{y} = F(\mathbf{x}) + \mathbf{e} \tag{3.3}$$

where  $\mathbf{e}$  is an error term that lumps measurement and model errors. When the process that is observed and the model that is used to describe the process is stochastic, i.e., when there is an unknown variability in the system that leads to different responses under the same external conditions, then  $\mathbf{e}$  also comprises this stochasticity. Often, the parameters of the model are not known and are estimated by searching for the parameter values that minimize the norm of  $\mathbf{e}$ . When using the Bayesian framework to acknowledge parameter uncertainty, the goal is to derive the posterior probability density function (pdf) of the model parameters of interest,  $\mathbf{x}$ , given the observations,  $\mathbf{y}$ , as expressed by Eq.(3.4)

$$p(\mathbf{x}|\mathbf{y}) = \frac{p(\mathbf{y}|\mathbf{x})p(\mathbf{x})}{p(\mathbf{y})} \tag{3.4}$$

where  $p(\mathbf{x}|\mathbf{y})$  is the posterior pdf of  $\mathbf{x}$  given  $\mathbf{y}$ ,  $p(\mathbf{y}|\mathbf{x}) \equiv L(\mathbf{x}|\mathbf{y})$  denotes the likelihood function of  $\mathbf{x}$ ,  $p(\mathbf{x})$  is the prior pdf of  $\mathbf{x}$ , the normalization factor  $p(\mathbf{y}) = \int p(\mathbf{y}|\mathbf{x})p(\mathbf{x})d\mathbf{x}$  is obtained from numerical integration over the parameter space so that  $p(\mathbf{x}|\mathbf{y})$  scales to unity. The quantity  $p(\mathbf{y})$  is generally difficult to estimate in practice but is not required for parameter inference. In the remainder of this study, we will focus on the unnormalized posterior:

$$p(\mathbf{x} | \mathbf{y}) \propto L(\mathbf{x} | \mathbf{y}) p(\mathbf{x}) \quad (3.5)$$

Moreover, in case of a uniform prior, Eq.(3.5) simplifies to  $p(\mathbf{x}|\mathbf{y}) \propto L(\mathbf{x}|\mathbf{y})$ . For numerical stability, it is often preferable to work with the log-likelihood function,  $\ell(\mathbf{x}|\mathbf{y})$ , instead of  $L(\mathbf{x}|\mathbf{y})$ . If we assume the error  $\mathbf{e}$  to be normally distributed, uncorrelated and heteroscedastic, the log-likelihood function can be written as

$$\ell(\mathbf{x}|\mathbf{y}) = -\frac{n}{2} \log(2\pi) - \sum_{i=1}^n \log(\sigma_i) - \frac{1}{2} \sum_{i=1}^n \frac{[y_i - F_i(\mathbf{x})]^2}{\sigma_i^2} \quad (3.6)$$

where  $n$  is the number of measurement data and the  $\sigma_i$  are the standard deviations of the residual errors  $e_i$ . Note that in our context, the subscript  $i$  refers to a combination of time and depth.

### 3.2.5 Markov chain Monte Carlo sampling

The aim of the inference is to estimate the posterior distribution of the model parameters,  $\mathbf{x}$ , given the available measurements  $\mathbf{y}$ :  $p(\mathbf{x}|\mathbf{y})$ . As an exact analytical solution of  $p(\mathbf{x}|\mathbf{y})$  is not available, we resort to Markov chain Monte Carlo (MCMC) simulation to generate samples from this distribution. The basis of this technique is a Markov chain that generates a random walk through the search space and iteratively finds parameter sets with stable frequencies stemming from the posterior pdf of the model parameters (see, e.g., (Robert and Casella, 2013) for a comprehensive overview of MCMC simulation). The MCMC sampling efficiency largely depends on the proposal distribution used to generate candidate solutions in the Markov chain. In this study, the state-of-the-art DREAM<sub>(ZS)</sub> (Laloy and Vrugt, 2012; ter Braak and Vrugt, 2008; Vrugt, 2016) algorithm is used to retrieve posterior samples. The DREAM<sub>(ZS)</sub> scheme evolves different interacting Markov chains in parallel. A detailed description of this sampling scheme, including convergence proof, can be found in the cited

literature and is thus not reproduced here.

The convergence of the MCMC sampling to the posterior distribution can be monitored by means of the potential scale reduction factor of Gelman and Rubin (Gelman and Rubin, 1992),  $\hat{R}$ . This requires using multiple Markov chains and is thus well suited for the multi-chain DREAM<sub>(ZS)</sub> sampler. For each sampled parameter, the Gelman and Rubin (Gelman and Rubin, 1992) approach compares the average within chain variance to the variance of all the chains mixed together. The smaller the difference between these two variances, the closer to 1 is the value of the  $\hat{R}$  statistic. A value of  $\hat{R}$  smaller than 1.2 for every parameter of interest is commonly considered as indicating official convergence of the sampling to a stationary distribution. In this work,  $\hat{R}$  is calculated regularly throughout sampling, using the last 50% of the sampled parameter sets. The mean acceptance rate (AR (%)) of the proposed transitions in the Markov chains is an important sampling property and is thus also reported. A too small fraction of accepted moves points out poor mixing of the chains due to a too wide proposal distribution. In contrast, an overly large acceptance rate suggests a too narrow proposal distribution, causing the Markov chains to remain in the close vicinity of their current locations. The optimal AR value depends on the proposal and target posterior distributions, but a range of 10–40% generally indicates good performance of DREAM<sub>(ZS)</sub>.

### 3.2.6 Dealing with model stochasticity and non-independent data errors

To represent the random nature of the root distribution in real field conditions, root architecture models internally draw realizations of some of their parameters from prescribed probability distributions (Tron et al., 2015). In other words, many of the parameters that are internally used in a given forward simulation by the model are randomly drawn from prespecified probability distributions. The parameters of these distributions (e.g., mean and standard deviation in case of a Gaussian distribution) are the actual RSA parameters and are to be set by the model user. Consequently, repeatedly using the same set of RSA parameter values leads to an ensemble of different outputs (such as  $R_{LD}$  in soil core samples). With increasing size of the output (i.e., with an increasing number of soil cores that are taken), the variability of the ensemble in terms of  $M_{RLD}$  and  $S_{RLD}$  (see Eq.(3.1) and Eq.(3.2)) will asymptotically converge to zero.

When using MCMC for Bayesian inference, the forward model is typically considered as

deterministic and a given input parameter set thus always has the same log-likelihood. Hence, DREAM<sub>(ZS)</sub> requires the log-likelihood of a given parameter set not to vary. To deal with forward model stochasticity, we therefore averaged the simulated data corresponding to a given input parameter set over a certain number of realizations, before computing the log-likelihood. Using the true model parameters, we studied how many realizations, i.e. sets of 15 soil cores, are needed to obtain a relatively stable log-likelihood estimate (red curve in Figure 3.2). It is observed that from 150 realizations or repetitions of 15 soil cores, the log-likelihood of the true parameters given the used measurements becomes approximately stable (red curve in Figure 3.2).

Nevertheless, a short preliminary MCMC trial using 150 simulated data realizations to calculate the log-likelihood led to a substantial overfitting of the measurement data, with the MCMC returning only log-likelihood values in the approximate 1030 - 1040 range after some 3000 iterations whereas the true parameter set has a log-likelihood of about 950 (red curve in Figure 3.2). We hypothesize that this overfitting is mainly due to unknown data error dependencies (correlations and higher-order dependencies) that are not accounted for by our classical uncorrelated Gaussian log-likelihood formulation that assumes independent data errors Eq.(3.6). A way to solve this overfitting problem is to inflate the used log-likelihood function by multiplying the standard deviations of the data errors by a constant factor. We did so herein and obtained the value of this inflation factor as follows. We computed 2 distributions of log-likelihoods, distributions I and II, always using the true parameter set and our classical uncorrelated Gaussian log-likelihood formulation:

- i) Distribution I is the distribution of 200 log-likelihoods that are calculated from 200 white noise realizations used to corrupt the mean log-likelihood (over 150 simulated data realizations). The white noise distribution has a diagonal covariance matrix that contains the 512 variances of the data errors computed in section 3.2.1(for this calculation, the error term,  $[y_i - F_i(\mathbf{x})]$  thus was randomly drawn from the assumed measurement error distribution). This distribution of log-likelihoods thus corresponds to the distribution that would be expected if the data errors were truly independent
- ii) Distribution II is the distribution of 200 log-likelihoods using each time a different realization as “observations” and the ensemble mean over 150 simulated realizations as the forward model simulation. This distribution of log-likelihoods thus somehow encodes the effect of dependencies between the data errors. In addition, this distribution is “wider”, i.e., has a larger 95% uncertainty interval, interquartile range (IQR).

Based on the comparison between distributions I and II (see Figure 3.3), one can estimate what the effect of the unknown data error dependencies on our classical uncorrelated Gaussian log-likelihood function is. More specifically, it is seen that for distribution I to have the same IQR as distribution II, the standard deviations of the data errors used to derive distribution I need to be multiplied by a value of 2. Therefore, in the remainder of this study, we inflated the log-likelihood function by multiplying the standard deviations of the data errors by 2.

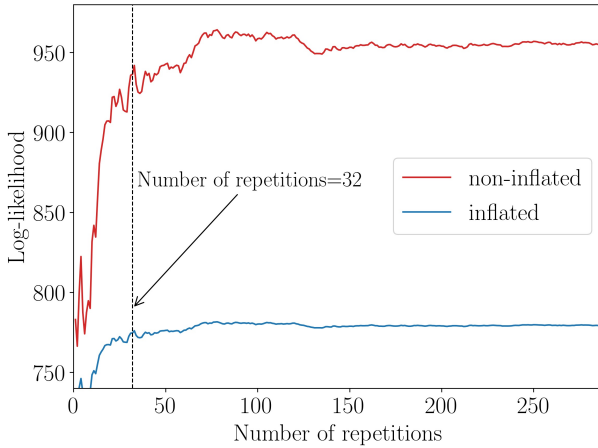


**Figure 3.2:** Evolution of the log-likelihood as a function of the number of repetitions, i.e. sets of 15 soil cores, used to average the simulated data before calculating the log-likelihood. The red line indicates changes in the classical log-likelihood while the blue line denotes changes in the inflated log-likelihood.

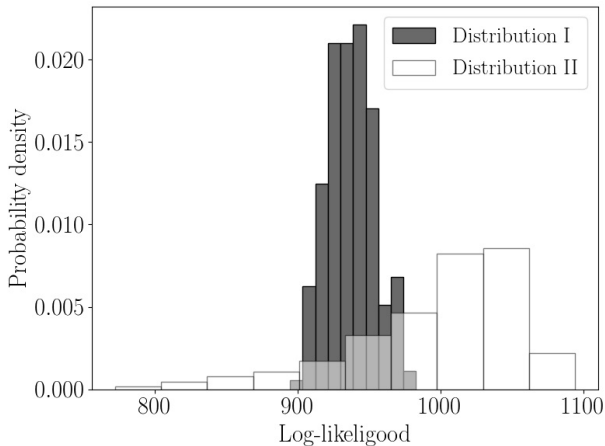


**Figure 3.3:** Distributions I and II used to compute the used inflation factor (see main text for details).

The inflation strategy described above was found to prevent overfitting, but the required averaging of the simulated data over 150 realizations makes it unfortunately too computationally-demanding for the MCMC to converge within a reasonable amount of time, given our available computational resources. In our case, each forward model run takes about 1-12 minutes, depending on the parameter combinations. When using DREAM<sub>(ZS)</sub> with the required minimum of 3 interacting Markov chains together with parallelizing the 150 realizations per proposed parameter set over 32 CPUs, it still incurs a computational cost of about 9-10 days to perform 500 MCMC iterations (that is, to achieve 167 transitions in each of the used 3 Markov chains). To make the MCMC sampling affordable given our available 32 CPUs, we therefore decided to perform 32 realizations only. Averaging the simulated data over 32 realizations instead of 150 makes that the loglikelihood remains stochastic to some extent. To deal with this remaining stochasticity, we proceeded as follows.

The likelihood of a certain parameter set  $\mathbf{x}$  for a given dataset  $\mathbf{y}$  is calculated from Eq.(3.6), where  $F(\mathbf{x})$  is the prediction by the model of the data. The problem now is that  $F(\mathbf{x})$  is stochastic and should be written as  $F(\mathbf{x},\boldsymbol{\varepsilon})$  where  $\boldsymbol{\varepsilon}$  represents a set of random numbers that varies from realization to realization. We can write  $F(\mathbf{x},\boldsymbol{\varepsilon}) = \langle F(\mathbf{x}) \rangle + \delta$  where  $\langle \cdot \rangle$  represents the expected value of  $F(\mathbf{x},\boldsymbol{\varepsilon})$  and  $\delta$  is the deviation from the expected value for a certain set  $\boldsymbol{\varepsilon}$ . If we take several sets of  $\boldsymbol{\varepsilon}$  (several repetitions) or if we take one large set of  $\boldsymbol{\varepsilon}$ , then  $F(\mathbf{x},\boldsymbol{\varepsilon})$  converges to  $\langle F(\mathbf{x}) \rangle$  and  $\delta$  to 0. The problem is that this may require a large number simulations and  $\|\delta\|$  will for a finite set of  $\boldsymbol{\varepsilon}$  always be larger than 0. As

a consequence,  $\ell(\mathbf{x}|\mathbf{y})$  will vary for the same parameter set from realization to realization because of variations in  $\boldsymbol{\varepsilon}$ . We can define a likelihood of a certain parameter set  $\mathbf{x}$  and a certain realization  $\boldsymbol{\varepsilon}$  of random numbers that represent the random nature or stochasticity of the root growth for a certain observation dataset as  $\ell(\mathbf{x}, \boldsymbol{\varepsilon}|\mathbf{y})$ .

In order to investigate the variation of the likelihood of a certain parameter set for a certain observation dataset that is obtained from a limited set of simulations, the likelihood of the ‘true’ parameter set was evaluated for 20 observation datasets and 15 sets of stochastic forward simulations of 32 realizations. This was done for 9 different ‘true’ parameter sets. This means that for each considered parameter set,  $\ell(\mathbf{x}, \boldsymbol{\varepsilon}|\mathbf{y})$  was evaluated for 15 different  $\boldsymbol{\varepsilon}$  vectors and 20  $\mathbf{y}$  observation vectors. From this data set of 300  $\ell(\mathbf{x}, \boldsymbol{\varepsilon}|\mathbf{y})$  values we calculated the overall mean, the mean standard deviation of the  $\ell(\mathbf{x}, \boldsymbol{\varepsilon}|\mathbf{y})$  values that were obtained for a given  $\mathbf{y}$  but for different  $\boldsymbol{\varepsilon}$ ,  $\text{stdev}\ell_{\boldsymbol{\varepsilon}}$ , and the standard deviation of  $\ell(\mathbf{x}, \boldsymbol{\varepsilon}|\mathbf{y})$  values that were averaged over  $\boldsymbol{\varepsilon}$ ,  $\text{stdev}\ell_{\mathbf{y}}$ . The  $\text{stdev}\ell_{\mathbf{y}}$  quantity thus reflects the impact of the differences between different observation datasets on  $\ell$  due to the noise on the experimental data (which in turn is caused by the random nature of the root growth process). In contrast,  $\text{stdev}\ell_{\boldsymbol{\varepsilon}}$  represents the impact on  $\ell$  of the stochastic noise associated with the simulation results due to the finite number of samples that are simulated. In Table 3.2, mean  $\ell$ ,  $\text{stdev}\ell_{\mathbf{y}}$ , and  $\text{stdev}\ell_{\boldsymbol{\varepsilon}}$  are shown for 9 parameter sets  $\mathbf{x}$ . (The parameters were chosen for simulations by systematically increasing the values from the lower bounds to the upper bounds, and P1 indicates the lowest, while the P9 indicates the highest values of the inferred parameters).

**Table 3.2:** Mean of log-likelihoods  $\ell$  of the true parameter set that are obtained from a combination of 20 different observations and 15 sets of forward simulations (each consisting of 15 realizations), standard deviation of the loglikelihoods due to observation dataset noise  $stdev\ell_{\mathbf{y}}$ , and due to stochastic simulation noise  $stdev\ell_{\boldsymbol{\varepsilon}}$  for 9 different parameter sets. See the main text for the calculation details of  $stdev\ell_{\mathbf{y}}$  and  $stdev\ell_{\boldsymbol{\varepsilon}}$ .

	Mean $\ell$	$stdev\ell_{\mathbf{y}}$	$stdev\ell_{\boldsymbol{\varepsilon}}$
<b>P1</b>	1211	6.8	2.2
<b>P2</b>	1128	8.6	2.6
<b>P3</b>	1046	8.7	2.7
<b>P4</b>	953	10.3	2.4
<b>P5</b>	780	13.2	3.8
<b>P6</b>	615	19.7	3.7
<b>P7</b>	526	16.1	3.5
<b>P8</b>	468	24.7	4.6
<b>P9</b>	429	20.1	6.5

Since the total number of RLD samples that is simulated for each log-likelihood evaluation is 32 times larger than the number of RLD samples in an observation dataset,  $stdev\ell_{\boldsymbol{\varepsilon}}$  is smaller than  $stdev\ell_{\mathbf{y}}$ . Table 3.2 also shows that the noise of the simulation results depends on the parameters. The parameter sets with a smaller loglikelihood have a larger standard deviation of the root growth parameters, which leads to more stochasticity and therefore to a larger variation in the loglikelihood.

Since the loglikelihood for a given observation dataset does not depend only on the parameter set but also on the set of random numbers,  $\boldsymbol{\varepsilon}$ , the parameter set  $\mathbf{x}$  and random number set  $\boldsymbol{\varepsilon}$  that jointly lead to the best match between the simulation results and observations will be selected by the MCMC. As sampling in the MCMC goes on and the algorithm always finds higher  $\ell(\mathbf{x}, \boldsymbol{\varepsilon}|\mathbf{y})$  for the same  $\mathbf{x}$  due to the forward model changing  $\boldsymbol{\varepsilon}$ , the chance of finding higher  $\ell(\mathbf{x}, \boldsymbol{\varepsilon}|\mathbf{y})$  values decreases and it becomes increasingly more difficult for the MCMC to find likelihoods that are higher (or equally high) for the same  $\mathbf{x}$  or for a parameter set that is close to  $\mathbf{x}$ . This will cause the MCMC to get ‘stuck’ around a certain  $\mathbf{x}$ .

To avoid this problem we propose to change the Metropolis acceptance rule of candidate parameter sets. The underlying idea is that a proposed parameter set,  $\mathbf{x}_2$ , should be accepted when its likelihood is not significantly smaller than the likelihood of the current state,  $\mathbf{x}_1$ . This can be tested by null hypothesis significance testing (NHST) if we have an

estimate of the variance of  $\ell(\mathbf{x}, \boldsymbol{\varepsilon}|\mathbf{y})$  due to variations in  $\boldsymbol{\varepsilon}$ . The hypotheses to be tested are:

$$H_0 : \ell(\mathbf{x}_2, \boldsymbol{\varepsilon}_2|\mathbf{y}) \geq \ell(\mathbf{x}_1, \boldsymbol{\varepsilon}_1|\mathbf{y})$$

$$H_1 : \ell(\mathbf{x}_2, \boldsymbol{\varepsilon}_2|\mathbf{y}) < \ell(\mathbf{x}_1, \boldsymbol{\varepsilon}_1|\mathbf{y})$$

If we assume that  $\ell(\mathbf{x}, \boldsymbol{\varepsilon}|\mathbf{y})$  is normally distributed with mean  $\mu = \ell(\mathbf{x}|\mathbf{y})$  and standard deviation  $\varepsilon = \text{stdev} \ell_{\cdot \boldsymbol{\varepsilon}}$ , then  $\ell(\mathbf{x}_2, \boldsymbol{\varepsilon}_2|\mathbf{y}) - \ell(\mathbf{x}_1, \boldsymbol{\varepsilon}_1|\mathbf{y})$  is normally distributed with mean  $\ell(\mathbf{x}_2|\mathbf{y}) - \ell(\mathbf{x}_1|\mathbf{y})$  and standard deviation  $\sqrt{2} \sigma$ . Considering testing at the 95% confidence level (that is, in 5% of the cases when we should accept  $\mathbf{x}_2$ , we reject it) then we should accept  $\mathbf{x}_2$  when:

$$\ell(\mathbf{x}_2, \boldsymbol{\varepsilon}_2|\mathbf{y}) - \ell(\mathbf{x}_1, \boldsymbol{\varepsilon}_1|\mathbf{y}) > -1.69 \sqrt{2} \sigma$$

whereas in classical MCMC (using a symmetric proposal distribution and a uniform prior distribution) the acceptance rule is

$$\ell(\mathbf{x}_2, \boldsymbol{\varepsilon}_2|\mathbf{y}) - \ell(\mathbf{x}_1, \boldsymbol{\varepsilon}_1|\mathbf{y}) > 0$$

According to our proposed approach, every proposal  $\mathbf{x}_2$  should thus be accepted with the following probability:

$$P = \exp(\ell(\mathbf{x}_2, \boldsymbol{\varepsilon}_2|\mathbf{y}) - \ell(\mathbf{x}_1, \boldsymbol{\varepsilon}_1|\mathbf{y}) + 1.69 \sqrt{2} \sigma) \quad (3.7)$$

Based on the analyses reported in Table 3.2, we suggest to set  $\sigma = 4$ .

## 3.3 Results

### 3.3.1 MCMC sampling and convergence

We ran our Python version of DREAM<sub>(ZS)</sub> (Laloy et al., 2017) in parallel over 32 CPUs for a total of 15,000 iterations (log-likelihood evaluations). The  $\hat{R}$ -convergence was satisfied for every parameter from iteration 5880 on and we thus discarded the first 2940 samples as burn-in. Figure 3.4 presents the evolution of the acceptance rate and variation of log-likelihoods throughout sampling. The final mean acceptance rate is about 30%. The loglikelihood varies from 750 to 800 since the sampling algorithm accepts the proposals that are slightly smaller than the current proposal when it propagates. Therefore, it clearly

indicates that our approach prevents the overfitting problem. Moreover, the distribution of likelihoods after burn-in points to the mean value of 774 with a standard deviation of 13.

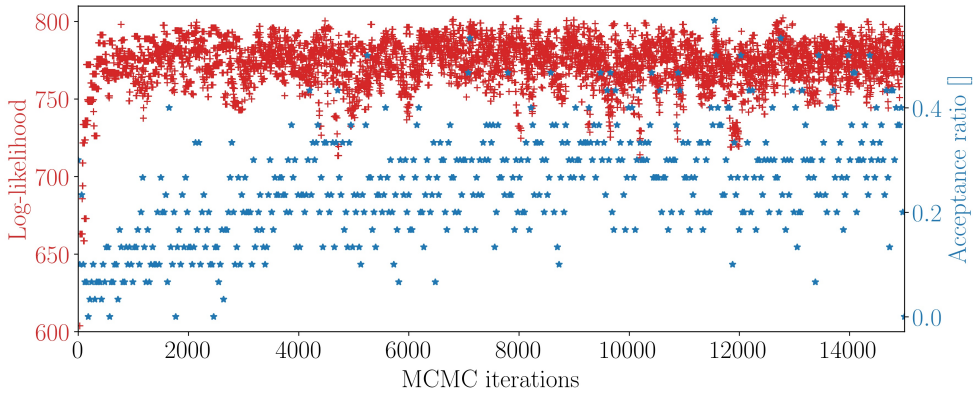


**Figure 3.4:** The trajectory of Log-likelihood and the MCMC acceptance rate throughout the sampling.

The  $NB$  parameter in the CRootBox model is considered as a plant parameter that determines how many primary roots emerge from the seed or next to the seed. This parameter is crucial in determining the total root length density of the sampling data. The tracer plot in Figure 3.5(a) shows that The three chains equilibrated around the true  $NB$  value after some 2000 iterations. The posterior uncertainty associated with  $NB$  is however relatively large (Figure 3.5(b)).

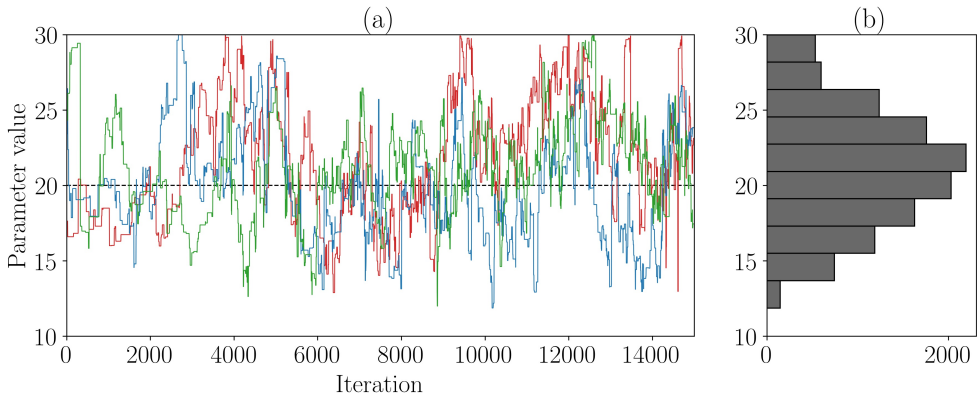


**Figure 3.5:** Left: Sampling trajectory of the  $NB$  parameter in each of the 3 Markov chains. Each chain is coded with a different color (green, blue, red) and the true value is denoted by the horizontal black dashed line. Right: Corresponding marginal posterior density plot computed after discarding the first 2940 samples as burn-in.

Figure 3.6 shows the evolution of three Markov chains for the 16 remaining parameters (each chain coded with a different color). The black horizontal lines show the true parameter values. It is noticeable that the sampled  $maxl0$  parameter values stabilize within the first 200 iterations and narrowly fluctuate around the true value. In addition, the sampled  $r0$ ,  $theta0$ ,  $ln0$ , and  $r0s$  values also converge to their true counterparts, but with larger fluctuations. The other sampled parameters show higher posterior variations, especially the higher-order root parameters.

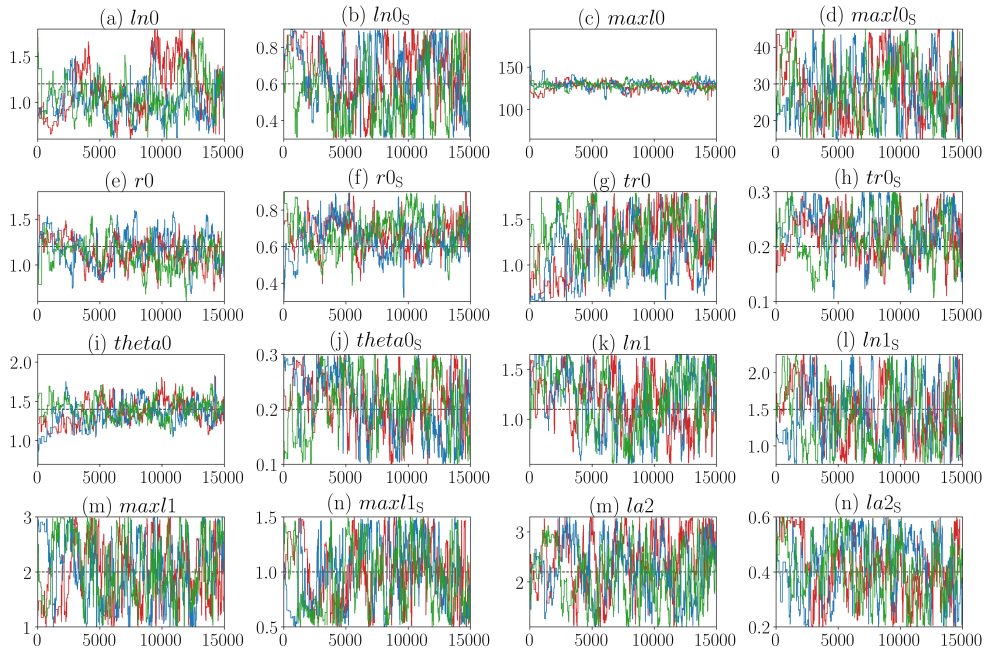


**Figure 3.6:** Tracer plots of MCMC sampling trajectories of the three parallel Markov chains. Each chain is coded by one different color. The dashed black lines show the true parameter values, and the y-axis indicates the lower and upper bounds of the uniform prior parameter distributions.

Figure 3.7 shows the marginal posterior probability distribution and maximum a posterior (MAP) value of each inferred parameter. The blue markers represent true values. The probability distributions of the  $maxl0$ ,  $r0$ ,  $r0s$ ,  $ln0$ , and  $theta0$  parameters are normally distributed and approximately centered around the corresponding true values. Unlike the other zero-order parameters,  $ln0s$ ,  $maxl0s$ ,  $tr0$ , and  $tr0s$  parameters are not resolved and display a wide posterior uncertainty. This is also the case for the higher-order parameters. Given that the number of collected posterior samples (12,060) is relatively small for such

a 17-dimensional search space, it is difficult to draw conclusions about the shape of the distributions for the parameters that are not well resolved.

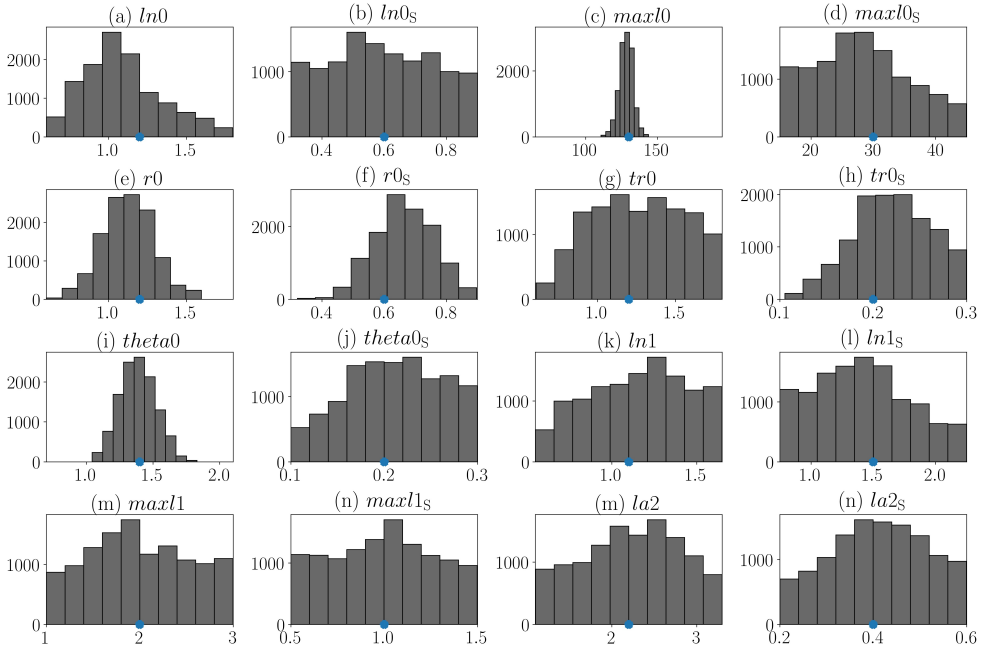


**Figure 3.7:** Marginal posterior probability density functions of sixteen parameters. The horizontal x-axes indicates the prior range of parameter values, and the y-axes present the probability. Blue marker represents the true parameter value.

### 3.3.2 Parameter correlations

A principal component analysis of parameter sensitivities was conducted before the Bayesian inference to have insights of parameter combinations that interact and could produce problematic inversion results. According to that previous study (Morandage et al., 2019), the first two principal components explained 92.5 % of the total variability in the sensitivity of the soil coring data obtained at the end of the growth period (Figure 3.8). The scatter plots in Figure 3.9 highlight some important parameter correlations, and please refer to Figure B.1 for a detailed description of parameter correlations. The posterior correlations observed between the parameters (Figure 3.9) are in agreement with the PCA analysis of sensitivities, especially with the first and second principal components. The parameters that came out of the PCA to have high loading correspond with the parameters

that were best resolved by the inversion ( $NB$ ,  $maxl0$ ,  $theta0$ ). Since measured data from different time intervals are used in the inversion while the performed PCA relied on the last observation time, the  $r0$  parameter, which did not have a higher influence in the PCA could also be inversely estimated with relatively high accuracy.

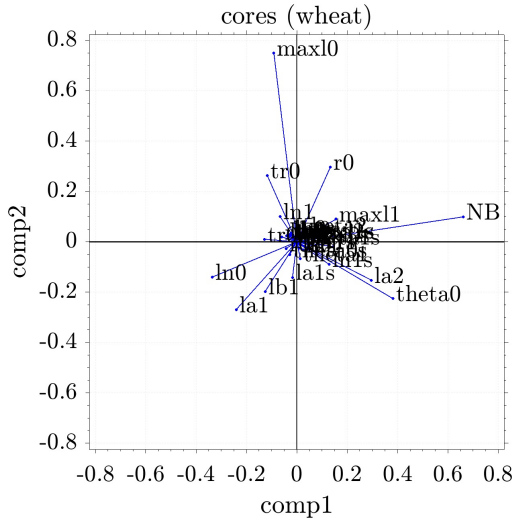


**Figure 3.8:** Biplot of principal component analysis of parameter loadings for the 1st and 2nd PCs of soil coring data (modified after (Morandage et al., 2019)).

The  $ln0$  parameter is related to the internodal distances of first-order roots on the the zero-order roots and thus controls how many lateral roots (first-order laterals) emerge from the zero-order roots. An increasing number of zero-order roots ( $NB$ ) and decreasing internodal distance ( $ln0$ ) both increase the root density. This implies that an increase in  $NB$  can be compensated by an increase in  $ln0$  (Figure 3.9-A), which is reflected in a higher positive correlation of the parameter estimates of  $NB$  and  $ln0$  as was also indicated by the PCA analysis (Figure 3.8).

The insertion angles of zero-order roots,  $theta0$  indicate the angle between the starting point of the root trajectory and vertical (towards the gravity) direction. Wider insertion angles lead to a broader spreading of the root system, while narrow angles tend to reduce the lateral spreading of roots. The insertion angle interacts with tropism parameter,  $tr0$  that determines how much the gravitational force influences root trajectory, i.e., higher values of tropism strength apply higher force on root tips to grow towards vertically along with the gravity. The higher gravitational force turns root tips towards the downward

direction and reduces the lateral spreading of the root system. Consequently, the insertion angle ( $\theta$ ) and gravitropism strength ( $tr$ ) of zero-order roots show a relatively high positive linear correlation with  $R = 0.77$  (Figure 3.9-B).

Figure 3.9-C shows a negative correlation between the mean root elongation rate ( $r$ ) and the standard deviation of the elongation rate ( $rs$ ). The negative correlation indicates the effect of the combination of parameter mean and its standard deviations. The well resolved  $maxl$  parameter (Figure 3.7c) determines the rooting depth of the entire root system. As shown in Fig. Figure 3.9-D, E, and F, and Figure B.1, the  $maxl$  parameter is generally not highly correlated with the other parameters and this is in agreement with our former PCA analysis. As discussed previously,  $tr$  and  $maxl$  parameters influence the root distribution deeper in the soil profile. As a consequence of interaction, these two parameters show a moderate negative correlation in both the PCA analysis test and the joint correlation plots (Figure 3.9-D). The  $\theta$  and  $NB$  are also moderately correlated according to PCA analysis (as shown in Figure 3.8), as well as in the posterior correlation (Figure B.1). However, the  $\theta$  and  $maxl$  parameters are not correlated to each other in posterior sampling ( $R=0$ , see and Figure 3.9-E). Furthermore, the parameter pairs,  $r-tr$  ( $R=-0.60$ ), and  $r-NB$  ( $R=-0.55$ ) show higher negative correlations, while  $ln\theta-\theta$  ( $R=0.47$ ) higher positive correlations (Figure B.1).

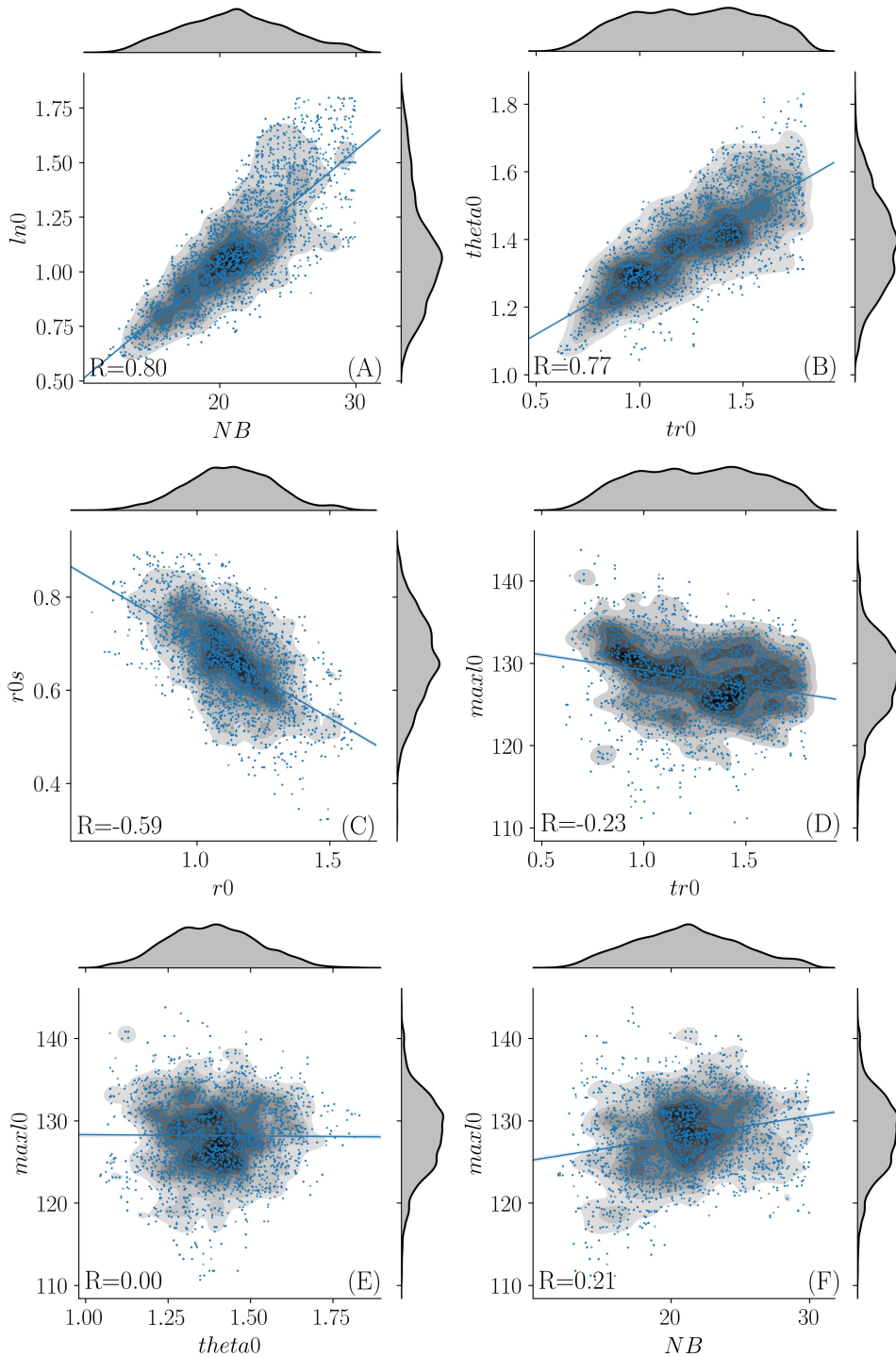


**Figure 3.9:** Scatter plot and corresponding marginal probability distributions and joint distribution of selected pairs of RSA parameters and respective with correlation factors.

### 3.3.3 Validation of inferred RSA parameters

We randomly selected ten sets of parameters from the posterior and the parameter set with the highest log-likelihood ( $\sim 800$  units) and ran the model with those parameters to compare the differences among RLD profiles that were derived from the true parameter set, measurement data, and estimated parameter sets. Figure 3.10 shows the simulated mean RLD profile (solid blue line), standard deviations (blue shaded area) of 32 realizations based on true parameter set, and RLD profiles of the mean (solid black line) and standard deviations (blue shaded area) for estimated parameters from the posterior sampling data. The red line indicates the measurement data used for this study. The posterior samples slightly overestimate the RLD between the depths of -10 cm and -100 cm in the soil profile.

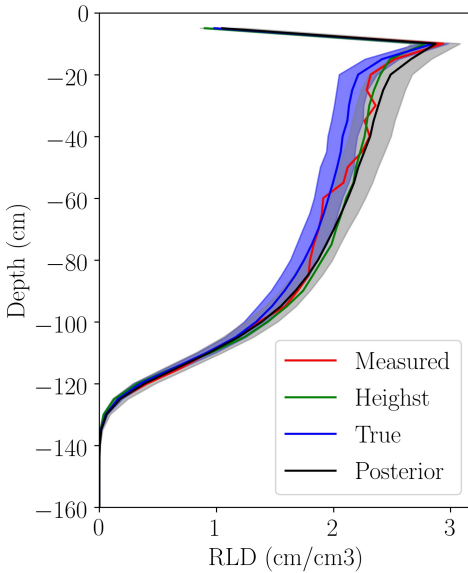


**Figure 3.10:** Root length density profiles that are simulated from the posterior samples (black) and from the true parameter set (blue), and the measurement data (red).

## 3.4 Discussion

In this study, we identified the potential challenges associated with the inference of RSA parameters from field sampling data using inverse modeling.

### 3.4.1 MCMC inversion run time for RSA parameter estimation

The requirement of higher computational demand and computing resources is one of the main drawbacks of the Bayesian approach (van de Schoot et al., 2014). Since the simulation of the root distribution in one virtual field plot requires simulating several root systems, our model took 2 min to 15 minutes in total for one forward model run. Additionally, it requires 32 repetitions to reduce the stochasticity of the model and the inversion algorithm completes only about 500 iterations per day. Thus, the total sampling run time for 15000 iterations is approximately 30 days on 32 computing nodes with 4 x AMD Opteron 6300 (Abu Dhabi) 2.3GHz CPU and 8.00 Gb RAM per each node. Although parallel implementation reduces the inversion time significantly, computing cost is still the limiting factor in the inverse parameter estimation.

### 3.4.2 Fixing problematic and highly correlated parameters from field observations

We highlighted that one of the main obstacles in inference is that the correlation of parameters that lead to difficulties in resolving parameters separately. Therefore, we propose to fix some parameters that can be measured in the field to improve the prediction uncertainty of the inferred parameters. Previous studies and field experiments indicate that the number of zero-order roots can be estimated from field methods by exposing the plant base and therefore used as a fixed parameter in inference improve the accuracy of other parameters because  $NB$  parameter is one of the most sensitive parameters that determine the total root length density of soil core data.

The influence of higher gravitropism strength compensates for the influence of higher insertion angle. Therefore, it is difficult to estimate the parameters independently and fixing one of these parameters would allow to estimate the other. The insertion angle and its variability can be measured directly from exposed root systems (Landl et al., 2018; Wu and Guo, 2014). This indicates that improving field methods to extract information about

parameters is helpful to reduce the uncertainty of the inversely estimated parameters.

### 3.4.3 Possibility of application on real field root sampling data

Our approach was tested on synthetic root sampling data, derived from root architecture parameters and root system simulation model. The main advantage of a synthetic experiment is that the influence of soil environmental conditions is neglected and inversely estimated parameters and true parameters are independent of growth medium. Thus, we assumed that the soil is homogeneous, and the soil moisture, penetration resistance, and other chemical and biological conditions did not vary in the soil. Therefore, in our simulations, RSA of the plant and sampling data are independent of varying soil conditions. However, these assumptions are not valid for root growth in real field conditions. Therefore, root architecture models used in root simulations should account for the effects of spatial and temporal variations in soil conditions and weather influence on root growth. Current root system architecture models are capable of incorporating soil information. However, the models should be tested with experimental field data to implement the functions or influences, which are specific to both plant type and soil conditions. Notably, most commonly used root growth functions, i.e., linear or exponential growth should be adjusted to account for C allocation and shoot-root communications.

## 3.5 Conclusions

In this study, we demonstrated using a synthetic experiment that soil core sampling data may contain enough information to inversely retrieve a few parameters ( $maxl0$ ,  $NB$ ,  $maxl0$ ,  $r0$ ,  $theta0$ ) of zero-order roots of wheat root system architectures based on a RSA model that simulates root growth in a field plot. Although the inferred parameters of the higher-order roots are not appropriately resolved in comparison to the true parameter values and show higher uncertainty, we argue that our proposed approach could be an important step towards retrieving RSA parameters by probabilistic inversion of field root sampling data. This work also provides useful insights about the challenges associated with the inverse estimation of RSA parameters by Markov chain Monte Carlo (MCMC) sampling, such as the long inversion run time and high computational demand, even when using parallel computing resources. Challenges associated with the RSA model stochasticity were addressed by averaging the simulated data associated with each parameter set over multiple

forward simulations. Since performing enough repetitions to get a fully stable likelihood was found intractable given our available computational resources, we adapted the Metropolis acceptance rule that is used to accept proposals in the Markov chain to account for the remaining likelihood stochasticity. Moreover, the observed overfitting problem could be solved by appropriately inflating the error variances in the likelihood. Importantly, we found that the uncertainty of the estimated parameters and correlated parameters cannot be resolved separately and therefore, care must be taken for selecting and fixing correlated parameters. Furthermore, since our simulations do not account for the impact from the growth medium and assume that roots grow in homogenous soil under the optimum conditions, we strongly recommended that this approach should be tested in future studies considering root simulations with site-specific soil and environmental conditions.

## Chapter 4

To which extent can explicit consideration of soil information explain observed differences in root growth? A simulation study.

**Adapted from:** Morandage S, Vanderborght J, Zoerner M, Cai G, Vereecken H, Schnepf A (2019), To Which Extent Can Explicit Consideration of Soil Information Explain Observed Differences in Root Growth? A Simulation Study  
*(manuscript in preparation for publication in Plant and Soil Journal)*

## 4.1 Introduction

Root system architecture models are essential tools to study root growth and functions because these models are capable of simulating root growth of specific crop types based on root architecture parameters and soil information (Dunbabin et al., 2013). Since root systems cannot be observed directly in the field, the detailed root system architecture of a plant and its interaction with the surrounding soil environment is challenging to study without modelling approaches. Therefore, in order to identify parameters that characterize the root system architecture and how it develops as a function of the soil conditions and properties, experimental field sampling data could be combined with model simulations using an inverse modeling framework (Morandage et al., 2019; Garré et al., 2012; Pagés et al., 2012; Ziegler et al., 2019; Vansteenkiste et al., 2014). However, these studies focused on the estimation of RSA parameters without considering the impact of growth medium and environmental factors. Therefore, the explicit consideration of those factors is required for characterizing the alteration of RSAs of field grown crops.

The application of the minirhizotron technique (MR) for minimally invasive observation of root growth and distribution patterns has been used successfully for a few decades (Rewald and Ephrath, 2013). The main advantage of this method is the ability to observe root growth in specific depths and locations of the soil profile during the entire growth period without damaging the soil domain. Nevertheless, this method has its limitations such as lack of conversion methods to volume-based root length densities, the influence of tubes on root growth and underestimation of root distribution within the first few centimeters of the soil profile (Majdi, 1996; Smit et al., 2000).

In order to study the effect of root growth in different types of soils in the same climatic conditions, minirhizotron facilities were established in Selhausen, Germany, where two sites that are 150 m apart from each other are characterized by a strong difference in stone content. The fine soil texture class in both sites is a silty loam. However, the stone contents are 60% and 4%, respectively. In the following, we will use the terms “stony soil” and “silty loam soil” to refer to the soils of these two sites. The differences in stone content could change soil temperature, nutrient content, and soil hydraulic properties (Naseri et al., 2019), which have a direct impact on root distribution and other plant functions. During the last four years of root observations, significant differences in root mass, root depth distribution and maximum rooting depth in two different sites were observed (Cai et al., 2016). The differences between sites are remarkably more significant than the differences between the years (growing periods) and crops. However, these observations and governing

factors cannot be explained without proper representation of the underlying root growth mechanism. Therefore, we examined the properties of soils and climatic conditions and their influence on root distribution with the help of a root architectural model.

Soil strength or soil penetration resistance is one of the most important factors (Kirby and Bengough, 2002), which determines the root's ability to overcome the soil's resistance against root extension. Roots may exhibit different characteristics and alterations in their original morphology, depending on the soil strength and compaction (Correa et al., 2019). It has been found that the elongation rates of roots decrease with increasing soil strength (Bengough et al., 1997, 2006; Houlbrooke et al., 1997; Taylor and Brar, 1991; Tracy et al., 2012), and thus root length density decreases with increasing penetration resistance (Pardo et al., 2000).

Plowing is conducted before sowing in most agricultural fields to loosen the soil and reduce mechanical resistance for root growth within the topsoil layer. This implies that soil compaction has adverse effects on root development (Buttery et al., 1998; Haling et al., 2011). As a consequence to lower rooting depths due to compaction, roots cannot extract water or nutrients from deep soils, and thus limit the plant growth and root water uptake capacity (Masle and Passioura, 1987; Pardo et al., 2000; Tardieu, 1994; Unger and Kaspar, 1994; Valentine et al., 2012), and affect the plant yield (Glab, 2011).

Roots require exerting force on soil particles or aggregates to extend through the soil. Depending on the soil composition, roots tend to change their path, displace obstacles and extend through it or easily penetrate through fine, less resistant materials (Whiteley and Dexter, 1984). During root growth, direction, elongation rate, and branching pattern may vary with the surrounding soil. From the point of view of a root, soil particles can appear as rigid surfaces, obstacles that cannot be replaced by the root tip, solid particles which are movable, or as a homogeneous fine soil (Kolb et al., 2017). Presence of large stones or granules may affect the rooting patterns of the crops because when a root tip meets an obstacle, which cannot be penetrated or pushed away by the root, root tends to change its growth direction by bending away from the obstacle to find another path (Bizet et al., 2016; Fakhri et al., 2017; Popova et al., 2013, 2016). Displacement of solid particles by roots depends on many factors such as soil depth, root diameter, solid diameter, and length of root segment and root type or plant type (Whiteley and Dexter, 1984).

It is found that the ability of roots to grow through soils is a function of root diameter ( $dR$ ) and grain diameter ( $dG$ ). If the aspect ratio ( $S = dR/dG$ ) is very small, root apex cannot displace, deform or penetrate through the obstacle (Kolb et al., 2017). Studies showed

that the length of lateral roots is shortened by adjacent obstacles and changes its path by changing growth direction as roots are sensitive to obstacles, even if obstacles are not in contact with root tips (Falik et al., 2005). Moreover, root growth in-between the space of the grains depends on existing pressure among the grains and root's ability to exert pressure (Wendell et al., 2011). These processes may lead roots to follow highly tortuous paths and primarily affect the rooting depth and structure of the root system, and thus the total soil volume explored by the root system could be limited. Therefore, studies on root growth simulations in granular soil are useful and necessary to provide better insights on how the distribution of roots changes with increasing amounts of large soil particles in the soil.

Clays undergo cycles of shrinking and swelling processes due to changes in water content during the seasonal climatic cycles. Soil cracks are formed in clayey soils as a result of this phenomenon. Cracks in clayey soils create weak passages, which allow roots to grow with minimum resistance while anchoring into the crack surfaces. These zones accumulate more water during rainfall or irrigation events and are more favorable to root functions during water stress periods than hard less permeable zones (Grismer, 1992). Since soil resistance is minimum within cracks, roots can reach higher depths (Tardieu, 1994). When undisturbed, root recolonization may occur due to the presence of pores created by the roots from previous growing seasons for many years. Similar to roots, other biological activities such as earthworm burrow create pore networks in the soil. Biopores create preferential paths of pore network, which are enriched with nutrients, and filled with organic materials and water that are essential to root growth (Landl et al., 2017; Nakamoto, 2000; Pagenkemper et al., 2014). Thus, roots can penetrate easily through biopores with minimum resistance, while anchoring to pore walls (Bengough et al., 2016).

Root growth rate depends not only on soil physical properties such as bulk density, water content, water potential, porosity and other soil textural properties (Gao et al., 2016; Vaz et al., 2013, 2011; Whalley et al., 2007) but also the force applied by the root tip on soil particles (Kolb et al., 2017). Bulk density of soil is a measure of soil compaction, which increases with the depth and influences root elongation rates (Shierlaw and Alston, 1984; Tardieu, 1994). Moreover, soil penetration resistance increases with decreasing matric potential (Eavis, 1972; Jin et al., 2013). When undisturbed, the bulk density of soil does not vary substantially with time. However, on the other hand, moisture content and soil matric potential vary with time. Soil moisture content fluctuates due to irrigation, precipitation, drought conditions or evapotranspiration with time and depth. Since the top 30 cm of the soil profile is highly exposed to atmospheric changes, penetration resistance is highly

variable with time at the topmost part of soil due to soil drying and wetting process (Hodgkinson et al., 2017). Therefore, root growth models should consider the temporal variations of soil strength to simulate root systems in the field successfully.

Soils absorb energy from sunlight and propagate heat energy from the top to deeper layers of the soil profile. In addition to radiation, the composition of the soil controls the temperature of the soil (Onwuka, 2016). Therefore, soils with different texture and stone content under the same climatic conditions exhibit different temperatures. Since upper soil layers are stronger influenced by the dynamics of aboveground environmental conditions than the deeper soil, much variability can be observed within the first few centimeters of the soil profile (Illston and Fiebrich, 2017). Previous studies showed that temperature changes the root system architecture since it has an impact on root length, rooting depth, root elongation rates, branching intensity, surface area, growth direction, and lateral branch angles (Kaspar and Bland, 1992; Macduff et al., 1986; Nagel et al., 2009; Onderdonk and Ketcheson, 1973; Vincent and Gregory, 1989). Several authors studied temperature effects on the growth of different plants; cotton grass (Ellis and Kummerow, 1982; Tardieu, 1994), cotton (McMichael and Quisenberry, 1993), alfalfa (Ellis and Kummerow, 1982), oilseed rape & barley (Macduff et al., 1986), and found that certain crops have a specific optimum temperature of reaching the maximum growth rate. Increasing temperature does not always increase the root elongation rate because after reaching the optimum temperature, root growth starts to decrease with increasing temperature (Drennan and Nobel, 1998; McMichael and Quisenberry, 1993), i.e., winter wheat shows root length increases with increasing temperature up to about 20 degrees and start to decrease thereafter (Huang et al., 1991). Furthermore, the optimum, minimum, and maximum limits of root development temperatures and rates vary with genotypes as well as crop types (Sattelmacher et al., 1990). Similar to roots, a similar trend was observed in shoot development (Vincent and Gregory, 1989). Therefore, to simulate temperature effects on root growth, it is important to consider the temperature dependency during the growth periods and also the depth dependency of temperature over the period (Hartmann et al., 2018).

Several simulation models were introduced to include soil physical, chemical and climatic features in the models by several authors, i.e. biopores (Landl et al., 2017), soil strength (de Moraes et al., 2018; Grant, 1993), root obstacle avoidance (Fakih et al., 2017), temperature (Nagel et al., 2009), and moisture content (de Moraes et al., 2018). The main challenge in this regard is the lack of dynamic soil and field root sampling data and to include complex soil structures and dynamics to models due to the lack of comparison between simulated root systems and field-derived root data.

In this study, we investigate by numerical modelling how much of the differences in root system development can be explained by the difference in stone content. We use the root architecture model CRootBox (Schnepf et al., 2018), in which stones can explicitly be represented as obstacles to root growth. As the stone content directly affects other soil properties such as soil temperature, water dynamics, and related soil penetration resistance, as well as crack formation, we will use dynamic experimental data from the field sites to inform CRootBox. Local soil environmental conditions reduce elongation rates of individual roots; this may result in a reduced overall root system length as compared to optimal conditions. In the field without stones, CRootBox will be informed about the observed large cracks that will result in changed root growth direction as well as increased elongation rates inside the cracks to a lower penetration resistance.

This paper is organized as follows. The methodology section describes the selection of RSA parameters and simulation of winter wheat and maize root systems to compare the differences between RLD data that are reported in the literature and simulated profiles. In this section, we explain the experimental field setup and rhizotube root observation and sampling. Then we introduce the simulation of root growth in static soil conditions and how the differences in topsoil bulk density, crack intensity, and stone content affect the rooting depths. The last part of this section contains the root system simulations based on measured soil properties from stony and silty loam soil in the rhizotron facilities. The results section includes rhizotubes measurement data, simulations of RLD based on static soil properties, sensitivity analysis and describe how combined use of those factors based on dynamic field measurements can reproduce the observed differences in root development between the two sites for two different crops. The discussion section explains how each of these factors influences the rooting patterns and the challenges associated with the application of the minirhizotron method on root studies. Finally, in the conclusions, we summarize the significant findings of this study.

## 4.2 Materials and methods

### 4.2.1 The root architecture model CRootBox

CRootBox root architecture model (Schnepf et al., 2018) was used to simulate the 3D root architectures of winter wheat and maize root systems for full vegetation periods (240 days for winter wheat and 120 days for maize). CRootBox simulates root systems with

pre-defined RSA parameters, and each parameter of the RSA model is described by mean and standard deviation values that assign stochasticity to simulated root systems. If not otherwise specified, the model CRootBox simulates root systems under optimal conditions. Root systems can be simulated with or without considering the soil and environmental factors that affect root growth and distributions. Each of these effects is implemented in CRootBox such that the RSA parameters are rescaled and root growth is subjected to changes in soil and environmental conditions of the growth medium and the locality.

### **4.2.2 Parameterization of the root architecture model for winter wheat and maize**

We parameterized the root system architectures for winter wheat and maize based on published RSA model parameters that are available in the parameter database of CRootBox. The winter wheat root systems were simulated based on parameters used by (Morandage et al., 2019) except for the emergence times of basal roots. While the focus of (Morandage et al., 2019) was on individual root traits such as intermodal distance or maximal root length, in this study we adapted the emergence times of primary roots in order to achieve dynamically realistic root length densities compared to field data. Thus, we assumed that basal roots may emerge until the plants reach maturation (180 days) and the emergence times of 20 basal roots were set to a 9-day time interval between two successive basal roots. For the simulation of the maize root system architectures, we used the RSA parameter set of (Postma and Lynch, 2011).

Since the simulations account for model stochasticity, each simulated root system represents similar but unique characteristic features. Therefore, we performed 100 simulations for each scenario (we performed only 10 repetitions of simulations for root growth with the influence of stones due to long simulation time). Since simulations of large number of root systems in a plot requires a higher computational cost and time, we simulated one root system and calculated the normalized root length density for a plot, taking into account a planting density of wheat and maize of 12 cm and 75 cm between rows and 3 cm and 13 cm distance between two plants, respectively. From the resulting root architectures, we computed root length density profiles for comparison against observed root length density profiles.

### 4.2.3 Field experiments

#### The experimental site:

We conducted field experiments at the rhizotron facilities in Selhausen, Germany (50°52'07.8" N 6°26'59.7" E). The experimental site consists of two rhizotron facilities, which are located approximately 150 m apart from each other. The upper rhizotron facility (F1) consists of silty loam soil with a higher percentage of gravel (>60%), characterized by low water holding capacity, and the lower rhizotron facility (F2) has a silty loam soil with a negligible amount of gravel content (<4%). Table 4.1 shows the particle size distribution of two rhizotron facilities. Each facility covers the area of 68.25 m<sup>2</sup> (7 m wide and 9.75 m long) and is separated into three subplots with three different water treatments. The first plot was kept dry using a sheltering system, which sheltered out the rainwater. The middle plot was fed by rainwater. The third plot was irrigated to supply the necessary plant water demand and to reduce the water stress. In this study, we used only the data collected from the rain-fed plot. Soil moisture content was measured hourly using the time-domain Reflectometry, TDR sensors (Campbell Scientific, Inc.), and the TDR data were converted to water content based on Topp equation (for the F2 facility), and with a combination of Topp equation and CRIM model (for the F1 facility). The MPS-2 sensors (Decagon Devices, Inc.) measure the soil water potential along with the soil temperature of both facilities half-hourly. In addition to MPS-2 sensors, soil water potentials were measured by the tensiometers (UMS GmbH München) hourly (see (Cai et al., 2016) for a detailed description of the installation setup and experimental procedure in the minirhizotron facilities in Selhausen). The IR sensors were used to measure hourly canopy temperatures, and we measured crop heights and LAI weekly during the entire growing seasons, to study the differences in above-ground shoot development in the two sites. Moreover, climatic data were collected from the climate station next to the field site.

#### Grain size analysis and soil classification:

The grain size distribution was obtained from the soil analysis of the Selhausen test site (Cai et al., 2016; Stadler et al., 2015; Weihermüller et al., 2007) (Table 4.1). The facility 2 (F2) consists of more than 96% of particles which are smaller than 2 mm in diameter. Therefore, it is unlikely to see an effect of stones on rooting patterns in the F2 facility. The detailed grain size analysis of fine fractions of both facilities is carried out by the previous studies (Cai et al., 2016). In order to determine the particle size distribution of stone fraction (> 2 mm) in the F1 facility, we collected a (240 mm\*250 mm\*65 mm) size block

of soil from the F1 facility. The soil sample was dried and stones ( $> 2$  mm) were separated from fine soil fraction ( $< 2$  mm). The stone fraction was further separated based on the diameter classes of 2 mm - 6.3 mm, 6.3 mm - 20 mm, and stones that are larger than 20 mm.

**Table 4.1:** Grain size distribution Selhausen test site according to ISO 14688-1:2002 (2002) modified after (Weihermüller et al., 2007) and (Stadler et al., 2015). The values with \* sign indicate volume fractions and the other values indicate the weight fractions.

Name	Particle size (mm)	Percentage				
		F1		F2		
		<30cm	>30cm	<30cm	>30cm	
<b>Gravel</b>	Coarse	20–63	*05	69	4	2
	Medium	6.3–20	*15			
	Fine	2.0–6.3	*20			
<b>Sand</b>		0.063–2.0	*10 (35)	37	13	11
<b>Silt</b>		0.002–0.063	*15 (52)	47	70	68
<b>Clay</b>		$\leq 0.002$	*05 (13)	16	17	21
<b>Porosity</b>			30 (33)	25	40	40

### Experimental design and agricultural management:

Winter wheat (*Triticum aestivum* L.) was sown on 26 October 2015 and harvested on 22 July 2016. Maize (*Zea mays*) was sown on 3 May 2017 and harvested on 12 September 2017. Winter wheat was sown at a population density of 450 plants  $m^{-2}$  with 3 cm distance between plants in a row and 12 cm distance between rows. A total number of 750 maize seeds were sown ( $\sim 10$  plants  $m^{-2}$ ) in 10 rows with inter-row spacing of 75 cm and 13 cm spacing between two plants within a row.

### Minirhizotron root observations:

Root growth was observed through horizontally installed 7 m long 6.4 cm in outer diameter transparent tubes using a Bartz minirhizotron camera system (VSI /Bartz Technology Corporation). Rhizotubes are installed horizontally at each facility at six different depths of 10, 20, 40, 60, 80, and 120 cm below the soil surface. There are three replicate tubes in each of the three different water treatment plots, with a total number of 54 tubes in each facility. The camera captures 1.65 cm in length and 2.35 cm wide real size images.

In each tube, images were taken at 20 positions from the left and right-hand sides of the tubes. We captured root images at weekly (or biweekly) time intervals during the growing seasons. We collected images from 22 measurement times during the winter wheat season and 12 times during the maize season. The collected images were processed using Rootfly root imaging software (Zeng et al., 2008) to trace all the root images and to calculate root count densities. The roots counted in each image were divided by the radius of the tube and width of the image to convert the root count densities to root length densities (see (Cai et al., 2016) for detailed information about the root length density conversions in minirhizotron method). Finally, we prepared the root arrival curves of each tube, and the root length density profiles of both facilities were compared. Furthermore, we calculated the total root length per soil surface area,  $L_T$  ( $\text{cm cm}^{-2}$ ) Eq.(4.1), of wheat and maize, and the  $RLD$  differences between upper and lower facilities.

$$L_T = \sum_{i=1}^6 RLD_i * d_i \quad (4.1)$$

where  $i=6$  ( $RLD$  measured at each depth), and  $d_i$  represents the soil thickness between the centers of adjacent tubes ( $d_i = [15, 15, 20, 20, 30, 20]$  cm).

### **Trench root counting:**

Trench root sampling was performed only for the maize crop to compare the differences in root distribution against the minirhizotron method. We excavated a 150 cm long and 160 cm deep, vertical trench, perpendicular to maize rows, next to rain-fed plots of both facilities (F1 & F2), just after the harvesting. The root intersections were counted in 3.75 cm\*3.75 cm mesh grid. Although the root counting data indicate the spatial distribution of roots with depth and distance from maize rows, we calculated only the average root count variation with depth, summing up the lateral distributions of root count densities as root counts per square centimeter into a depth profile (Figure C.7).

### **Visual observation of root systems:**

We visually investigated the structural features present in two different soil types at the end of the maize-growing season. The excavated pit for the trench-root counting was used to observe the influence of the stones, how the roots develop around the obstacles to find plausible growth directions in the upper rhizotron facility (F1). In the lower rhizotron facility, we observed the root growth within the cracks and rooting patterns in the biopores.

Sample photos were taken to demonstrate the influence the structural features (Figure C.10).

#### 4.2.4 Influence of static soil physical properties on simulated root growth patterns

In this section, we describe how root architecture models simulate the effect of prominent structural features, i.e. stones, cracks, and top soil loosening vs compaction in tilled vs non-tilled soils, on root length density distributions and maximum rooting depth.

##### **Role of soil cracks on rooting depth:**

The influence of cracks on root growth was simulated using the approach of (Landl et al., 2017). This approach considers cracks or macropores as anisotropies to the preferred root growth direction. In addition to root orientation in cracks, the root elongation rate was increased by 200% from its original values when roots grow inside macropores because the root elongation increase with decreasing bulk densities. We assumed that the loose materials inside macropores have the bulk density closer to  $1 \text{ g cm}^{-3}$ . Therefore, we used the differences in root elongation rates based on the field soil ( $1.55 \text{ g cm}^{-3}$ ) and loosely packed soil ( $1 \text{ g cm}^{-3}$ ) (Valentine et al., 2012). Since cracks and macropores have a similar influence on root growth patterns, except the differences in shape and the orientations, we assumed that the proposed approach is valid to simulate root growth in cracks for winter wheat and maize crops. To test the effect of the number of cracks present in the soil, we defined a  $100 \text{ cm} \times 100 \text{ cm} \times 160 \text{ cm}$  homogeneous soil domain and set seed in the center of the soil domain at 3 cm depth. In this soil domain, we tested five scenarios with 5 mm wide uniform cracks that represent increasing crack intensities of 0, 2, 5, 10, 20 cracks  $\text{m}^{-1}$ .

##### **Stone content and root obstacle avoidance:**

The model CRootBox uses signed distance functions to simulate root growth in confined geometries (Schnepf et al., 2018). The signed distance function determines the distance of a given point ( $x$ ) to the nearest boundary of the object Eq.(4.2). If the value is positive ( $x$ ) is inside  $\Omega$  (inside the boundary). Negative sign indicates the outside the boundary or

zero indicates on the boundary (Osher and Fedkiw, 2003).

$$f(x) = \begin{cases} d(x, \partial\Omega), & x \in \Omega^+ \\ -d(x, \partial\Omega), & x \in \Omega^- \end{cases} \quad (4.2)$$

Using such signed distance functions to represent the stones' geometry explicitly, root tip heading during growth is changed until the new position of the root tip is outside of any stones (Figure 4.1). Because of numerous deviations due to impenetrable obstacles, final root length distribution may substantially alter in comparison to roots grown in fine-grained soils.

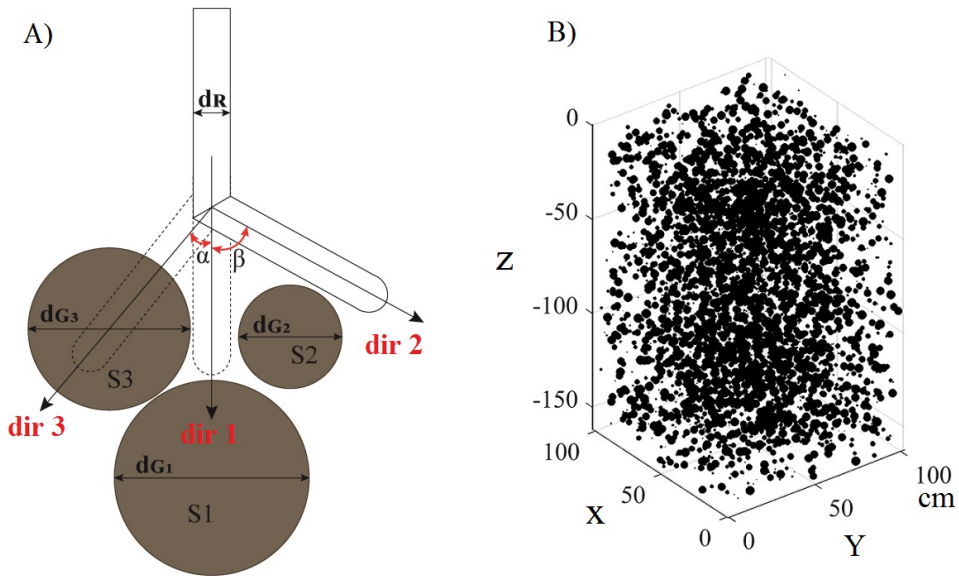


**Figure 4.1:** Deflection of the root segments due to obstacle avoidance; root grows downward direction towards an obstacle, S1, and cannot be penetrated and change its direction to find a suitable direction while turn alpha degree left-hand side and prevented by another stone (S3); therefore it needs to change beta degrees right-hand side and find new growth direction (A). Packing of stones in different diameter classes to occupy the entire domain (160\*100\*100 cm soil block) based on compositions given in Table 4.2 to grow one root system (B).

In order to study the dependence of root growth as a function of stone content, we selected five scenarios with increasing packing densities to evaluate how increasing stone content affects rooting depths (sensitivity analysis with five different packing densities). Based

on the grain size analysis of the stony soil of the F1 facility, we categorized grain size distribution as percentages of spheres with 40, 20, 10, 5, and 2.5 mm in radius. We assumed that the stones, which have a radius smaller than 2.5 mm can be considered as movable obstacles by roots and do not affect the growth direction of root trajectories, while the stones with a diameter higher than 5 mm cannot be replaced by roots and therefore, roots tend to find an alternative path. In CRootBox, we selected grain positions and diameter classes randomly to place all particles inside the selected soil domain. The size of the soil domain was chosen as a 160 cm deep and 100 cm\*100 cm wide soil block to simulate a root system inside that domain. The domain was packed based on the composition of stones, given in Table 4.2 for each scenario. Then, we repeated each scenario ten times to calculate the mean vertical root distributions with 1 cm depth intervals. Finally, we evaluated the changes in rooting depth as a function of increasing packing density for both wheat and maize crops.

**Table 4.2:** *Distribution of particle sizes and respective percentages of stony soils used to simulate root growth under different scenarios.*

Scenario	Size (diameter) of the percentage of the particle's volume fraction (%)					
	8 cm	4 cm	2 cm	1 cm	0.5 cm	< 0.5 cm
<b>S1</b>	0.00	0.00	0.00	0.00	0.00	100.00
<b>S2</b>	0.625	2.50	5.00	5.00	10.00	75.00
<b>S3</b>	1.25	3.75	7.50	7.50	15.00	62.50
<b>S4</b>	2.50	5.00	10.00	10.00	20.00	50.00
<b>S5</b>	3.75	6.25	12.50	12.50	25.00	37.5

#### Root system response to different topsoil bulk densities:

The root development of winter wheat and maize were simulated based on the changes in soil bulk densities of the top 30 cm of the soil profile. We simulated 5 scenarios with increasing soil bulk densities of 1.3, 1.4, 1.5, 1.6, 1.7 g cm<sup>-3</sup> of the soil profile. Based on the changes in soil bulk densities, the elongation rates were modified. We obtained root elongation rates of wheat at different bulk densities based on laboratory studies published by (Colombi et al., 2017) for wheat and (Popova et al., 2016) for maize (Table 4.3) and rescaled the elongation rates accordingly (Figure 4.2). However, the root growth patterns in the soil below the 30 cm depths were not changed as the effect of loosening and hardening is less influential in deeper soil. It should be noted that the elongation rates of these parameters

were derived based on the early stages of the plants and we assumed that the other root architecture parameters are not considerably influenced by soil strength or penetration resistance. Finally, the root systems of winter wheat and maize crops were simulated 100 times for each scenario to calculate the mean root length density distribution with varying degrees of soil bulk densities in the topsoil.

**Table 4.3:** *Root elongation rates of winter wheat (Colombi et al., 2017) and maize (Popova et al., 2016) observed in the soils with different bulk densities.*

Scenario	Bulk density (g cm <sup>-3</sup> )	Elongation rate- wheat (cm day <sup>-1</sup> )	Elongation rate- maize (cm day <sup>-1</sup> )
S1	1.3	2.28	3.50
S2	1.4	1.67	2.86
S3	1.5	1.18	2.25
S4	1.6	0.80	1.63
S5	1.7	0.40*	1.00

\**extrapolated value*

## 4.2.5 Influence of dynamic soil conditions on root growth patterns

### Soil temperature:

To adapt root elongation according to measured soil temperatures, we rescaled the optimum elongation rates with a temperature-dependent impedance factor calculated using temperatures measured half-hourly at six different soil depths (10, 20, 30, 60, 80, and 120 cm) (wheat-Figure C.1 & maize-Figure C.4). The field derived temperature values were obtained from decagon MPS-2 sensors installed in Selhausen rhizotron facility during the 2015 November and 2016 July winter wheat, and from 2017 May to 2017 September for the maize growing season. The impedance factors were assigned to the CRootBox model as grid-based values. When roots arrive at a certain depth, elongation rates are rescaled based on the impedance factor of that depth at the given time, according to (Clausnitzer and Hopmans, 1994) Eq.(4.3).

$$imp_r = \sin \pi(T)^{\sigma} \quad (4.3)$$

where

$$T = \frac{tem - tem_{min}}{tem_{max} - tem_{min}} \quad \text{and} \quad \sigma = \frac{\log(0.5)}{\log\left(\frac{T_{opt} - tem_{min}}{tem_{max} - tem_{min}}\right)}$$

for  $T_{opt} < 0.5 * (tem_{min} + tem_{max})$

and

$$T = \frac{tem - tem_{max}}{tem_{min} - tem_{max}} \quad \text{and} \quad \sigma = \frac{\log(0.5)}{\log\left(\frac{T_{opt} - tem_{max}}{tem_{min} - tem_{max}}\right)}$$

for  $T_{opt} > 0.5 * (tem_{min} + tem_{max})$

tem is the measured soil temperature,  $T_{opt}$  is the genotype-specific optimal temperature for root growth,  $tem_{max}$  is the maximum and  $tem_{min}$  is the minimum temperature within which root elongation occurs. Maximum, minimum and optimum temperature values of winter wheat were set to 25°C, 2°C, and 16.3°C respectively (Porter and Gawith, 1999), and for maize were set to 40.1°C, 12.6°C and 26.3°C (Sánchez et al., 2014). We simulated the root systems, according to the temperature dynamics of stony soils (F1) and silty loam soils (F2). The root development was measured at given six depths, and root arrival curves of six depths of the two sites were compared with arrival curves of roots that were simulated under the optimal conditions.

### Moisture content:

We evaluated the temporal changes in penetration resistance as a result of water content and matric potential. Similar to temperature data, we rescaled the elongation rate, according to the impedance factor in two field sites taking measurements of water content and matric potential variation in 30-minute time intervals at six different depths. Penetration resistance was modified at each time step based on the water content using the general equation (Vaz et al., 2013) Eq.(4.4), which depends on the normalized bulk density ( $\rho b^*$ ), and normalized moisture content  $sp$ .

$$PR = \exp^{[1.5(\pm 0.06) + 2.18(\pm 0.09) * \rho b^* - 4(\pm 0.16) sp]} \quad (4.4)$$

$$Sp = \frac{\theta_v - \theta_p}{\theta_s - \theta_p}, \quad \text{and} \quad \rho b^* = \frac{\rho b - \rho b_{min}}{\rho b_{max} - \rho b_{min}}$$

where  $\theta_v$  is the volumetric water content,  $\theta_s$ - saturation (= porosity),  $\theta_p$ - permanent wilting point,  $\rho_b$ - bulk density,  $\rho_{bmin}$ - minimum soil bulk density,  $\rho_{bmax}$ - maximum soil bulk density. We selected maximum bulk density of  $1.6 \text{ g cm}^{-3}$  and a minimum of  $1.4 \text{ g cm}^{-3}$  in the F1 and F2 facilities respectively (we assumed that the bulk density of the fine soil material in the F1 facility are equal to the bulk density of the soil in the F2 facility). The wilting points of the soils were set to 0.05 and 0.2 for F1 and F2 facilities and the penetration resistant at each time step and depth was derived based on measured water content (wheat-Figure C.2 & maize-Figure C.5) and porosity values. Then we used Eq.(4.5) with measured soil water potentials (wheat-Figure C.3 & maize-Figure C.6) to derive the impedance factor for root elongation (Bengough et al., 1997; Dexter and Hewitt, 1978; Tardieu, 1994).

$$imp_v = \frac{R}{R_{max}} = \left( -\frac{\psi_0}{\psi_w} + \exp^{-0.6931(P_R/P_{R1/2})} \right) \quad (4.5)$$

where  $R_{max}$  is the maximum rate of root elongation,  $\psi_0$  is the metric potential,  $\psi_w$  the matric potential at wilting point (-1500 kPa), and  $P_R$  is the Penetrometer resistance and  $P_{R1/2}$  is the penetration resistance value at which root elongation rate decreases to half of its maximum value. The  $P_{R1/2}$  values were obtained from the measurement data of wheat-(Colombi et al., 2017) and maize-(Bengough et al., 2011) published in the literature. Finally, we simulated wheat and maize root systems from the rescaled growth rates to calculate the RLD changes at hourly time intervals. The resultant curves were compared between and among optimum root growth conditions to investigate the changes in root systems as a function of soil strength.

### **Combining all effects based on field data to simulate root development in the two field sites:**

Finally, we combined all the individual effects based on F1 (stony soil) and F2 (silty loam soil) to simulate root systems and to calculate the final root length density distributions of wheat and maize root systems. The influence of stones as obstacles is only affecting root growth in the F1 facility. We adjusted the elongation rates, according to dynamic changes in temperature, water content, water potential, and soil bulk densities and respective penetration resistance values. The impedance to single root elongation as affected by individual physical properties is shown in Figure 4.2 for both wheat and maize. Each of those impedance factors was multiplied to calculate the combined impedance factors in simulations.

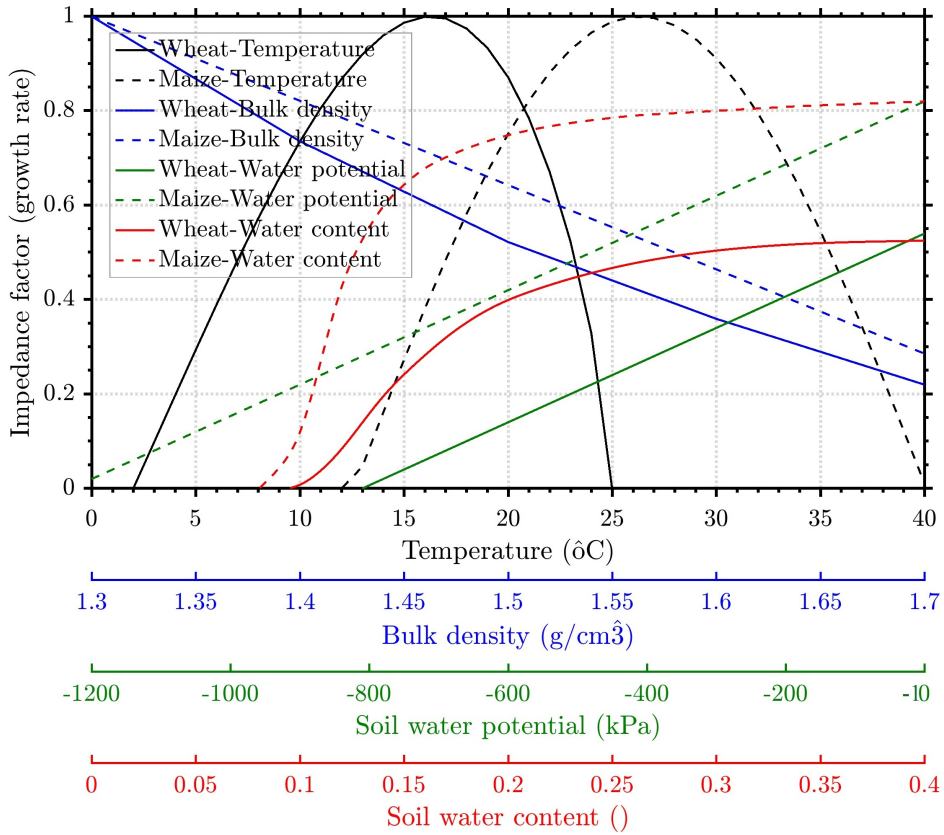


**Figure 4.2:** The relationship between relative root elongation rates (wheat and maize) and the properties of growth medium; soil temperature (Clausnitzer and Hopmans, 1994), soil bulk density (wheat (Colombi et al., 2017) and maize (Popova et al., 2016)), and soil water potential and soil moisture content (Bengough et al., 1997; Dexter and Hewitt, 1978) of soils with  $1.55 \text{ g cm}^{-3}$  of bulk density.

## 4.3 Results

### 4.3.1 Comparison between measured root arrival curves of winter wheat and maize in stony and silty loam soil

Figure 4.3 shows root arrival curves (RAC), root length densities with respect to time, measured at 10, 20, 40, 60, 80, and 120 cm soil depths of winter wheat (blue lines) and

maize (green lines) obtained during the 2015-2016 and 2017 growing seasons. Winter wheat roots arrived at 10, 20, and 40 cm depths in both silty loam (F2) and stony soils (F1) within the first three weeks after sowing. In general, the F1 facility shows the highest root length density in the top layer and decreasing with depth. This behavior is the same for both crops. F2 facility has differently shaped root length density profiles, with the largest value at a depth of 60-80 cm. In both experimental facilities, winter wheat reached its maximum root development approximately after 200 days of sowing and maize after 100 days after sowing. After reaching the maximum growth stages, root decay could be observed.

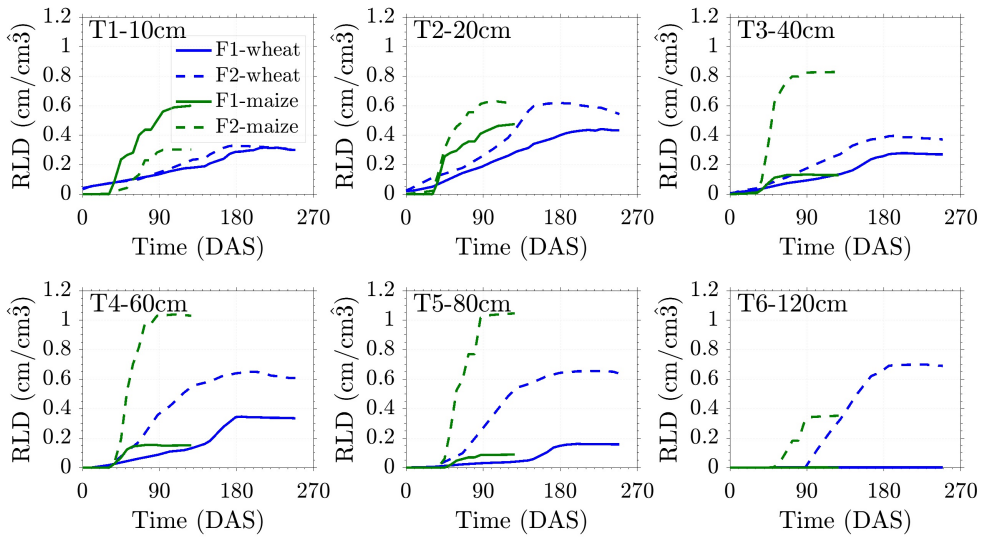


**Figure 4.3:** Root length density changes with days after sowing (root arrival curves) observed in rhizotubes, which are located at T1-10 cm, T2-20 cm, T3-40 cm, T4-60 cm, T5-80 cm, and T6-120 cm depths.

Winter wheat roots reach up to 40 cm depths of both facilities within the first month after sowing. However, roots reached at 60 cm depth after 50 days in silty loam soil, while it took 60 days for the roots in the stony soil to reach the same depth. We observed the arrival of first wheat roots to the tubes located at 80 cm depth in 85 days after sowing, while it took 120 days for the first roots to arrive at the same depth in the F1 facility. The observed maximum rooting depth of stony soils was 80 cm, and the roots were first observed after 110 days (We observed a negligible number of roots at 120 cm depth in stony soils after 160 days). It took 120 days for roots to arrive at the 120 cm depth of silty loam soil. For maize, the first root arrival times to the tubes that are located in 40, 60, 80 cm depths of the F1 facility in comparison to the F2 facility, were delayed 10, 12, 15 days, respectively.

### 4.3.2 Simulated and measured root length density (RLD) distributions of winter wheat and maize plants in soils with high and no stone content

Figure 4.4 compares the root length density profiles obtained from RSA simulations and minirhizotron images at the end of each growing season of winter wheat and maize crops. The blue lines indicate the simulated root length density profiles. The grey shaded area is the envelope of available published root length density profiles, encompassing many different environmental conditions and thus representing a range of plausible root length density values. The root length densities obtained from CRootBox model simulations fit well within that range for both crops. The RLDs obtained from our MR measurements, however, are only comparable to that range for maize grown in the stony loam soil. Wheat from MR observations shows a lower RLD in top soil layers compared to literature range and model simulations in both facilities. MR-based RLD of maize in the silty loam has a convex shape with maximum value at 60-80 cm depth. Interestingly, this rather unusual shape was corroborated by the root intersection density (RID) obtained from trenches in the year 2017 (Figure C.7). Based on the MR data, the total root length of the F2 facility is 255% for wheat and 350% for maize higher than in the F1 facility at the end of the growing periods. This indicates that the soil conditions profoundly reduce the root growth in stony soil.

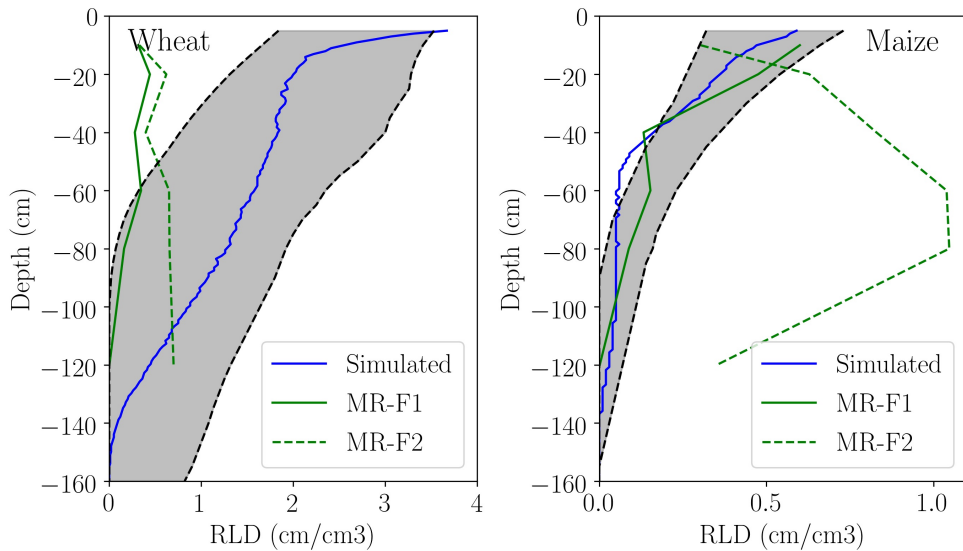


**Figure 4.4:** Root length density distribution of winter wheat and maize at the end of the growing seasons measured by the minirhizotron method (green) plotted against the simulated RLD curves (blue). The solid green lines indicate the measurements from the F1 facility, and the dashed green lines indicate the F2 facility MR measurements. The gray shaded areas indicate root length density profiles derived based on measured data from the literature of wheat (Palta et al., 2004; Wasson et al., 2014; Xu et al., 2016; Xiying et al., 2009) and maize (Buczko et al., 2008; Gao et al., 2010; Mekonnen et al., 1997; Postma and Lynch, 2012; Zhan and P Lynch, 2015; Zhuang et al., 2001).

### 4.3.3 Root growth in macropores

Figure 4.5 compares the changes in root distribution simulated for in roots grown in homogeneous soil and soils with macropores. The maximum rooting depth increases with increasing density of cracks in both crops. However, the maximal increase is <20 cm.

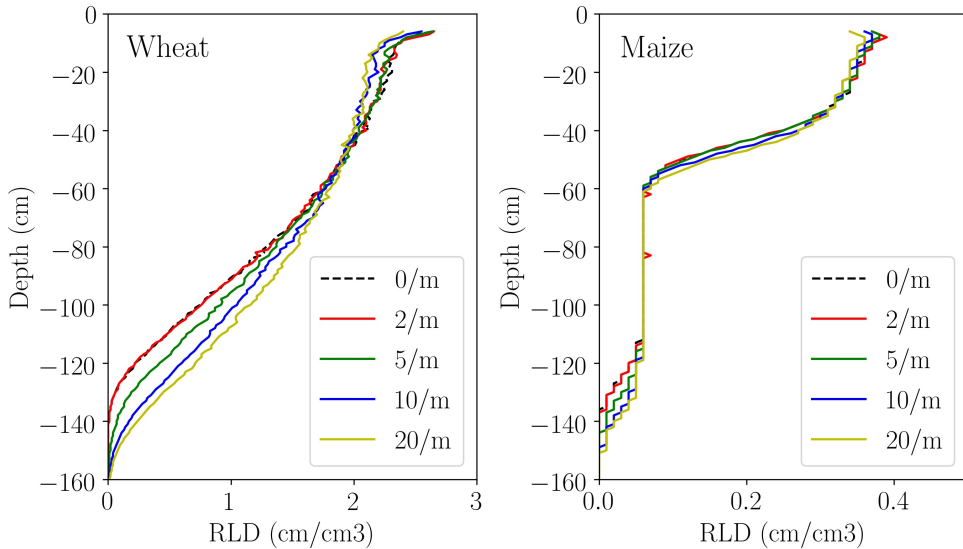


**Figure 4.5:** Comparison between simulated root growth patterns in homogeneous soil (black dashed line) and soils with the influence of crack densities, plotted as root length density profile at the end of the growing seasons of wheat (left) and maize (right).

#### 4.3.4 Root obstacle avoidance

Simulations of wheat and maize root systems in soil without obstacles (S1) show the highest rooting depth amongst the scenarios. When packing density (proportion of stone content) increases, rooting depths decrease and fractions of the root system at shallower depth increase (Figure 4.6), because root trajectories follow highly tortuous paths and decrease the rooting depths. This observation implies that the root growth towards the direction of gravity is disturbed by the larger particles. Maximum rooting depths of simulated winter wheat and maize with the same amount of stones as in the soil of the F1 facility (F1) are reduced by about 10 cm and 20 cm respectively (blue line) compared to simulations in soil without stones.

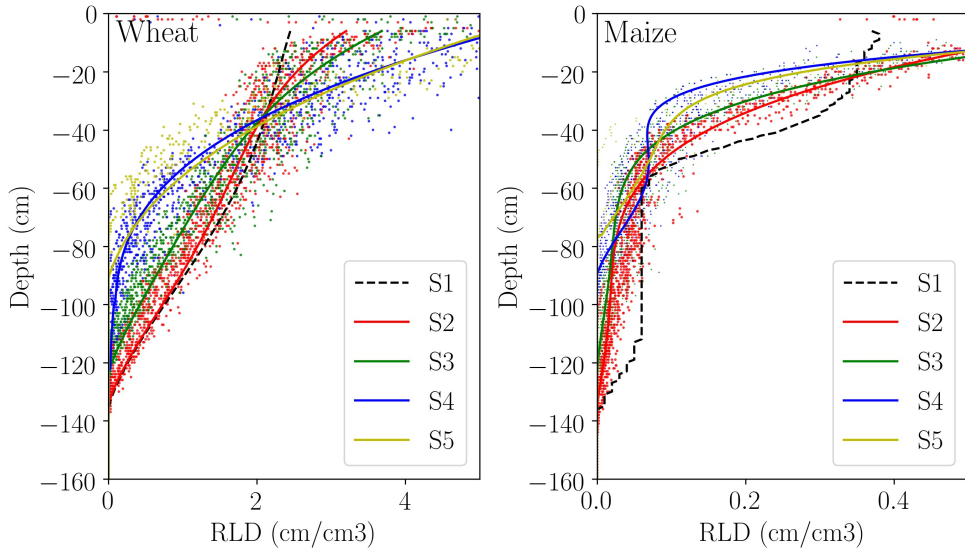


**Figure 4.6:** The relationship between root length density destitution (left-wheat and right-maize) and packing density of stones that are higher than 5 mm in diameter. Particle compositions are defined as increasing packing density of different sizes of particles;  $P1$  indicates the root growth without the influence of stones and  $S4$  indicates the experimental grain size distribution of the upper rhizotron facility ( $F1$ ), and  $S2$ ,  $S3$ , and  $S5$  consist of 25%, 50% and 125% of  $S4$  fractions respectively

### 4.3.5 Root growth in loose and compacted topsoil

Figure 4.7 shows the root length density profiles computed from simulated root systems grown in soils with different topsoil layer (<30 cm) bulk densities. The simulated profiles indicate that the hardening of topsoil has a significant influence only on the wheat crop as the bulk densities of  $1.7 \text{ g cm}^{-3}$  and  $1.6 \text{ g cm}^{-3}$  cause a reduction in root development, and the loosening soil does not have a long term impact on wheat crops. Maize does not have any effect on changes in topsoil bulk densities at the end of the growing period. However, the changes in elongation rates due to changes in topsoil bulk densities cause delays in reaching the maximum rooting depth and root maturation. In other words, rooting depths may differ at different growth stages (results are not shown).

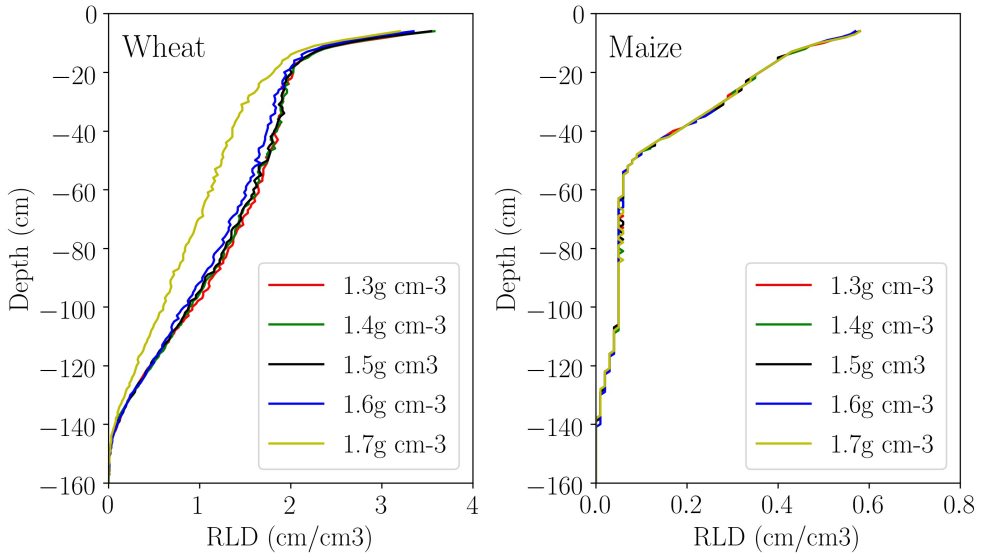


**Figure 4.7:** Root length density distribution patterns observed with varying degrees of bulk densities between  $1.3 \text{ g cm}^{-3}$  and  $1.7 \text{ g cm}^{-3}$  of topsoil layer ( $<30 \text{ cm}$ ), which undergoes hardening and loosening of soil due to plowing and compaction.

### 4.3.6 Sensitivity analysis of static soil properties on rooting depth

The effect of changes of crack intensity, stone content, and bulk densities of topsoil layer on maximum rooting depth is summarized in Figure 4.8. The amount of stones in the soil and the size of the stones have a considerable influence on the maximum rooting depth of both wheat and maize crops. The maximum rooting depth of wheat was reduced by about 55 cm, while maize accounts for 40 cm decrease in rooting depth when roots distribute in soils consist of 62.5 % of stones. Cracks provide favorable conditions for deep root systems, indicating 15 cm, and 20 cm increase in rooting depths of maize and wheat, respectively. Although increasing topsoil bulk density causes reductions in total root length densities of wheat, the maximum rooting depths of wheat and maize crops are not affected.

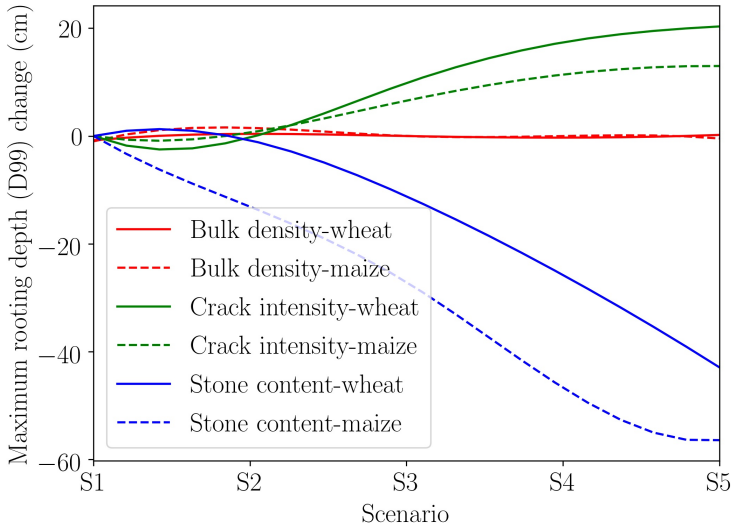


**Figure 4.8:** Sensitivity analysis for the maximum rooting depths (D99) of wheat (solid lines) and maize (dashed lines) with varying degrees of soil bulk density of topsoil (red lines), crack intensity (green lines), and stone content (blue lines).

### 4.3.7 Soil temperature

The measured soil temperature of the stony soil is approximately  $2^{\circ}\text{C}$  higher than the one of the silty loam soil (Figure C.1 -wheat, and Figure C.4 -maize). The differences in temperature cause faster root growth in the stony soil (Figure 4.9). Winter wheat undergoes temperatures ranging from  $0^{\circ}\text{C}$  during the winter to  $30^{\circ}\text{C}$  in the spring and maize experience from  $5^{\circ}\text{C}$  to  $35^{\circ}\text{C}$  temperature during the growth period. Notably, the below zero temperatures between February and March months cause a reduction in elongation rates (in some cases, stop the root elongation due to freezing temperatures).

For wheat, the temperatures are far from optimal in both facilities. In the top layers, root development is only delayed and reaches the same root length density than the optimal temperature at a later time. In the deepest depth (120 cm), root growth is reduced and does not catch up at later times. There is also a small difference in root length densities caused by the temperature difference between the two facilities. Compared to wheat, the temperatures are not as far from optimal for maize in both facilities. However, less than optimal temperatures hit the maize in the early phase, just after germination.

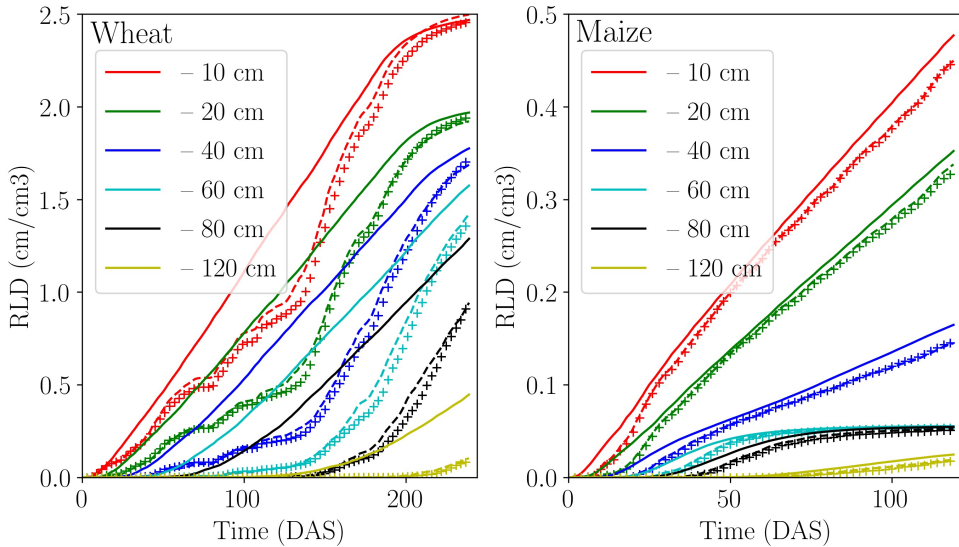


**Figure 4.9:** Simulated mean root arrival curves for winter wheat during the 2015-2016 growing season (left) and 2017 maize growing season (right) considering the influence of temperature on root growth in stony soil, F1 (dashed line) and silty loam soil, F2 (+ markers), plotted against the optimal temperature conditions (solid continuous line) at depths 10, 20, 40, 60, 80, and 120 cm.

### 4.3.8 Root growth in soils with soil strength as dependent on measured soil water content

The silty loam soil with higher water holding capacity in the F2 facility shows higher developments of wheat roots than in the F1 facility in measurement data. Although simulated root development of F1 and F2 facilities are highly affected by penetration resistance within the first six months in comparison to optimum soil (Figure 4.10), differences in root development between two sites do not vary significantly with time. Temporal variation of dry and wet weather conditions caused higher penetration resistance and stopped root growth in some time periods. Maize indicates a similar root growth pattern for changes in moisture conditions. .

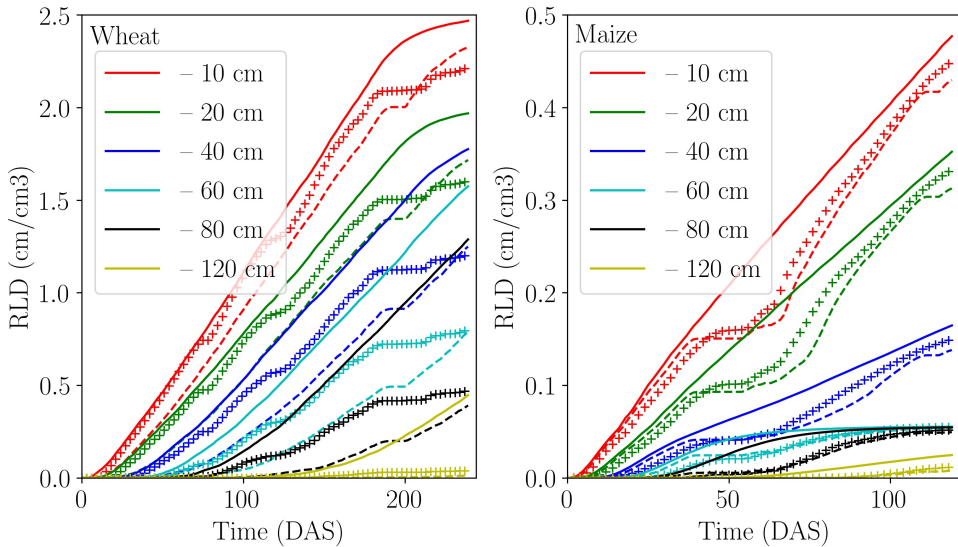


**Figure 4.10:** Simulated mean root arrival curves for winter wheat during the 2015-2016 growing season (left) and 2017 maize growing season (right) considering the influence of soil strengths in the fine material of stony soil, F1 (dashed line) and silty loam soil, F2 (+ markers), plotted against the optimal soil conditions (solid continuous line) at depths 10, 20, 40, 60, 80, and 120 cm.

### 4.3.9 Comparison between field sampling data and simulation results that include all measured soil information and its effect on root growth

Figure 4.11 compares the measured RLD data (winter wheat rhizotube root observation data during the 2015-2016 growing season and maize in 2017) and corresponding root system simulation results based on the measured soil information. Simulated winter wheat root systems in the stony soil are limited to a rooting maximum of 60 cm, while measurements show roots up until a depth of 120 cm. The simulated RLD of the top 10 cm of the soil profile of wheat roots is almost 4-5 times higher than the measured data. Simulated and MR-observed RLD of wheat in the silty loam soil have adverse trends with depth. The simulated RLD of wheat in silty loam soil decreases, while the measured RLD of wheat increases with depth.

Although the maximum rooting depth of simulated maize root systems is limited to 80 cm

in stony soil, the simulated and the measured RLD within the first 40 cm of stony soil show a good agreement. However, simulated and measured root growth in silty loam soil does not show comparable results, except for the first 10 cm depth. Thus, the observed field root growth patterns of winter wheat and maize in stony and silty loam soils are not adequately explained by the simulation results that explicitly consider the soil physical properties in root growth (see Figure C.8 & Figure C.9 for the simulation of root arrival curves of wheat and maize respectively based on measured data).

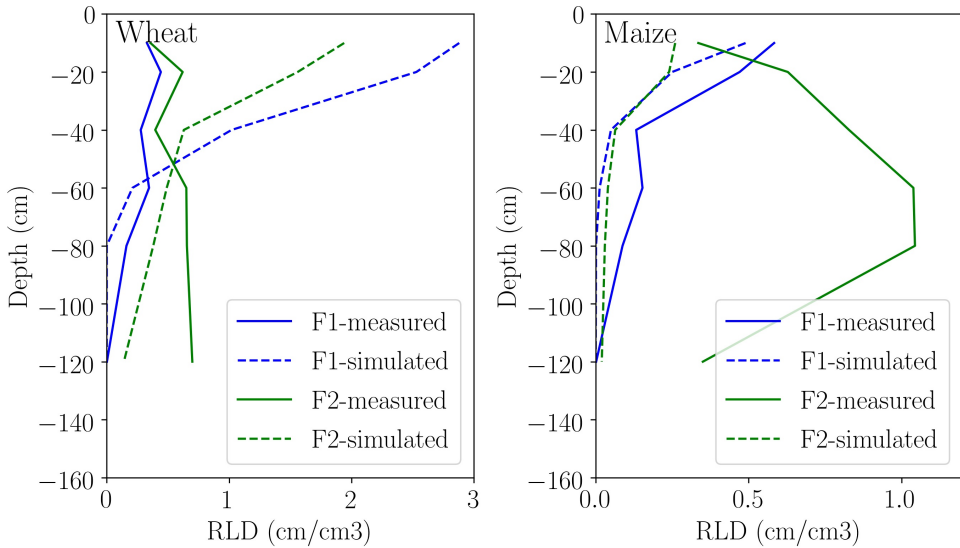


**Figure 4.11:** Comparison between simulated and measured root length density profiles of wheat (left) and maize (right) considering the influence of physical properties of stony, F1 and silty loam soil, F2.

Table 4.4 compares the differences between measured and simulated root system measures of wheat and maize crops. Simulated maximum observable rooting depths of wheat, simulated based on the measurements of stony soil reach at 80 cm depth while wheat roots reach 120 cm in silty loam soil. This indicates that the simulated wheat root systems of F1 soil underestimate the actual measured rooting depths. Although simulated maize roots arrived at 120 cm depth in simulations and are comparable with the measured data, the RLD values are significantly smaller than that of measured data. Total root length densities of both measured and simulated data are not comparable and the highest difference can be observed in the simulated and measured roots of maize in silty loam soil. The maximum root length density of the F1 facility was observed within the first 20 cm in both simulated

and measured data of wheat and maize crops. However, the F2 facility shows an opposite pattern in the measurement data such that the simulated maximum RLD values were observed at 10 cm depths, while the measured maximum RLD of wheat and maize were observed at 120 and 80 cm depths respectively in the F2 facility. The median root arrival time at the different depths indicate that the measured and simulated root system data has significant differences in arrival time periods.

**Table 4.4:** Differences in F1 facility in comparison to F2 facility between simulated and measured root growth patterns of wheat and maize crops concerning the  $D_{max}$ ,  $T_c$ ,  $RMm$ , and  $At$  root system measures.

Root System measure	Wheat		Maize	
	$\Delta(\%Mes.)$	$\Delta(\%Sim.)$	$\Delta(\%Mes.)$	$\Delta(\%Sim.)$
<b>Dmax</b>	0.0%	33%	0.0%	0.0%
<b>Tc</b>	60%	16%	80%	5%
<b>RMm</b>	83%	0.0%	88%	0.0%
<b>At</b>	10cm	5%	9%	5%
	20cm	2%	14%	2%
	40cm	32%	38%	9%
	60cm	74%	31%	12%
	80cm	60%	–	1%
	120 cm	–	–	62%

$D_{max}$ - maximum observable rooting depth

$T_c$ - total root length density

$RMm$ - depth at which maximum RLD observed

$At$ - median root arrival times at 10, 20, 40, 60, 80, 120 cm depths

## 4.4 Discussion

### 4.4.1 Similarities between simulated and literature root length density profiles

The root length density profiles of winter wheat and maize, simulated based on the published RSA parameters of winter wheat (Morandage et al., 2019) with slight modification, and maize (Postma and Lynch, 2011) are comparable with the RLD data published in the literature. However, we observed that the literature data for RLD's of wheat and maize is highly variable and, is challenging to summarize into a narrow distribution. Some studies show that the RLD values as high as  $60 \text{ cm cm}^{-3}$  and lower values such as  $0.5 \text{ cm cm}^{-3}$  is also reported for mature root systems (Ephrath et al., 1999; Mekonnen et al., 1997; Zuo et al., 2006). This means that the root length densities vary with several factors such as sampling location, soil type, climate, and genotypes. However, most of the data indicate similar characteristics in the shape of RLD curve; a higher proportion of roots were observed at the first 40 cm of the profile and the RLD decrease with the depth, and the roots of wheat and maize could reach up to 200 cm deep into the soil profile.

Although the sensors measure the soil hydraulic properties of the bulk soil (stones + fine soil), roots experience mostly the influence of fine materials of soil, as roots do not explore the stone fraction of soil. Therefore, soil hydraulic properties that determine the root-soil penetration resistant in fine soil fraction should be rescaled and the effect of stones should be excluded from the calculations of effective soil water content and soil matric potential values (Naseri et al., 2019). However, our simulations of root growth in stony soil do not account for the influence of stones on soil hydraulic properties on fine soil. Therefore, the overall root development could have been affected due to a lack of rescaled measured water content and water potential values.

### 4.4.2 Differences in RLD's in simulations, literature data, rhizotube observations, and trench profile data

Our field data are useful to compare the growth rates at different depths during the whole life cycle of the crops because, in comparison to other field methods, minirhizotron root observations provide information about the dynamics of root systems. The comparison between field measurements, based on rhizotron facilities and the literature data (and

simulated profiles) indicates significant differences depending on the soil and crop types. The root growth in soil with a higher stone content (F1 facility) shows that only the shapes of the RLD curves of winter wheat show similar characteristics to literature data, but the absolute RLD values of minirhizotron data highly underestimate the literature data, which is almost four times higher than that of MR data. Nevertheless, MR data of maize in F1 facility show a similar shape than the literature data; On the other hand, the MR data obtained from both winter wheat and maize crops in the experimental site with silty loam soil (F2) are not comparable with the literature data, regarding both the shape of the RLD curve and the absolute RLD values. Although we speculate that the installation of rhizotubes influences the root growth, the root count densities (trench profile data-Figure C.7) of maize prove that the shapes of root counting data are in agreement with the MR data. This means that the influence of tubes that act as obstacles to root growth does not have a significant impact on the accuracy of MR data of maize crop. Furthermore, our MR data show a good agreement with other studies that are published based on MR root sampling data, especially the underestimation of RLD at the first 30-40 cm in the soil profile, such as for wheat (Postic et al., 2019) and maize (Hulugalle et al., 2015; Samson and Sinclair, 1994). It is reported that the underestimation of RLD at the first 40 cm is a major limitation, which is identical to MR methods for the other crops as well (Chen et al., 2018; Liao et al., 2015; Parker et al., 1991; Svane et al., 2019).

Some authors suggested the reasons for lack of correlation between MR data and other methods is that lack of contact between soil and tubes and the influence of tubes. However, we observed that this applies only to fine-grained soils and the shape of RLD profile of stony soil indicates comparable results to other field methods and simulated profiles, except for the lower root mass. The following reasons may be responsible for the mismatch reported in our MR data and also the MR method in general, based on our observations: The root lengths or roots counts that are measured in rhizotube images needed to be converted to root length densities as the length of roots per cubic centimeter of soil; therefore the methods proposed in this study and the other studies could result in the erroneous calculations due to certain assumptions. Next, the Influence of tubes has a major impact on changing the root growth patterns, such as illumination effects, changing growth directions and stimulates the growth of lateral branches.

Moreover, the space in between tube and soil matrix could accommodate additional roots and the accumulation of roots around the tubes might be higher in the deeper zones of the soil, indicating that the tubes in deeper depth are more favorable for excess development of roots around rhizotubes. In addition to that, some MR experiments conduct using angular

or vertical tubes. Therefore, the roots could grow along the downward direction with the tube and thus show higher root mass around the tubes in comparison to the rest of the soil domain. However, the tubes in the Selhausen facility are installed horizontally, this effect may not have a great impact on our observations. Furthermore, when sampling root systems of row crops such as maize, the sampling locations are highly influential in root length density values, i.e., image capturing locations that are close to the plant base might show a higher amount of roots than the locations far apart from the plant base. Therefore, MR approach requires to make sure that the sampling scheme is representative of the whole plot. More importantly, the installation of rhizotubes for several growing seasons prevents agricultural practices such as plowing and field preparation before sowing the seeds. Therefore, the compaction of topsoil increases with time, in our field the plowing was not conducted during the last 5 years, and the sowing was mainly performed with creating holes for the placement of seeds. Therefore, we noticed approximately 7 cm subsidence in the soil in the F2 facility (the F1 facility indicated only 2-3 cm of soil subsidence). Therefore, the tube in 10 cm is located at the seeding depth ( $\sim 5$  cm), and fewer amounts of roots could be observed by the camera.

Moreover, the F2 facility consists of large amounts of soil cracks (Figure C.10). Therefore, most of the roots tend to grow along cracks and easily develop roots at the deeper layers of soil in the F2 facility since the moisture content is higher than the shallow depths. Finally, the most influential factor and most of the factors are dependent on the lack of plowing and soil homogenizing processes before sowing. This led to preserving existing macroscopic structures in the soil for years and forms a hard crust at first 20-30 cm depths. Therefore, the lack of loose soil prevents the development of roots in the first few centimeters of the soil. In contrast, the F1 facility does not undergo heavy compaction due to the presence of large stones.

#### **4.4.3 How differences in stone contents affect the other soil properties**

The results of experimental data predominantly show how much variability in root length density, rooting depth and growth rate is affected by the growth medium as a result of the stone content differences in two different soils. Since the plants were grown only 150 m apart from each other, we can assume that the plants experienced the same climatic conditions. The presence of stones in the F1 facility causes slight changes in temperature since the heat capacity of stony soil is higher than silty loam soil. Therefore, we observed approximately

2°C temperature difference between both facilities. Since the topmost layer is exposed to atmospheric heat exchanges, the temperature at the top 20 cm in the soil profile fluctuates rapidly as day and night temperature changes and highly sensitive to seasonal changes. The slight difference in temperature in two soil types influences a slightly faster root growth in the F1 facility than the F2 facility. Since the F2 facility has favorable conditions for root growth in the deeper in the soil profile due to the abundance of water, root penetration resistance and relative growth rate are faster than the stony soil in the F1 facility and are further confirmed by the simulation results. Stony soils consist of large pore spaces that are not connected and the stones prevent lateral extension of root branches and reduce the total RLD of stony soil.

Although both experimental sites receive the same amounts of water, soil composition determines the water availability to the plant growth. The water received from rainfall or irrigation on stony soils drain faster and show higher moisture content only after a rainfall event at the upper soil layers. Moisture contents in the topmost layers fluctuate rapidly with the climatic changes such as precipitation and evaporation. The soil moisture content variation with depth could also be affected considerably with size and the proportion of stones. The water holding capacity also causes leaching losses of nutrients. Therefore, root growth and root mass might be reduced in the F1 facility and affect the overall crop performance. Furthermore, the roots can only absorb a limited amount of nutrients from the stony soil as a limited volume of soil is explored by the root system because most of the minerals in stony soil are not water-soluble ions and roots are not directly in contact with soils due to the presence of larger pores in stony soils (Figure C.10).

#### **4.4.4 Simulations of root systems based on soil type and root distribution patterns and the potential role of macropores as a governing factor of deep root systems**

Simulations are not sensitive to differences in soil bulk densities on root length density distribution (see Figure 4.8). This implies that plowing practices do not significantly contribute to the overall root distribution as a result of changes in root elongation rates. However, in simulations, we assume that the other RSA parameters are not attributed to changes in bulk densities. This could lead to erroneous interpretations as some studies indicate the observation of higher root mass in zones with lower bulk densities. Therefore, further studies are required for simulations of the effect of bulk densities on rooting patterns

The increasing proportions of stones or granules that are not replaced by the roots tend to restrict root growth deeper into the soil as shown in Figure 4.6. A systematic increase in the proportion of stone content reduces the rooting depths up to 70 cm in both crops. This means that the stones prevent roots from reaching deeper to capture water and nutrients and the soil exploration capability of roots is reduced by stones. Since the acquisition of resources is limited, shoot growth is affected and the available carbon supply to root system can be decreased significantly. Therefore, the measured lower RLD in stony soil can be explained by the presence of higher stone content in the F1 facility. Moreover, we assumed that a threshold diameter (5 mm) of stones, which act as obstacles to root growth. However, in real conditions, many factors such as the adjacent soil matrix, depth and type roots also determine the root's ability to replace stones (Whiteley and Dexter, 1984).

Simulated profiles indicate that increasing crack intensities lead to deeper penetration of roots than that of homogeneous soil. However, the difference is unexpectedly smaller than the published data that consider the effect of macropores on changes in root growth patterns (Han et al., 2015; Perkons et al., 2014). The main reason could be that the maximum length of primary roots reaches to its maximum length faster (shorten the maturation time) due to excessive root elongation rates and stop growing with time. Because in simulations, only the root growth rates (root tip elongation rate) are modified when roots grow inside the macropores, and the changes of other parameters such as lateral branching intensities and the lengths of branches are not modified to account the effect of macropores due to lack of experimental data on those effects. Moreover, the influence of abundance of water, nutrients and other cell functions in macropores that stimulate root growth are not considered in the simulations. Therefore, models need to be adapted to account for these factors to simulate the root in accordance with field-grown crops.

The most striking observation of the experimental data is that the root developments in large quantities below the 60 cm depth in the F2 facility. This observation cannot be explained by the factors considered in the simulation study. Although we observed roots up to 120 cm depth using minirhizotron camera, the excavated profiles show that the maize roots grow up to 170 cm depth in silty loam soil, while maximum rooting depth of maize does not exceed 100 cm in stony soil. Therefore, we hypothesized that the presence of macropores (as shown in Figure C.10, most roots were observed in deep cracks and biopores) in silty loam soil stimulates the root growth deeper in the soil profile as the soil has higher moisture content and possibly more nutrients.

The main challenge of determining the effect of macropores on root growth is the uncertainty of measurements and lack of understanding of rooting patterns inside macropores in

the field conditions. Root elongation through cracks and biopores depends on the ability of the roots to find a crack. The roots grow through crack may re-enter the soil depending on the strength of the adjacent soil domain, root thickness or size of the crack (Whiteley and Dexter, 1984). If cracks provide favorable conditions for roots to grow, the probability of re-entering back to the soil domain is highly decreased. Moreover, the diameter of biopores and the number of biopores are essential factors to estimate the root distributions. The presence of a large number of pores in the soil is not a good indication of deep roots, which depend on the occupancy of roots in the pores and the ability of roots to find pores. Moreover, these features vary with climatic conditions (Hodgkinson et al., 2017). Therefore, care must be taken to define the size of biopores and methods to estimate the size and number of biopores, which varies from centimeter to micrometer scale (Wuest, 2001). This implies that the simulations that are based on simplified assumptions are not sufficient to quantify the measured differences in root distribution patterns in highly heterogeneous soil. Therefore, future models should consider the above additional factors for studies on root growth that consider the influence of soil and environmental conditions.

#### 4.4.5 The alteration of root traits and root system architecture

The most significant observation in field root sampling observed as a function of time is that the differences in growth speed, maximum rooting depths, distribution of root at different depths and the total number of roots (root mass).

##### **Rooting depth:**

Based on the visual inspection of excavated profiles, we observed a large number of soil cracks and biopores in the F2 facility (silty loam soil). Although we excavated soils after the maize growing season, these soil structures were undisturbed after the construction of the experimental sites. Therefore, we can assume that the soil structures were not altered considerably with time. Consequently, roots can easily penetrate these weak zones and grow deep into the soils because the roots face less resistance from surrounding soils and absorb water and nutrients from the pores or crack walls while anchoring into the pore/crack walls. We could observe the areas (different positions of root images taken by the camera with the same tube) where root length densities are very low at the same depths as observed in rhizotube images (results are not included). These areas can be identified as the zones, where roots prefer to avoid and to follow paths with lower resistance.

It is remarkable to observe that most of the root mass of stony soil is located within the first 60 cm in wheat and 40 cm in maize. A very few roots were observed at the 120 cm depth, which is the maximum observable depth of the rhizotubes. However, root distributions of silty loam soil indicate that the roots penetrate more than 120 cm depth. Notably, most of the roots were observed within 60-120 cm depth. This observation indicates that the roots follow fewer resistant paths and develop longer lateral roots in the deeper layers, which have higher moisture content. Visual observations show that the presence of cracks and biopores in silty loam soil and tortuous root growth around large stones (Figure C.10). Since connected pores or weak zones are not present in the stony soil, penetration of roots is restricted and reduces the maximum rooting depths.

Root simulations show that the temperature does not play a significant role in rooting depths. A fewer number of roots (as RLD) were increased at deeper depth in stony soils, which we did not observe in the field simulations. The main reason could be that the measured temperature has negligible effects of elongation rates, as the temporal variations do not contribute much to the final root distribution in comparison to other factors. Interestingly, the observed higher RLD in deeper in the soil in the F2 facility, and higher RLD in top horizons of the F1 facility cannot be explained based on temperature differences. The field observations also contradict the simulation results of temperature-dependent root growth as temperature induces roots to grow deeper in the F1 facility.

The higher impendence in the root elongation rate in the stony soil than the silty loam soil can be explained as a result of combined effects of higher bulk density, low water content, and higher matric potential, which increase the root-soil penetration resistance. Since wheat did not experience water stress during the development stage, we cannot observe the differences in root length densities simulated by the data obtained from the 2015-2016 period. However, maize shows a smaller RLD at 60 and 80 cm depths in the F1 facility due to lower matric potential and water content. The maximum rooting depth of simulated root systems in soil with the stone content similar to the F1 facility indicates that the rooting depth decrease by about 20 cm and proportional to the stone content. Thus the simulation results only partially explain the differences in field measurements.

### **Total root length:**

The differences in root distribution can be interpreted mainly based on the properties of the two different soils. The first 30 cm of the F1 facility consists of 50% of stone content and soils below 30 cm consist of 69% of stones. A higher percentage of stones could act as

obstacles to root growth, prevent preferential growth directions of seminal roots, and root branches. The root length density of the F1 facility is lower than the F2 facility in MR data and the root counting data validated the MR data because root intersection densities measured from trench profiles in the stony soil are lower than the silty loam soil (Figure C.7). Since the F1 facility consists of large fractions of stones, nutrient and water uptake efficacy could be reduced because of lacking contact between soil and roots due to the presence of larger pores. Therefore, root development was highly influenced by the differences in stone content in the soil. This observation cannot be explained using simulation results due to the lack of additional information in the model, i.e., alterations of RSA parameters such as changes in branching patterns, changes in lengths of lateral roots in addition to growth rates. Therefore, the model needs to include parameters derived from experimental data to simulate the increase of root length densities due to changes in different soils.

### **Elongation rate:**

When undisturbed, the bulk density of soil increases with the depth. However, our soil analysis results show that the bulk density of silty loam soil varies between  $1.5 \text{ g cm}^{-3}$  and  $1.6 \text{ g cm}^{-3}$  with depth. Since the soil in the F2 facility consists of biopores and cracks, local heterogeneity can be observed in different zones in the same depth. Therefore, a large number of samples are needed to estimate highly precise bulk density values. Although the bulk density of soils in our experimental site does not vary systematically with depth, we observed the changes in soil water potential with the depth during the growing season due to seasonal changes. Studies found that the soil strength and penetration resistance are increased with decreasing (more negative) soil matric potential (Taylor and Brar, 1991). We observed higher matric potentials during the rainy periods in the upper layers while deeper layers remain wet in the F1 facility. However, during dry periods, different patterns could be observed. This implies that, although the bulk density does not change with depth, temporal changes in soil water potentials indirectly change the root elongation rates. On the other hand in the F1 facility, the methods used in the estimation of bulk density of fine-grained soils cannot be applied successfully to stony soil because the presence of large stones leads to difficulties in sampling and inaccurate measurements of soil volume at different depths.

### 4.4.6 Relationship between shoot development and root distribution as a function of properties

The root system of a plant has a direct influence on the overall crop performance. Shoot and root development of plants are decreased by increasing the percentage of stones or granules in the soil (Alexander and Miller, 1991). In order to evaluate the shoot-root relationship, we compared crop developments in the 2015-2016 winter wheat and 2017 maize seasons. There are significant differences between shoot development in two soils as shown in the differences in LAI and crop heights (Figure 4.12). At the beginning of the growing periods, crop development was not highly affected by the differences in stone content; however, during the development stage, crop shows considerable differences in aboveground crop development. Root growth in stony soils has a significant restriction in resource capturing, as the root distribution is limited in space, especially shallower root systems prevent plants from accessing deep water and nutrients. Since stony soils have low water contents, water stress can be observed in plants growing in stony soil, and consequently, reduce the plant development. Similar to water, nutrients are also limited in the same manner as well as the limited amount of non-bounding ions in soils due to the abundance of stones. Therefore, stony soils show limited shoot development, lower LAI, and crop heights in both winter wheat and maize crops than the crops grow in the silty loam soil. Thus crops in stony soil indicate much less overall plant performance.

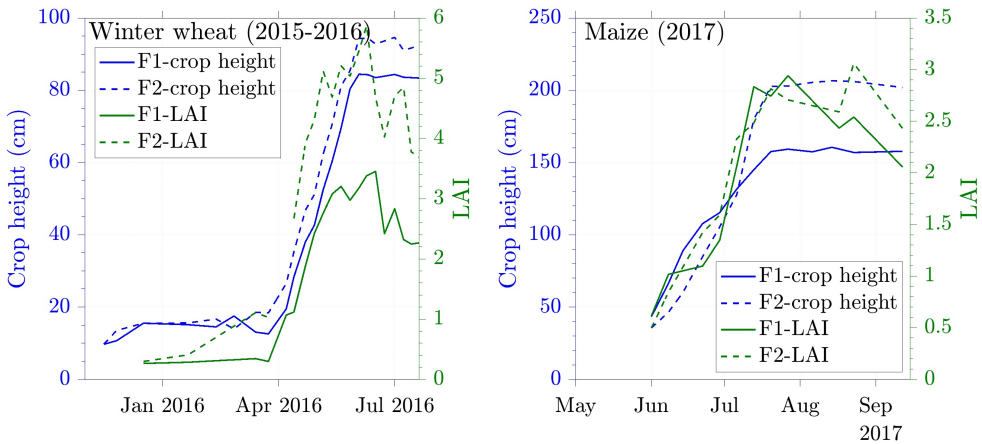


**Figure 4.12:** Leaf area index (LAI) and crop height of winter wheat (left) and maize (right) change with time in plants grow in stony soil, F1 (solid line) and silty loam soil, F2 (dashed line).

#### 4.4.7 Suggestions for model improvements

The selected soil properties cannot fully explain the differences in rooting patterns. There are notable differences in total root lengths and root length density varies with depth, measured in stony soils and silty loam soils. The current model does not have sufficient information to account for the differences in RLDs. Because in addition to differences in soil physical properties, many additional factors contribute to the development of a root system such as nutrient supply, carbon allocation and shoot development. The main drawback in most simulation models is that there are simplified assumptions and a lack of functional relationships derived from experiments for specific crops. Therefore, stepwise improvement of root models is required to strengthen the understanding between experimental data and root system simulations by adding more soil and plant-specific information RSA models.

### 4.5 Conclusions and outlook

In this study, we investigated the differences in root distribution of both wheat and maize crops as a result of the differences in stone content on crops grown in the same climatic conditions. The soil with a higher stone content reduces the rooting depths, total root length den densities, and root arrival times at specific depth of crops, in comparison to soil with a negligible amount of stones. Moreover, the differences in stone content change the soil temperature up to 2°C, and soil hydraulic properties also affected as the stony soil tends to drain water faster than the silty loam soil. In order to simulate these effects, we implemented the functions published in the literature that explains the changes in root growth patterns of soil physical properties and simulated virtual field root systems based on the measured soil information and published root architecture parameters using root architecture model CRootBox. The simulated RLD profiles of winter wheat and maize crops based on the RSA parameters can reproduce realistic root system architectures successfully and are comparable with the measured RLD's, reported in the literature. There are significant differences between the RLD data obtained from MR methods of this study and other studies and core sampling data published in the literature. Our simulation results imply that the variation of temperature and soil penetration resistant due to changes in moisture content depending on the season and depth has temporal influences, which cause delays of roots to reach a certain depth at specific periods and slightly affect the maximum rooting depth. Next, the macropores in fine-grained soil and the presence of large stones alter the growth direction and distribution of root systems that ultimately change the root

length density distribution.

Moreover, the comparison between measured and simulated data indicate that the significant differences in root development that observed between the two different soil types, based on the differences in structural and soil physical properties cannot be reproduced successfully by the model. Especially, the higher root development observed in macropores simulated by the model is not sensitive enough to reproduce the measured differences. We speculated that the differences in crop growth and development in the different soils that could have been caused by water, nutrient stress, and C limitation in the two soils. Therefore, the results emphasize the need to link RSA models to growth models that represent the impact of stresses and resource allocation on plant growth and its feedbacks on root development.

# Chapter 5

## Synthesis

### 5.1 General Conclusions

Since obtaining the information about detailed root system architecture and root traits from field-grown crops are vital for plant breeding programs and for root architecture models to evaluate the resource capturing efficiency of plant's root systems and other modeling approaches, we intended to investigate whether the data obtained from classical field sampling methods contain enough information about root system architecture of plants, and how each parameter of the root system responds to the observed variation of the field sampling data (chapter 2). With the overview of the parameter sensitivities, the possibility of estimating the most sensitive parameters was carried out in a Bayesian framework based on soil core sampling data derived from synthetic experiments (chapter 3). However, our approach was based on synthetic experiments and the influence of the growth medium was neglected. Thus we studied the possibility of incorporating soil and climatic factors that affect root growth patterns to the RSA model and evaluated the differences in root distribution between simulation results and measured data of winter wheat and maize crops that were grown in two different soil types at the rhizotron facility in Selhausen, Germany (chapter 4).

In general, the application of field sampling methods for studying root distribution and understanding of “the hidden half” of plants has been conducted during the last couple of decades. The improvements in field sampling techniques for obtaining detailed RSA information have continuously been investigated. However, the main research gap in this regard was whether field root sampling data contain enough information about the RSA of

plants and how to develop a systematic sampling procedure and methodological approach for obtaining such information. The main outcome of this research demonstrates that field root sampling data contain quantifiable information, especially the parameters of zero-order roots and could be inferred successfully with the help of root architecture modeling and Bayesian inference.

### 5.1.1 Parameter sensitivities and correlations of RSA model

The evaluation of sensitivities of different field sampling methods and respective characteristic root system measures to RSA parameters was conducted based on a virtual root system simulation and field sampling of winter wheat and maize crops with the help of a mathematical modeling approach. Although a few studies have been conducted based on RSA models to characterize virtual field sampling data, in this study, we demonstrated the use of all RSA parameters for simulations of entire growth periods of mature field-grown root systems and sampling schemes; coring, trenching, and minirhizotron observations to represent a realistic field sampling approaches and subsequent field data analysis. With the help of root architecture model CRootBox, simulation of large number of root systems with detailed root architecture parameters and root sampling from soil coring, root impact counting in vertical profiles walls and root image capturing through transparent rhizotubes, it was possible to produce synthetic field sampling data for this study to resemble real field experimental procedures. The simulated field data could be used to compute the uncertainty of field sampling data and sensitivities of root system measures to root system architecture parameters. The sensitivity analysis results revealed that some RSA parameters, especially the parameters of zero-order roots have higher sensitivities and lower non-linear effects, while the higher-order roots have lower sensitivities and highly non-linear effects on characteristic root system measures of different sampling results and the parameter sensitivities are specific to crop types and sampling methods.

Overall, the numbers ( $NB$ ), maximum length ( $maxl0$ ), and inter-branch distance ( $ln0$ ) of zero-order roots are the most influential parameters that determine the root length density and total root mass of root systems. The minirhizotron method provides more information about the dynamic parameters such as elongation rates of zero-order roots ( $r0$ ), while coring and trench profile methods are more sensitive to parameters associated with the spatial distribution of root systems. Moreover, the higher sensitivities of the number of zero-order roots ( $NB$ ), and elongation rates ( $r0$ ) of our sensitivity analysis results based on minirhizotron observations are comparable with a similar study conducted by (Garré

et al., 2012).

Furthermore, principal component analysis of sensitivities was carried out and thus specific correlations between parameters could be identified with respective root system measures. The PCA results indicated that parameter pairs, such as the number of zero-order roots ( $NB$ ) and inter-branch distances ( $ln0$ ), insertion angle ( $theta0$ ) and gravitropism strength ( $tr0$ ) of zero-order roots are highly correlated and could be compensated with each other. Nevertheless, these results could provide useful insights about the sensitivity, non-linearity, and correlation of parameters, which are vital information for characterizing RSA traits from field sampling data.

### 5.1.2 Inference of RSA parameters

With the overview of parameter sensitivities and characteristic root system measures that reflect the root growth patterns of winter wheat crops, we selected virtual core sampling data to investigate the possibility of approximation of RSA parameters utilizing a Bayesian framework. Based on the sensitivity analysis results we selected 17 most sensitive parameters out of 37 RSA model parameters of the winter wheat root system to estimate using Markov chain Monte Carlo DREAMzs sampler. We identified the prior knowledge of the parameters, selection of most sensitive parameters, the influence of parameter correlations, and minimize the model stochasticity as the most important steps that need to be addressed carefully. The major challenge in the inference, namely the model stochasticity, could be resolved with iterating over multiple times of forward model simulations of each proposed sample. However, iterating over multiple times requires a significant amount of computational time and the use of parallel computing resources could minimize the long sampling run time, which is the primary constraint in Bayesian inference. The next challenge could be identified as the complex data dependencies that lead to an overfitting problem, which could be solved by inflating the likelihood and adjusting the MCMC acceptance rule for accepting MCMC transitions that do not significantly change the likelihood value.

The inference results demonstrated that the maximum length or zero-order roots ( $maxl0$ ) could be estimated with higher accuracy and lower uncertainty from the RLD data of core samples. Nevertheless, the narrowly centered approximate posterior distributions of numbers ( $NB$ ), elongation rate ( $r0$ ), insertion angles ( $theta0$ ) of zero-order roots could also be estimated, but with higher uncertainty. However, the other zero-order and higher-order root parameters are not well resolved and indicate higher posterior uncertainty due to higher correlations among parameters and lower sensitivity. Furthermore, the inference results

are consistent with the results of sensitivity analysis and principal component analysis (Morandage et al., 2019).

In general, the results further proved that core sampling data contain sufficient information that reflects some information about root system architectures. Therefore, this approach could be identified as an auspicious step towards characterizing detailed RSAs of different genotypes based on large amounts of data collected from field sampling studies (Wasson et al., 2014)

### **5.1.3 Differences in measured and simulated root distribution of soils with different stone contents**

The RSA parameters, obtained from the published literature, that used to simulate and to calculate the root length density profiles of winter wheat and maize root systems are consistent with most of the measured RLD data published in the literature, indicating that the CRootBox, root architecture model could be used to simulate analogous to field-grown root systems. The measured differences between root growth patterns in stony soil and silty loam soil in the same climatic conditions demonstrate that the root growth, distribution, and root system architectures of plants are highly attributed to the growth medium. Hence, it is crucial to study the influence of soil conditions that affect rooting patterns for studying plant dynamics and simulating root growth in RSA models.

The functions published in the literature to include the soil and environmental factors that affect changes could be implemented in root architecture model CRootBox to simulate root systems based on the measured soil information to compare with the measured root growth patterns in the same conditions. The simulation results indicate that the temporal variation of temperature and soil moisture conditions have a temporal influence on root growth due to seasonal changes and at specific depths and slightly change the rooting patterns in different soil types. However, macroscopic soil structural properties such as stone content and the presence of macropores are highly influential in determining the maximum rooting depths. The measured data demonstrate that the deeper and faster root growth patterns of winter wheat and maize in silty loam soil, while the root length density and rooting depths of both crops are lower in the stony soil. However, simulations overestimate the root density above 40 cm and underestimate below 40 cm depths in the soil of both crops, in comparison to rhizotube observations. This indicates that the simulations are not representative of measured root growth observed in minirhizotron facilities indicating the lack of all stress

conditions that are present in field conditions in simulation results. Therefore, root growth models should consider the effects of nutrient stress, and adaptations of root systems in different environmental conditions should be investigated in detail.

Although the simulations contrasting with measured rhizotube RLD data, the comparisons should be made with another sampling method such as soil coring data to investigate whether the differences are independent of sampling methods. The underestimation of roots in topsoil and overestimation of roots in deep soil is reported as a major drawback in the minirhizotron method which was already emphasized in the literature. Nevertheless, our field measurements imply that this interpretation is valid only for the root growth measurements in fine-grained soil and the shape of the root length density curve of stony soil is not affected. The main reason could be that the presence of stones prevents the preferential growth of roots in stony soil. However, our explanations regarding the different patterns observed in MR data should be further validated and the application of minirhizotron data for root studies requires calibration with other field root sampling methods.

## 5.2 Outlook

In this research, we presented the use of virtual experiments to obtain information about the detailed root system architectures or root traits from field-grown crops. This research proves that the aggregated information from field root sampling methods, soil coring, trench root counting, and minirhizotron methods, contain the information related to parameters of RSA of winter wheat and maize crops. Thus, field sampling schemes could be used to understand the detailed RSA of crops. Although this study considered only the simulations of wheat and maize crops, this approach is not restricted to specific crop types, and therefore applicable to other crop types to understand the influence of each RSA parameter of root systems on root growth patterns. The Bayesian inference approach was successfully applied to inversely estimate zero-order root parameters from soil coring data of winter wheat. Future studies will extend this approach to further field sampling methods and different crop types. Technical challenges associated with long computation times of the inversion, dealing with parameter correlations, model stochasticity, lack of prior range of parameters, and influence of growth medium and environment of plants should also be resolved in future attempts. Our simulation results of root architecture development as influenced by measured field-data at high temporal resolution are a step in this direction.

# Appendix A





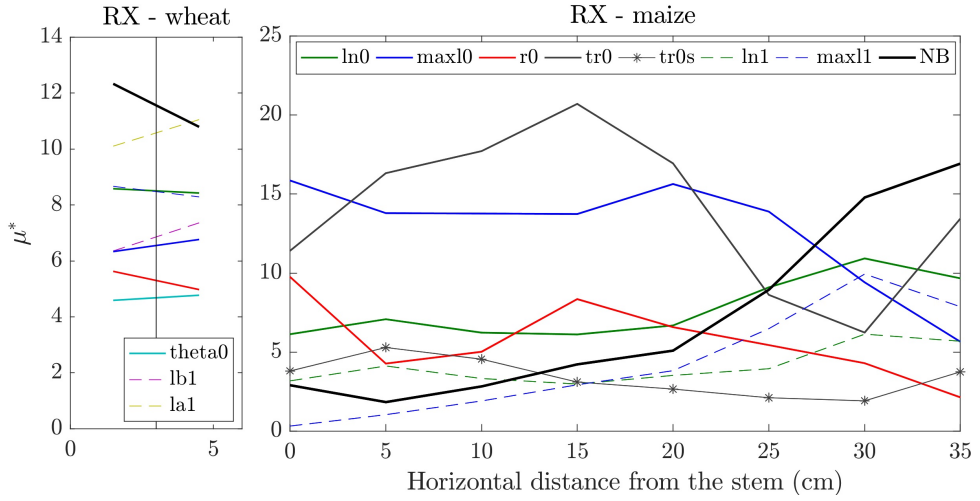


**Figure A.3:** Normalized means of absolute elementary effects ( $\mu^*$ ) of the most sensitive RSA parameters on root impact densities in vertical transects of trench profiles (RX) at different distances from the stem for winter wheat (left) and maize (right) 240 days and 180 days after sowing, respectively.

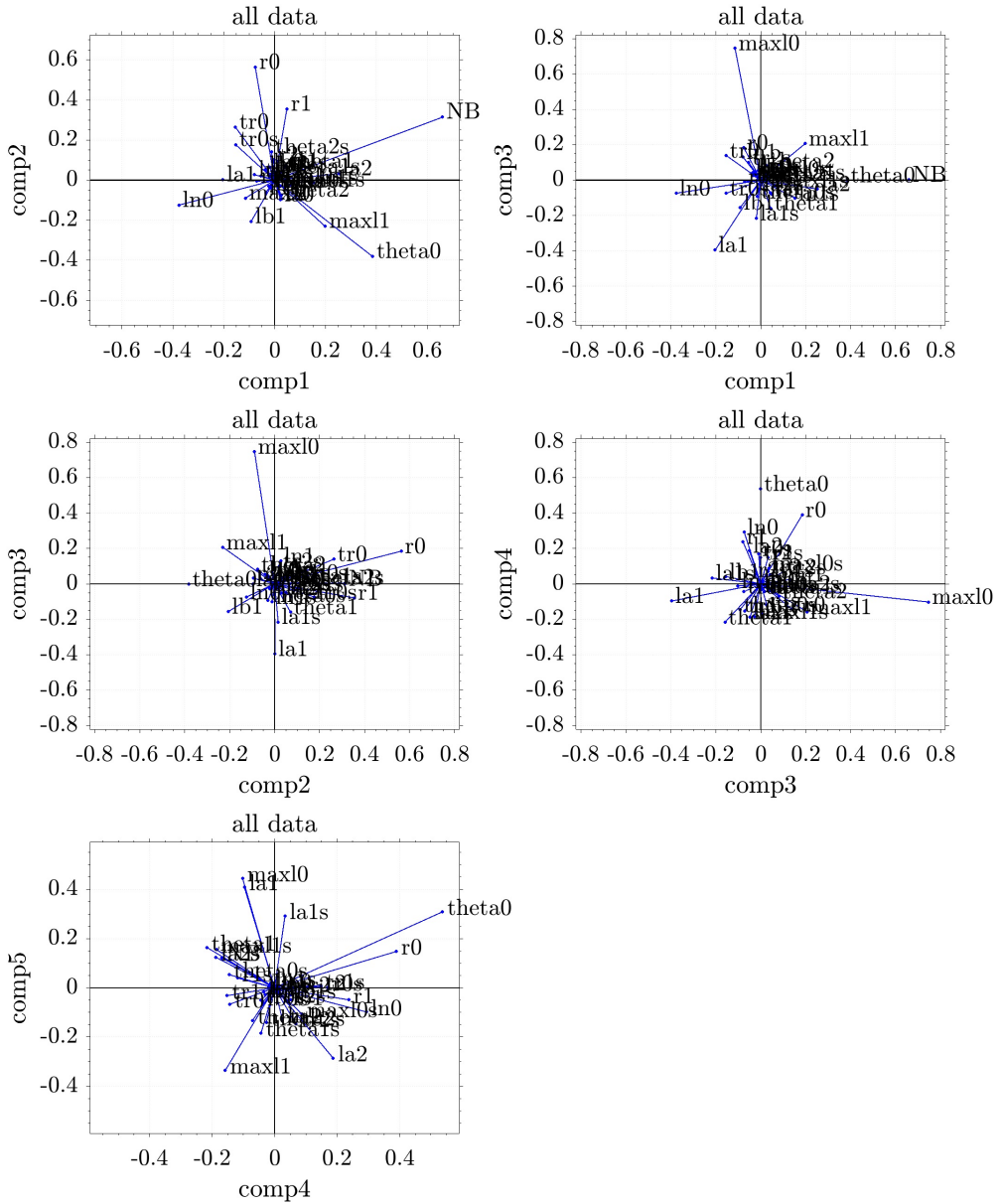


**Figure A.4:** Biplots of parameter loadings for different PCs when all data are combined for the wheat crop.

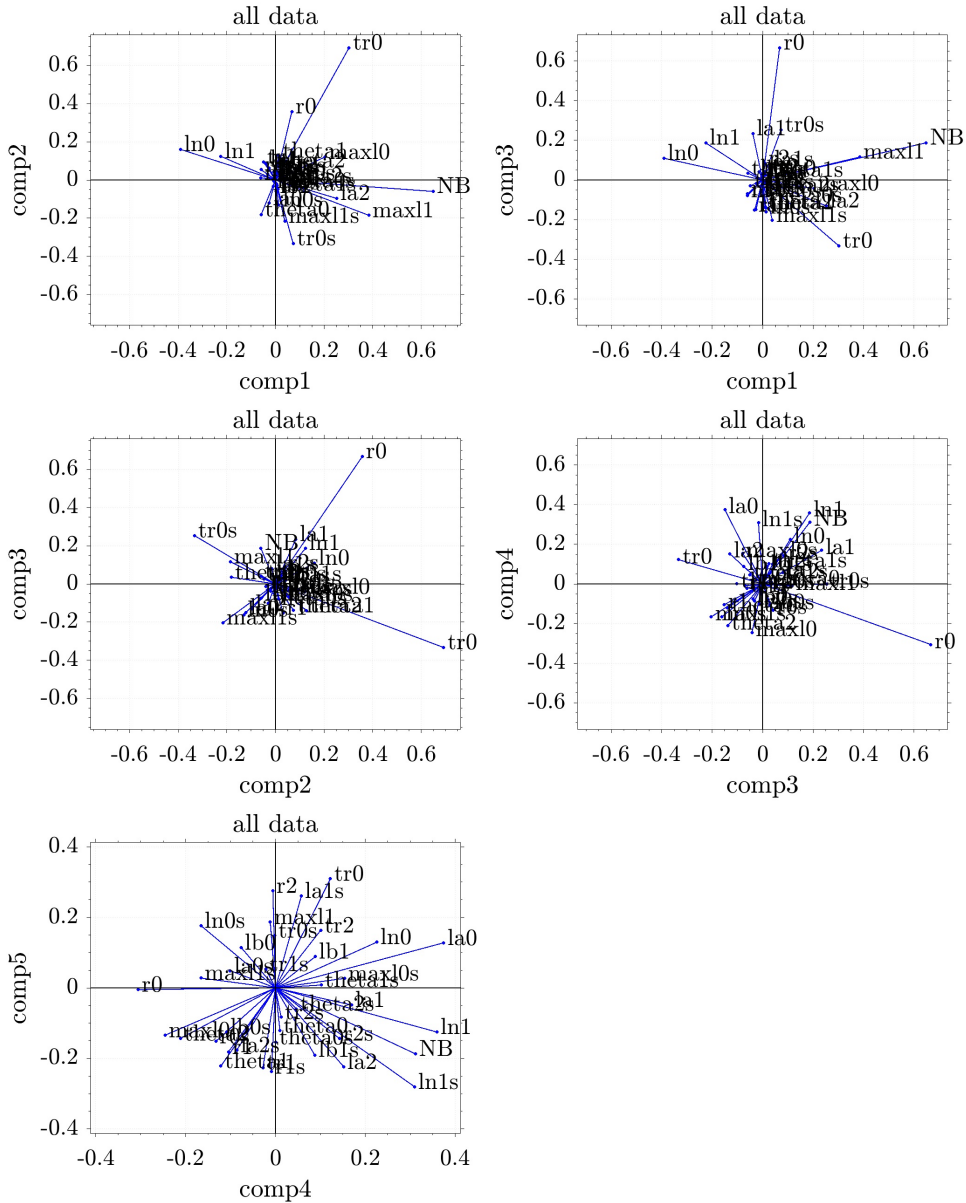


**Figure A.5:** Biplots of parameter loadings for different PCs when all data are combined for the maize crop.

# Appendix B

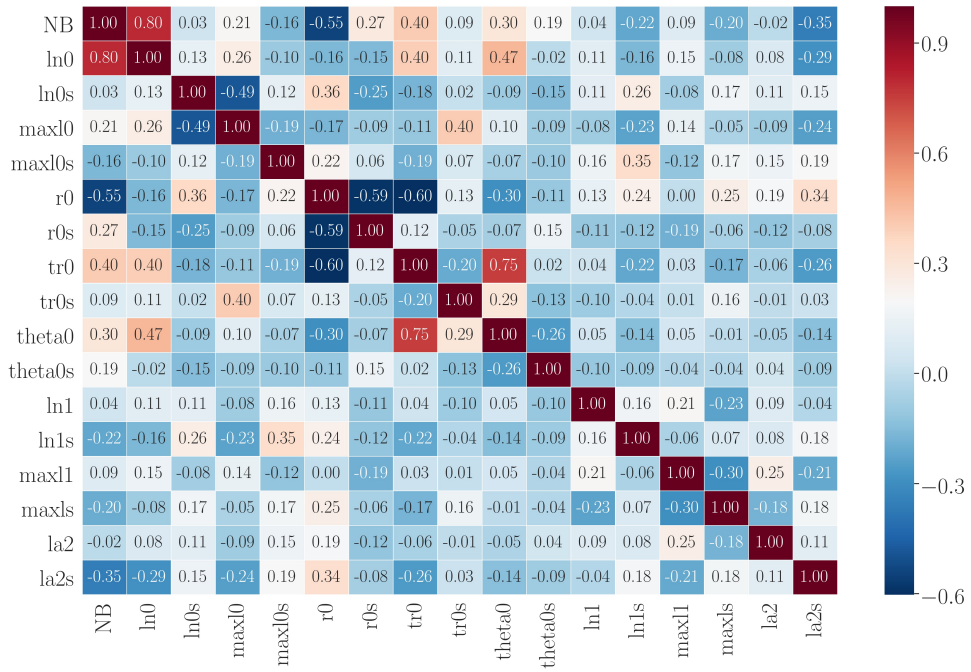


**Figure B.1:** Correlation matrix of all the inferred parameters. The Heat map shows the variation of correlations from higher negative correlations (blue) to higher positive correlations (red).

# Appendix C

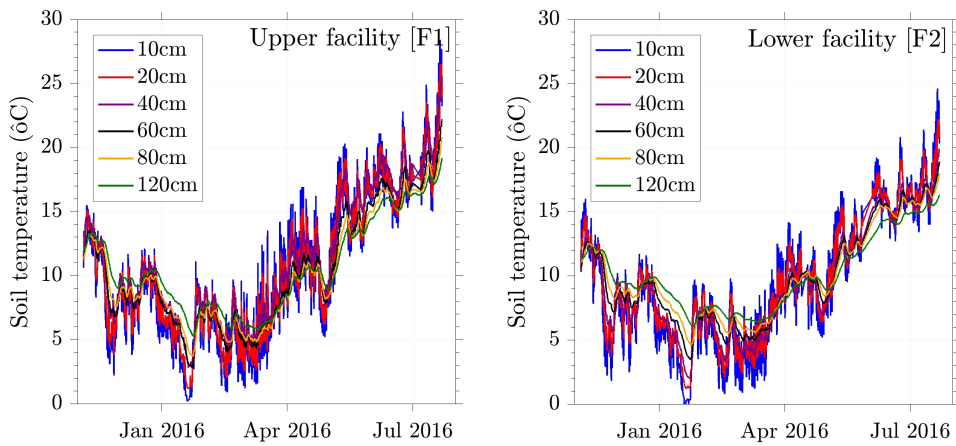


**Figure C.1:** Soil temperature changes during the study period of winter wheat growing season (Nov 2015-Jul 2016) measured by the MPS-2 sensors installed at the F1 facility (left) and the F2 facility (right).

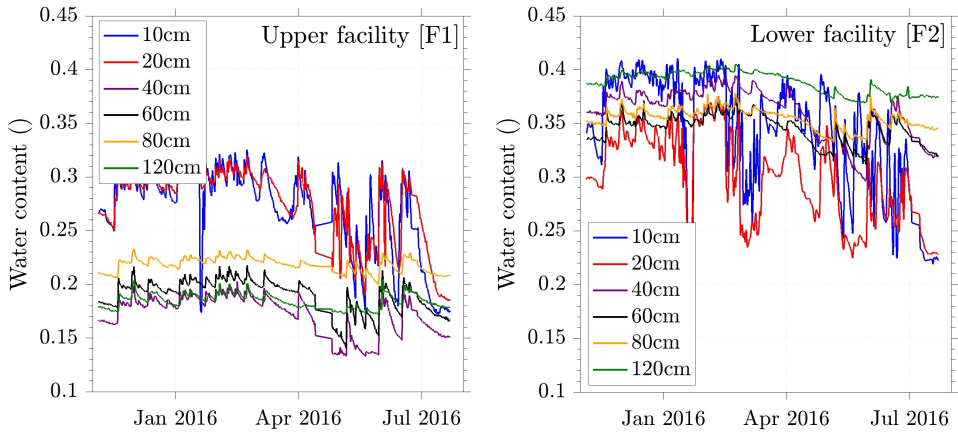


**Figure C.2:** Soil moisture content changes during the study period of winter wheat growing season (Nov 2015-Jul 2016) measured by the TDR sensors installed at the F1 facility (left) and the F2 facility (right).

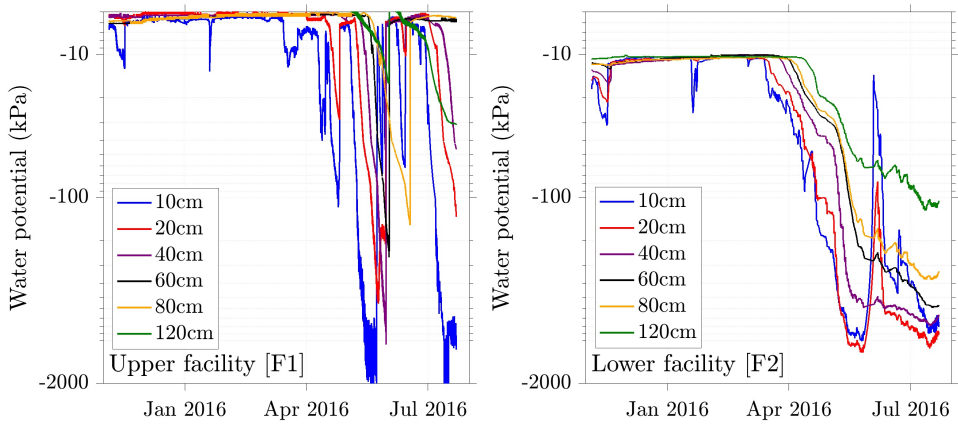


**Figure C.3:** Soil water potential changes during the study period of winter wheat growing season (Nov 2015-Jul 2016) measured by the MPS-2 sensors installed at the F1 facility (left) and the F2 facility (right).

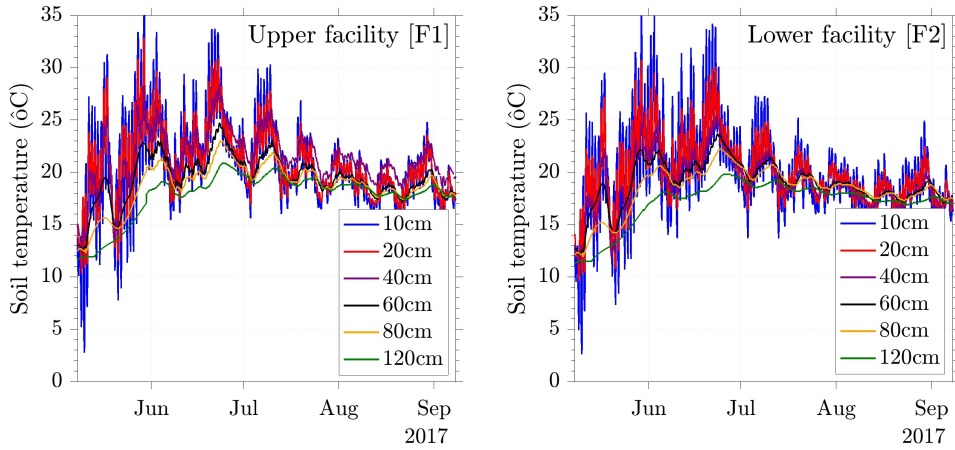


**Figure C.4:** Soil temperature changes during the study period of maize growing season (May 2017-Sep 2017) measured by the MPS-2 sensors installed at the F1 facility (left) and the F2 facility (right).

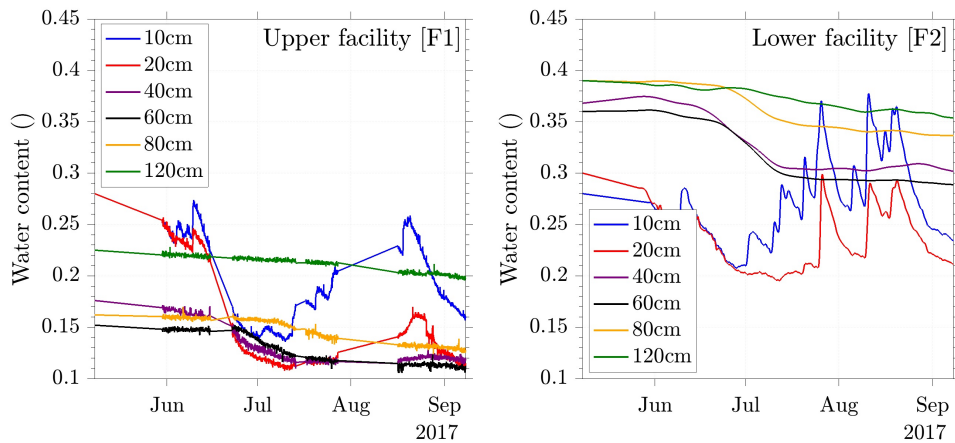


**Figure C.5:** Soil moisture content changes during the study period of maize growing season (May 2017-Sep 2017) measured by the TDR sensors installed at the F1 facility (left) and the F2 facility (right).

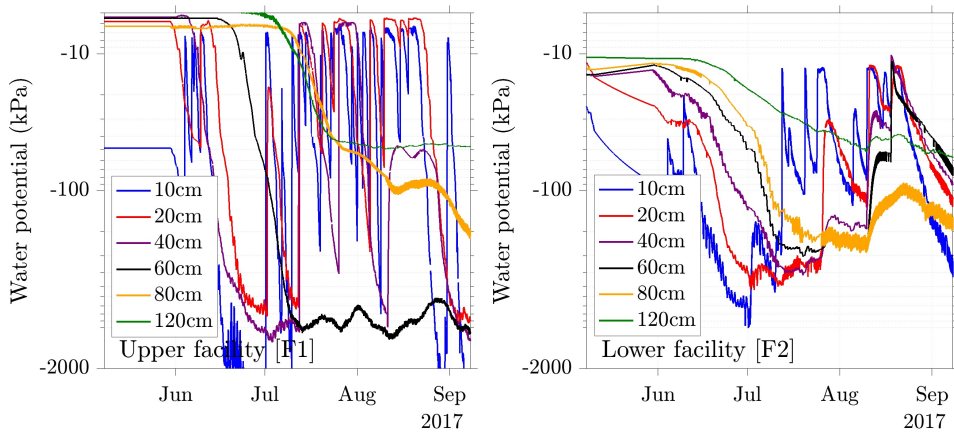


**Figure C.6:** Soil water potential changes during the study period of maize growing season (May 2017-Sep 2017) measured by the MPS-2 sensors installed at the F1 facility (left) and the F2 facility (right).

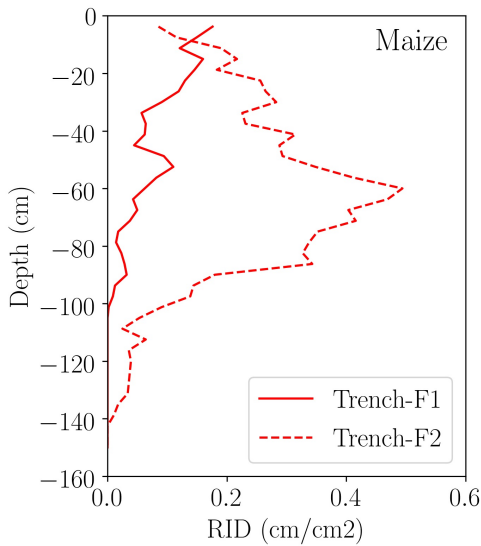


**Figure C.7:** Root intersection density distribution of maize at the end of the growing season measured by the trenching method. The solid red line indicate the measurements from the F1 facility, and the dashed red line indicate the F2 facility measurements.

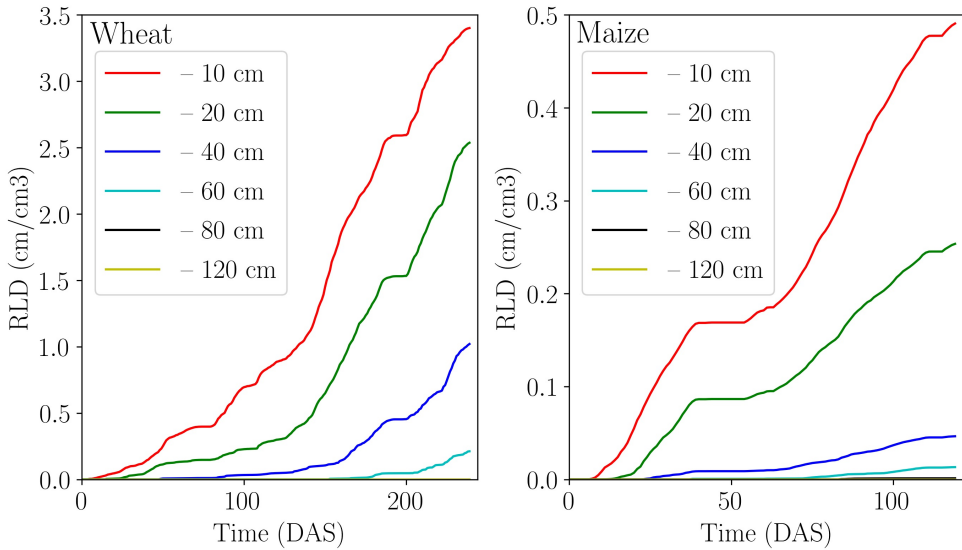


**Figure C.8:** Simulated mean root arrival curves for winter wheat during the 2015-2016 growing season (left) and 2017 maize growing season (right) based on measured soil properties of F1 facility.

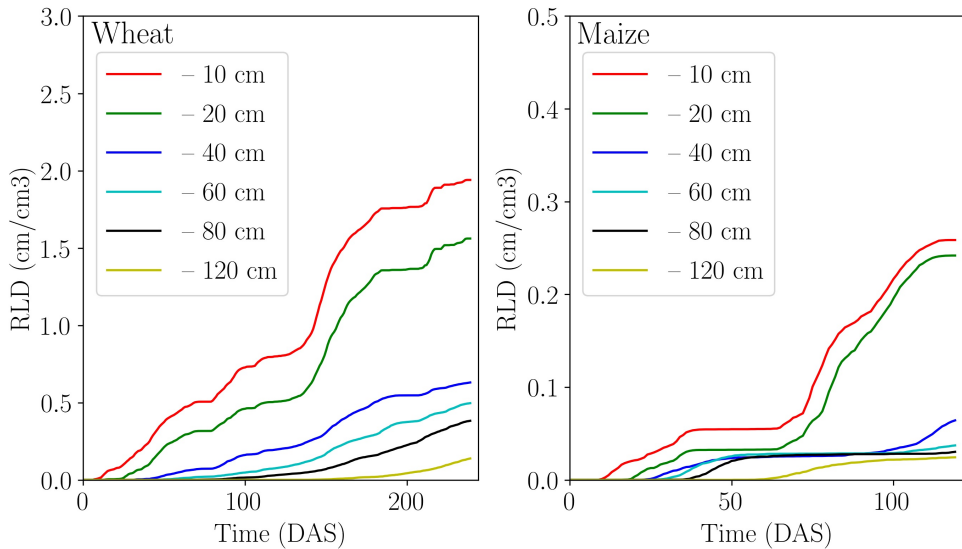


**Figure C.9:** Simulated mean root arrival curves for winter wheat during the 2015-2016 growing season (left) and 2017 maize growing season (right) based on measured soil properties of F2 facility.

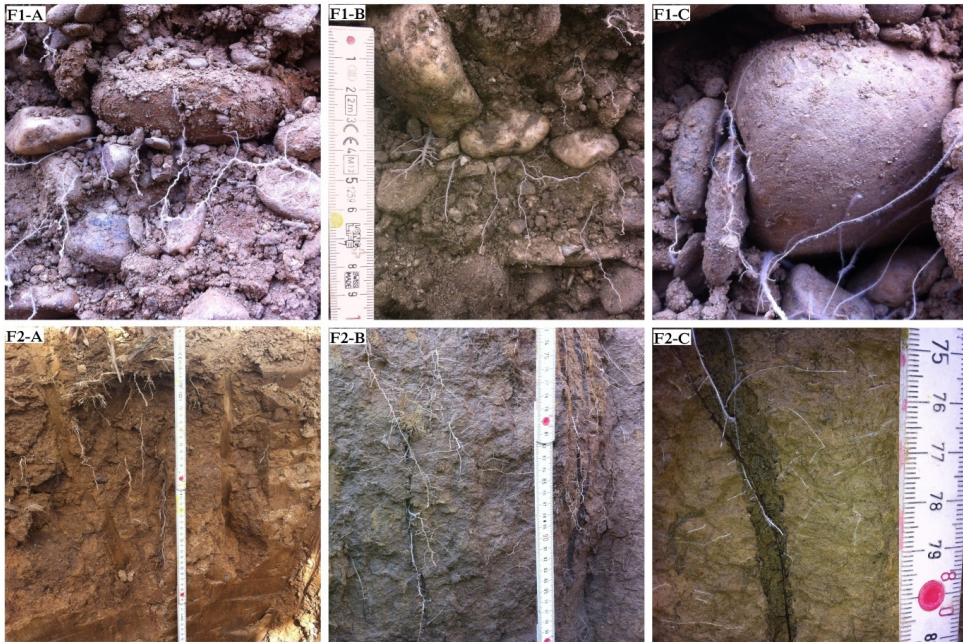


**Figure C.10:** Photographs showing macroscopic soil structures and rooting patterns of maize observed in the upper rhizotron facility (top) and the lower rhizotron facility (bottom). F1A, F1B, and F1C represent how the roots grow around large stones to find suitable paths. F2A demonstrates the root growth in a deep vertical crack. F2B shows the root growth on a vertical crack surface. F2C shows root growth inside a biopore and dead roots from the previous growing seasons

## Acknowledgement

My major gratitude goes to my supervisors Prof. Dr. Andrea Schnepf and Prof. Dr. Jan Vanderborght from Forschungszentrum Jülich for accepting me as a Ph.D. student, and for their guidance, motivation, enthusiasm, immense knowledge, dedication, patience and support during the past four years. I highly appreciate their suggestions, lots of discussions to understand the complex problems and advise which helped me to complete my Ph.D. dissertation. Besides my supervisors, I would like to thank the director of IBG-3, Prof. Dr. Harry Vereecken for his encouragement, insightful comments, and suggestions.

I gratefully appreciate the financial support from the project Transregional Collaborative Research Centre 32 (TR32), which is funded by the Deutsche Forschungsgemeinschaft (DFG) and the German Federal Employment Agency (Bundesagentur für Arbeit).

I am very grateful to Dr. Eric Laloy from Belgian Nuclear Research Centre (SCK-CEN) for providing DREAMzs code for inversion and his collaboration during the last three years. I really appreciate the support from Dr. Daniel Leitner from Simulationswerkstatt Linz (Austria) for helping me with the root architecture model CRootBox and the implementation of root growth functions in it. I am also thankful to Mukund ponkule and hardelauf Horst for their support for fixing the problems in codes and simulations, and Thomas Schuster for software installation and maintenance of my office computer.

I am very grateful for the support and the time spent together in the field with Gaochao Cai and Mirjam Zörner, including translating the abstract to the German version. I also wish to express my appreciation to the colleagues of IBG-3, especially for Cheng Sheng, Li Dazi, and Tian Jie. I express my gratitude to Normen Hermes, Huu Thuy Nguyen, Hubert Hüging for assistance to carry out field experiments. My gratitude also extends to the members of our research group Prof. Guillaume Lobet, Dr. Magdalena Landl, Asta Kunkel, Trung Hieu Mai, Xiao-Ran Zhou, Helena, Deepanshu, and Emil.

Finally, I would like to thank my parents and sisters family for their continuous support and encouragement throughout my academic life. I would also like to appreciate the free education system in Germany, without which I would not have realized my dream to further my studies.

Shehan Morandage  
Forschungszentrum Jülich  
December 2019

# Bibliography

- Alexander, K. G. and Miller, M. H. (1991). The effect of soil aggregate size on early growth and shoot-root ratio of maize (*Zea mays* L.). *Plant and Soil*, 138(2):189–194.
- Araus, J. L. and Cairns, J. E. (2014). Field high-throughput phenotyping: the new crop breeding frontier. *Trends Plant Sci*, 19(1):52–61.
- Atkinson, J. A., Pound, M. P., Bennett, M. J., and Wells, D. M. (2019). Uncovering the hidden half of plants using new advances in root phenotyping. *Curr Opin Biotechnol*, 55:1–8.
- Ayachit, U. (2015). *The ParaView Guide: A Parallel Visualization Application*. Kitware.
- Azevedo, M. C. B. d., Chopart, J. L., and Medina, C. d. C. (2011). Sugarcane root length density and distribution from root intersection counting on a trench-profile. *Scientia Agricola*, 68:94–101.
- Bardgett, R. D., Mommer, L., and De Vries, F. T. (2014). Going underground: root traits as drivers of ecosystem processes. *Trends in Ecology & Evolution*, 29(12):692–699.
- Bengough, A. G., Bransby, M. F., Hans, J., McKenna, S. J., Roberts, T. J., and Valentine, T. A. (2005). Root responses to soil physical conditions; growth dynamics from field to cell. *Journal of Experimental Botany*, 57(2):437–447.
- Bengough, A. G., Bransby, M. F., Hans, J., McKenna, S. J., Roberts, T. J., and Valentine, T. A. (2006). Root responses to soil physical conditions; growth dynamics from field to cell. *J Exp Bot*, 57(2):437–47.
- Bengough, A. G., Croser, C., and Pritchard, J. (1997). A biophysical analysis of root growth under mechanical stress. *Plant and Soil*, 189(1):155–164.
- Bengough, A. G., Loades, K., and McKenzie, B. M. (2016). Root hairs aid soil penetration by anchoring the root surface to pore walls. *J Exp Bot*, 67(4):1071–8.

- Bengough, A. G., McKenzie, B. M., Hallett, P. D., and Valentine, T. A. (2011). Root elongation, water stress, and mechanical impedance: a review of limiting stresses and beneficial root tip traits. *Journal of Experimental Botany*, 62(1):59–68.
- Bingham, I. J. and Bengough, A. G. (2003). Morphological plasticity of wheat and barley roots in response to spatial variation in soil strength. *Plant and Soil*, 250(2):273–282.
- Bizet, F., Bengough, A. G., Hummel, I., Bogeat-Triboulot, M. B., and Dupuy, L. X. (2016). 3D deformation field in growing plant roots reveals both mechanical and biological responses to axial mechanical forces. *J Exp Bot*, 67(19):5605–5614.
- Bodner, G., Alsalem, M., Nakhforoosh, A., Arnold, T., and Leitner, D. (2017). RGB and Spectral Root Imaging for Plant Phenotyping and Physiological Research: Experimental Setup and Imaging Protocols. *J Vis Exp*, (126).
- Bodner, G., Nakhforoosh, A., Arnold, T., and Leitner, D. (2018). Hyperspectral imaging: a novel approach for plant root phenotyping. *Plant Methods*, 14(84):17.
- Bodner, G., Nakhforoosh, A., and Kaul, H.-P. (2015). Management of crop water under drought: a review. *Agronomy for Sustainable Development*, 35(2):401–442.
- Böhm, W. (1979a). *Excavation Methods*, pages 5–19. Springer Berlin Heidelberg, Berlin, Heidelberg.
- Böhm, W. (1979b). *Profile Wall Methods*, volume 33 of *Ecological Studies (Analysis and Synthesis)*, book section 6, pages 48–60. Springer, Berlin, Heidelberg.
- Bouma, T. J., Nielsen, K. L., and Koutstaal, B. (2000). Sample preparation and scanning protocol for computerised analysis of root length and diameter. *Plant and Soil*, 218(1):185–196.
- Bucksch, A., Burridge, J., York, L. M., Das, A., Nord, E., Weitz, J. S., and Lynch, J. P. (2014). Image-based high-throughput field phenotyping of crop roots. *Plant Physiol*, 166(2):470–86.
- Buczko, U., Kuchenbuch, R. O., and Gerke, H. H. (2008). Evaluation of a core sampling scheme to characterize root length density of maize. *Plant and Soil*, 316(1):205.
- Buttery, B. R., Tan, C. S., Drury, C. F., Park, S. J., Armstrong, R. J., and Park, K. Y. (1998). The effects of soil compaction, soil moisture and soil type on growth and nodulation of soybean and common bean. *Canadian Journal of Plant Science*, 78(4):571–576.

- Cai, G., Vanderborght, J., Klotzsche, A., van der Kruk, J., Neumann, J., Hermes, N., and Vereecken, H. (2016). Construction of Minirhizotron Facilities for Investigating Root Zone Processes. *Vadose Zone Journal*, 15.
- Cai, G., Vanderborght, J., Langensiepen, M., Schnepf, A., Hüging, H., and Vereecken, H. (2018). Root growth, water uptake, and sap flow of winter wheat in response to different soil water conditions. *Hydrology and Earth System Sciences*, 22(4):2449–2470.
- Campolongo, F., Cariboni, J., and Saltelli, A. (2007). An effective screening design for sensitivity analysis of large models. *Environmental Modelling & Software*, 22(10):1509–1518.
- Chen, J., Liu, L., Wang, Z., Sun, H., Zhang, Y., Lu, Z., and Li, C. (2018). Determining the effects of nitrogen rate on cotton root growth and distribution with soil cores and minirhizotrons. *PLOS ONE*, 13(5):1–14.
- Chen, X., Ding, Q., Błaszczewicz, Z., Sun, J., Sun, Q., He, R., and Li, Y. (2017). Phenotyping for the dynamics of field wheat root system architecture. *Scientific Reports*, 7.
- Clark, R. T., MacCurdy, R. B., Jung, J. K., Shaff, J. E., McCouch, S. R., Aneshansley, D. J., and Kochian, L. V. (2011). Three-Dimensional Root Phenotyping with a Novel Imaging and Software Platform. *Plant Physiology*, 156(2):455–465.
- Clausnitzer, V. and Hopmans, J. W. (1994). Simultaneous modeling of transient three-dimensional root growth and soil water flow. *Plant and Soil*, 164(2):299–314.
- Colombi, T., Kirchgessner, N., Walter, A., and Keller, T. (2017). Root Tip Shape Governs Root Elongation Rate under Increased Soil Strength. *Plant Physiol*, 174(4):2289–2301.
- Comas, L. H., Becker, S. R., Cruz, V. M. V., Byrne, P. F., and Dierig, D. A. (2013). Root traits contributing to plant productivity under drought. *Frontiers in Plant Science*, 4:442.
- Correa, J., Postma, J. A., Watt, M., and Wojciechowski, T. (2019). Soil compaction and the architectural plasticity of root systems. *Journal of Experimental Botany*, 70(21):6019–6034.
- Couvreur, V., Vanderborght, J., Beff, L., and Javaux, M. (2014). Horizontal soil water potential heterogeneity: simplifying approaches for crop water dynamics models. *Hydrol. Earth Syst. Sci.*, 18(5):1723–1743. HESS.

- Creber, H., Davies, M., and Francis, D. (1993). Effects of temperature on cell division in root meristems of natural populations of *Dactylis glomerata* of contrasting latitudinal origins. *Environmental and Experimental Botany*, 33(3):433 – 442.
- de Dorlodot, S., Forster, B., Pagés, L., Price, A., Tuberosa, R., and Draye, X. (2007). Root system architecture: opportunities and constraints for genetic improvement of crops. *Trends in Plant Science*, 12(10):474–481.
- de Moraes, M. T., Bengough, A. G., Debiassi, H., Franchini, J. C., Levien, R., Schnepf, A., and Leitner, D. (2018). Mechanistic framework to link root growth models with weather and soil physical properties, including example applications to soybean growth in Brazil. *Plant and Soil*, 428(1-2):67–92.
- De Ruijter, F. J., Veen, B. W., and Van Oijen, M. (1996). A comparison of soil core sampling and minirhizotrons to quantify root development of field-grown potatoes. *Plant and Soil*, 182(2):301–312.
- Del Bianco, M. and Kepinski, S. (2018). Building a future with root architecture. *J Exp Bot*, 69(22):5319–5323.
- Dexter, A. R. and Hewitt, J. S. (1978). The deflection of plant roots. *Journal of Agricultural Engineering Research*, 23(1):17–22.
- Dietrich, D. (2018). Hydrotropism: how roots search for water. *Journal of Experimental Botany*, 69(11):2759–2771.
- Donald, R. G., Kay, B. D., and Miller, M. H. (1987). The Effect of Soil Aggregate Size on Early Shoot and Root-Growth of Maize (*Zea-Mays-L*). *Plant and Soil*, 103(2):251–259.
- Drennan, P. M. and Nobel, P. S. (1998). Root growth dependence on soil temperature for *Opuntia ficus-indica*: influences of air temperature and a doubled CO<sub>2</sub> concentration. *Functional Ecology*, 12(6):959–964.
- Dunbabin, V. M., Postma, J. A., Schnepf, A., Pagés, L., Javaux, M., Wu, L., Leitner, D., Chen, Y. L., Rengel, Z., and Diggle, A. J. (2013). Modelling root–soil interactions using three–dimensional models of root growth, architecture and function. *Plant and Soil*, 372(1):93–124.
- Dupuy, L., Gregory, P. J., and Bengough, A. G. (2010). Root growth models: towards a new generation of continuous approaches. *Journal of Experimental Botany*, 61(8):2131–2143.

- Eavis, B. W. (1972). Soil physical conditions affecting seedling root growth. *Plant and Soil*, 36(1-3):613–622.
- Ellis, B. and Kummerow, J. (1982). Temperature effect on growth rates of *Eriophorum vaginatum* roots. *Oecologia*, 54:136–137.
- Ephrath, J. E., Silberbush, M., and Berliner, P. R. (1999). Calibration of minirhizotron readings against root length density data obtained from soil cores. *Plant and Soil*, 209:201–208.
- Fakih, M., Delenne, J.-Y., Radjai, F., and Fourcaud, T. (2017). Modeling root growth in granular soils: effects of root stiffness and packing fraction. volume 140, page 14013.
- Falik, O., Reides, P., Gersani, M., and Novoplansky, A. (2005). Root navigation by self inhibition. *Plant, Cell & Environment*, 28(4):562–569.
- Fan, J. L., McConkey, B., Wang, H., and Janzen, H. (2016). Root distribution by depth for temperate agricultural crops. *Field Crops Research*, 189:68–74.
- Fan, Y., Miguez-Macho, G., Jobbágy, E. G., Jackson, R. B., and Otero-Casal, C. (2017). Hydrologic regulation of plant rooting depth. *Proceedings of the National Academy of Sciences*, 114(40):10572–10577.
- Fang, S., Clark, R., and Liao, H. (2012). *3D Quantification of Plant Root Architecture In Situ*, pages 135–148. Springer Berlin Heidelberg, Berlin, Heidelberg.
- Feldman, L. (1994). *The Maize Root*, pages 29–37. Springer New York, New York, NY.
- Figuroa-Bustos, V., Palta, A. J., Chen, Y., and Siddique, H. M. K. (2018). Characterization of Root and Shoot Traits in Wheat Cultivars with Putative Differences in Root System Size. *Agronomy*, 8(7).
- Frasier, I., Noellemeyer, E., Fernández, R., and Quiroga, A. (2016). Direct field method for root biomass quantification in agroecosystems. *MethodsX*, 3:513–519.
- Gao, W., Hodgkinson, L., Jin, K., Watts, C. W., Ashton, R. W., Shen, J., Ren, T., Dodd, I. C., Binley, A., Phillips, A. L., Hedden, P., Hawkesford, M. J., and Whalley, W. R. (2016). Deep roots and soil structure. *Plant Cell Environ*, 39(8):1662–8.
- Gao, Y., Duan, A., Qiu, X., Liu, Z., Sun, J., Zhang, J., and Wang, H. (2010). Distribution of roots and root length density in a maize/soybean strip intercropping system. *Agricultural Water Management*, 98(1):199–212.

- Garré, S., Pagés, L., Laloy, E., Javaux, M., Vanderborght, J., and Vereecken, H. (2012). Parameterizing a Dynamic Architectural Model of the Root System of Spring Barley from Minirhizotron Data. *Vadose Zone Journal*, 11(4).
- Gelman, A. and Rubin, D. B. (1992). Inference from Iterative Simulation Using Multiple Sequences. *Statistical Science*, 7(4):457–472.
- Gilland, B. (2002). World population and food supply: can food production keep pace with population growth in the next half-century? *Food Policy*, 27(1):47–63.
- Glab, T. (2011). Effect of soil compaction on root system morphology and productivity of alfalfa (*Medicago sativa* L.). *Polish Journal of Environmental Studies*, 20(6):1473–1480.
- Gorim, L. Y. and Vandenberg, A. (2017). Root Traits, Nodulation and Root Distribution in Soil for Five Wild Lentil Species and *Lens culinaris* (Medik.) Grown under Well-Watered Conditions. *Front Plant Sci*, 8:1632.
- Grabarnik, P., Pagès, L., and Bengough, A. G. (1998). Geometrical properties of simulated maize root systems: consequences for length density and intersection density. *Plant and Soil*, 200(2):157–167.
- Grant, R. F. (1993). Simulation model of soil compaction and root growth. *Plant and Soil*, 150(1):1–14.
- Gregory, P. (2009). Measuring root system architecture: Opportunities and challenges.
- Gregory, P. J. (2006). *Roots and the Architecture of Root Systems*, pages 18–44. Blackwell Publishing Ltd.
- Grismer, M. E. (1992). Cracks in irrigated clay soil may allow some drainage. *California Agriculture*, 46(5):9–11.
- Haling, R. E., Simpson, R. J., Culvenor, R. A., Lambers, H., and Richardson, A. E. (2011). Effect of soil acidity, soil strength and macropores on root growth and morphology of perennial grass species differing in acid-soil resistance. *Plant Cell Environ*, 34(3):444–56.
- Hamada, A., Nitta, M., Nasuda, S., Kato, K., Fujita, M., Matsunaka, H., and Okumoto, Y. (2012). Novel QTLs for growth angle of seminal roots in wheat (*Triticum aestivum* L.). *Plant and Soil*, 354(1):395–405.
- Han, E., Kautz, T., Perkons, U., Uteau, D., Peth, S., Huang, N., Horn, R., and Köpke, U. (2015). Root growth dynamics inside and outside of soil biopores as affected by

- crop sequence determined with the profile wall method. *Biology and Fertility of Soils*, 51:847–856.
- Hang Lai Thi Thu, Köpke Ulrich, K. T. (2011). Quantifying root length density from soil auger samples: comparison of methods and effects of sample size. Master's thesis, Rheinische Friedrich-Wilhelms-Universität Bonn.
- Hartmann, A., Šimůnek, J., Aidoo, M. K., Seidel, S. J., and Lazarovitch, N. (2018). Implementation and Application of a Root Growth Module in HYDRUS. *Vadose Zone Journal*, 17.
- Hines, K. E. (2015). A primer on Bayesian inference for biophysical systems. *Biophys J*, 108(9):2103–13.
- Hoad, S., Russell, G., Kettlewell, P., and Belshaw, M. (2004). Root system management in winter wheat: practices to increase water and nitrogen use. Report, The Home-Grown Cereals Authority.
- Hochholdinger, F. (2016). Untapping root system architecture for crop improvement. *J Exp Bot*, 67(15):4431–3.
- Hochholdinger, F. and Tuberosa, R. (2009). Genetic and genomic dissection of maize root development and architecture. *Current Opinion in Plant Biology*, 12(2):172–177.
- Hodgkinson, L., Dodd, I. C., Binley, A., Ashton, R. W., White, R. P., Watts, C. W., and Whalley, W. R. (2017). Root growth in field-grown winter wheat: Some effects of soil conditions, season and genotype. *Eur J Agron*, 91:74–83.
- Houlbrooke, D. J., Thom, E. R., Chapman, R., and McLay, C. D. A. (1997). A study of the effects of soil bulk density on root and shoot growth of different ryegrass lines. *New Zealand Journal of Agricultural Research*, 40(4):429–435.
- Huang, B.-R., Taylor, H., and McMichael, B. (1991). Growth and development of seminal and crown roots of wheat seedlings as affected by temperature. *Environmental and Experimental Botany*, 31(4):471 – 477.
- Hulugalle, N., Broughton, K., and Tan, D. (2015). Root growth of irrigated summer crops in cotton-based farming systems sown in Vertosols of northern New South Wales. *Crop and Pasture Science*, 66:158–167.
- Illston, B. G. and Fiebrich, C. A. (2017). Horizontal and vertical variability of observed soil temperatures. *Geoscience Data Journal*, 4(1):40–46.

- Javaux, M., Schröder, T., Vanderborght, J., and Vereecken, H. (2008). Use of a Three-Dimensional Detailed Modeling Approach for Predicting Root Water Uptake. *Vadose Zone Journal*, 7(3).
- Jin, K., Shen, J., Ashton, R. W., Dodd, I. C., Parry, M. A., and Whalley, W. R. (2013). How do roots elongate in a structured soil? *J Exp Bot*, 64(15):4761–77.
- Judd, L. A., Jackson, B. E., and Fonteno, W. C. (2015). Advancements in Root Growth Measurement Technologies and Observation Capabilities for Container-Grown Plants. *Plants (Basel)*, 4(3):369–92.
- Kalogiros, D. I., Adu, M. O., White, P. J., Broadley, M. R., Draye, X., Ptashnyk, M., Bengough, A. G., and Dupuy, L. X. (2016). Analysis of root growth from a phenotyping data set using a density-based model. *Journal of Experimental Botany*, 67(4):1045–1058.
- Kaspar, T. C. and Bland, W. L. (1992). SOIL TEMPERATURE AND ROOT GROWTH. *Soil Science*, 154(4).
- Kc, K. B., Dias, G. M., Veeramani, A., Swanton, C. J., Fraser, D., Steinke, D., Lee, E., Wittman, H., Farber, J. M., Dunfield, K., McCann, K., Anand, M., Campbell, M., Rooney, N., Raine, N. E., Acker, R. V., Hanner, R., Pascoal, S., Sharif, S., Benton, T. G., and Fraser, E. D. G. (2018). When too much isn't enough: Does current food production meet global nutritional needs? *PLOS ONE*, 13(10):e0205683.
- Kücke, M., Schmid, H., and Spiess, A. (1995). A comparison of four methods for measuring roots of field crops in three contrasting soils. *Plant and Soil*, 172(1):63–71.
- Kirby, J. and Bengough, A. (2002). Influence of soil strength on root growth: experiments and analysis using a critical-state model. *European Journal of Soil Science*, 53(1):119–127.
- Kolb, L. N., Gallandt, E. R., and Mallory, E. B. (2017). Impact of Spring Wheat Planting Density, Row Spacing, and Mechanical Weed Control on Yield, Grain Protein, and Economic Return in Maine. *Weed Science*, 60(2):244–253.
- Kuchenbuch, R. O., Gerke, H. H., and Buczko, U. (2009). Spatial distribution of maize roots by complete 3D soil monolith sampling. *Plant and Soil*, 315(1):297–314.
- Kuijken, R. C. P., van Eeuwijk, F. A., Marcelis, L. F. M., and Bouwmeester, H. J. (2015). Root phenotyping: from component trait in the lab to breeding. *Journal of Experimental Botany*, 66(18):5389–5401.

- Kumar, K., Prihar, S. S., and Gajri, P. R. (1993). Determination of root distribution of wheat by auger sampling. *Plant and Soil*, 149(2):245–253.
- Kutschera, L. (1960). *Wurzelatlas mitteleuropäischer Ackerunkräuter und Kulturpflanzen*, page 574. DLG-Verlags-G.m.b.H., Frankfurt/M.
- Laboski, C., Dowdy, R., Allmaras, R., and Lamb, J. (1998). Soil strength and water content influences on corn root distribution in a sandy soil. *Plant and Soil*, 203(2):239–247.
- Laloy, E., Herault, R., Lee, J., Jacques, D., and Linde, N. (2017). Inversion using a new low-dimensional representation of complex binary geological media based on a deep neural network. *Advances in Water Resources*, 110:387–405.
- Laloy, E. and Vrugt, J. A. (2012). High-dimensional posterior exploration of hydrologic models using multiple-try DREAM<sub>(ZS)</sub> and high-performance computing. *Water Resources Research*, 48(1).
- Landl, M., Huber, K., Schnepf, A., Vanderborght, J., Javaux, M., Glyn Bengough, A., and Vereecken, H. (2017). A new model for root growth in soil with macropores. *Plant and Soil*, 415(1):99–116.
- Landl, M., Schnepf, A., Vanderborght, J., Bengough, A. G., Bauke, S. L., Lobet, G., Bol, R., and Vereecken, H. (2018). Measuring root system traits of wheat in 2D images to parameterize 3D root architecture models. *Plant and Soil*, 425(1):457–477.
- Leitner, D., Felderer, B., Vontobel, P., and Schnepf, A. (2014). Recovering Root System Traits Using Image Analysis Exemplified by Two-Dimensional Neutron Radiography Images of Lupine. *Plant Physiology*, 164(1):24–35.
- Leitner, D., Klepsch, S., Bodner, G., and Schnepf, A. (2010). A dynamic root system growth model based on L-Systems. *Plant and Soil*, 332(1):177–192.
- Leong, L.-S. and Savage, V. R. (2013). *THE SECOND GREEN REVOLUTION: A REVIEW OF THE CHALLENGES AND PROSPECTS*, pages 405–437. WORLD SCIENTIFIC.
- Liao, R., Bai, Y., Liang, H., An, S., Ren, S., Cao, Y., Le, Z., Lu, J., and Liu, J. (2015). Root growth of maize as studied with minirhizotrons and monolith methods. *Archives of Agronomy and Soil Science*, 61(10):1343–1356.
- Lipiec, J., Siczek, A., Sochan, A., and Bieganski, A. (2016). Effect of sand grain shape on root and shoot growth of wheat seedlings. *Geoderma*, 265(Supplement C):1–5.

- Lobet, G., Pound, M. P., Diener, J., Pradal, C., Draye, X., Godin, C., Javaux, M., Leitner, D., Meunier, F., Nacry, P., Pridmore, T. P., and Schnepf, A. (2015). Root System Markup Language: Toward a Unified Root Architecture Description Language. *Plant Physiology*, 167(3):617–627.
- Lynch, J. (1995). Root Architecture and Plant Productivity. *Plant Physiology*, 109(1):7–13.
- Lynch, J. P. (2007). Roots of the Second Green Revolution. *Australian Journal of Botany*, 55(5):493–512.
- Lynch, J. P. (2013). Steep, cheap and deep: an ideotype to optimize water and N acquisition by maize root systems. *Ann Bot*, 112(2):347–57.
- Macduff, J. H., Wild, A., Hopper, M. J., and Dhanoa, M. S. (1986). Effects of temperature on parameters of root growth relevant to nutrient uptake: Measurements on oilseed rape and barley grown in flowing nutrient solution. *Plant and Soil*, 94(3):321–332.
- Maeght, J.-L., Rewald, B., and Pierret, A. (2013). How to study deep roots—and why it matters. *Frontiers in Plant Science*, 4:299.
- Majdi, H. (1996). Root sampling methods - Applications and limitations of the minirhizotron technique. *Plant and Soil*, 185(2):255–258.
- Majdi, H., Smucker, A. J. M., and Persson, H. (1992). A comparison between minirhizotron and monolith sampling methods for measuring root growth of maize (*Zea mays* L.). *Plant and Soil*, 147(1):127–134.
- Masle, J. and Passioura, J. (1987). The Effect of Soil Strength on the Growth of Young Wheat Plants. *Functional Plant Biology*, 14:643–656.
- McMichael, B. and Quisenberry, J. (1993). The impact of the soil environment on the growth of root systems. *Environmental and Experimental Botany*, 33(1):53 – 61.
- Meister, R., Rajani, M. S., Ruzicka, D., and Schachtman, D. P. (2014). Challenges of modifying root traits in crops for agriculture. *Trends Plant Sci*, 19(12):779–88.
- Mekonnen, K., Buresh, R. J., and Jama, B. (1997). Root and inorganic nitrogen distributions in sesbania fallow, natural fallow and maize fields. *Plant and Soil*, 188(2):319–327.
- Meunier, F., Couvreur, V., Draye, X., Vanderborght, J., and Javaux, M. (2017). Towards quantitative root hydraulic phenotyping: novel mathematical functions to calculate plant-scale hydraulic parameters from root system functional and structural traits. *Journal of Mathematical Biology*, 75(5):1133–1170.

- Morandage, S., Schnepf, A., Leitner, D., Javaux, M., Vereecken, H., and Vanderborght, J. (2019). Parameter sensitivity analysis of a root system architecture model based on virtual field sampling. *Plant and Soil*, 438(1-2):101–126.
- Morris, E. C., Griffiths, M., Golebiowska, A., Mairhofer, S., Burr-Hersey, J., Goh, T., von Wangenheim, D., Atkinson, B., Sturrock, C. J., Lynch, J. P., Vissenberg, K., Ritz, K., Wells, D. M., Mooney, S. J., and Bennett, M. J. (2017). Shaping 3D Root System Architecture. *Curr Biol*, 27(17):R919–R930.
- Morris, M. D. (1991). Factorial Sampling Plans for Preliminary Computational Experiments. *Technometrics*, 33(2):161–174.
- Muñoz Romero, V., Benítez-Vega, J., López-Bellido, R. J., Fontán, J. M., and López-Bellido, L. (2010). Effect of tillage system on the root growth of spring wheat. *Plant and Soil*, 326(1):97–107.
- Nagel, K. A., Kastenholz, B., Jahnke, S., van Dusschoten, D., Aach, T., Mühlich, M., Truhn, D., Scharr, H., Terjung, S., Walter, A., and Schurr, U. (2009). Temperature responses of roots: impact on growth, root system architecture and implications for phenotyping. *Functional Plant Biology*, 36(11):947–959.
- Nakamoto, T. (2000). The Distribution of Wheat and Maize Roots as Influenced by Biopores in a Subsoil of the Kanto Loam Type. *Plant Production Science*, 3(2):140–144.
- Naseri, M., Iden, S. C., Richter, N., and Durner, W. (2019). Influence of Stone Content on Soil Hydraulic Properties: Experimental Investigation and Test of Existing Model Concepts. *Vadose Zone Journal*, 18.
- Nations, U. (2019). *The Sustainable Development Goals Report 2019*.
- Ndour, A., Vadez, V., Pradal, C., and Lucas, M. (2017). Virtual Plants Need Water Too: Functional-Structural Root System Models in the Context of Drought Tolerance Breeding. *Front Plant Sci*, 8:1577.
- Onderdonk, J. J. and Ketcheson, J. W. (1973). Effect of soil temperature on direction of corn root growth. *Plant and Soil*, 39(1):177–186.
- Onwuka, B. (2016). Effects of soil temperature on Some Soil properties and plant growth. *Journal of Agricultural Science and Technology*.
- Osher, S. and Fedkiw, R. (2003). *Signed Distance Functions*, pages 17–22. Springer New York, New York, NY.

- Paez-Garcia, A., Motes, C. M., Scheible, W. R., Chen, R., Blancaflor, E. B., and Monteros, M. J. (2015). Root Traits and Phenotyping Strategies for Plant Improvement. *Plants (Basel)*, 4(2):334–55.
- Pagenkemper, S. K., Puschmann, D. U., Peth, S., and Horn, R. (2014). Investigation of Time Dependent Development of Soil Structure and Formation of Macropore Networks as Affected by Various Precrop Species. *International Soil and Water Conservation Research*, 2(2):51–66.
- Pagés, L., Bruchou, C., and Garré, S. (2012). Links Between Root Length Density Profiles and Models of the Root System Architecture. *Vadose Zone Journal*, 11(4).
- Pagés, L. and Picon-Cochard, C. (2014). Modelling the root system architecture of Poaceae. Can we simulate integrated traits from morphological parameters of growth and branching? *New Phytologist*, 204(1):149–158.
- Pagés, L., Vercambre, G., Drouet, J.-L., Lecompte, F., Collet, C., and Le Bot, J. (2004). Root Typ: a generic model to depict and analyse the root system architecture. *Plant and Soil*, 258(1):103–119.
- Pagés, L., Xie, J., and Serra, V. (2013). Potential and actual root growth variations in root systems: modeling them with a two-step stochastic approach. *Plant and Soil*, 373(1):723–735.
- Palta, J., M, L., and IRP, F. (2004). Rooting patterns in wheat differing in vigour is related to the early uptake of nitrogen in deep sandy soils.
- Pardo, A., Amato, M., and Chiarandà, F. Q. (2000). Relationships between soil structure, root distribution and water uptake of chickpea (*Cicer arietinum* L.). Plant growth and water distribution. *European Journal of Agronomy*, 13(1):39–45.
- Parker, C. J., Carr, M. K. V., Jarvis, N. J., Puplampu, B. O., and Lee, V. H. (1991). An evaluation of the minirhizotron technique for estimating root distribution in potatoes. *The Journal of Agricultural Science*, 116(3):341–350.
- Passioura, J. B. (2002). ‘Soil conditions and plant growth. *Plant, Cell & Environment*, 25(2):311–318.
- Passot, S., Couvreur, V., Meunier, F., Draye, X., Javaux, M., Leitner, D., Pagès, L., Schnepf, A., Vanderborght, J., and Lobet, G. (2018). Connecting the dots between computational tools to analyse soil–root water relations. *Journal of Experimental Botany*, 70(9):2345–2357.

- Perkons, U., Kautz, T., Uteau, D., Peth, S., Geier, V., Thomas, K., Lütke Holz, K., Athmann, M., Pude, R., and Köpke, U. (2014). Root-length densities of various annual crops following crops with contrasting root systems. *Soil and Tillage Research*, 137(Supplement C):50–57.
- Pierret, A., Doussan, C., Capowiez, Y., Bastardie, F., and Pages, L. (2007). Root functional architecture: A framework for modeling the interplay between roots and soil. *Vadose Zone Journal*, 6(2):269–281.
- Pingali, P. L. (2012). Green Revolution: Impacts, limits, and the path ahead. *Proceedings of the National Academy of Sciences*, 109(31):12302–12308.
- Popova, L., Tonazzini, A., Russino, A., Sadeghi, A., and Mazzolai, B. (2013). *Embodied Behavior of Plant Roots in Obstacle Avoidance*, pages 431–433. Springer Berlin Heidelberg, Berlin, Heidelberg.
- Popova, L., van Dusschoten, D., Nagel, K. A., Fiorani, F., and Mazzolai, B. (2016). Plant root tortuosity: an indicator of root path formation in soil with different composition and density. *Ann Bot*, 118(4):685–698.
- Porter, J. R. and Gawith, M. (1999). Temperatures and the growth and development of wheat: a review. *European Journal of Agronomy*, 10(1):23–36.
- Postic, F., Beauchêne, K., Gouache, D., and Doussan, C. (2019). Scanner-Based Minirhizotrons Help to Highlight Relations between Deep Roots and Yield in Various Wheat Cultivars under Combined Water and Nitrogen Deficit Conditions. *Agronomy*, 9(6):1–19.
- Postma, J. A., Kuppe, C., Owen, M. R., Mellor, N., Griffiths, M., Bennett, M. J., Lynch, J. P., and Watt, M. (2017). OpenSimRoot: widening the scope and application of root architectural models. *The New phytologist*, 215(3):1274–1286.
- Postma, J. A. and Lynch, J. P. (2011). Root Cortical Aerenchyma Enhances the Growth of Maize on Soils with Suboptimal Availability of Nitrogen, Phosphorus, and Potassium. *Plant Physiology*, 156(3):1190–1201.
- Postma, J. A. and Lynch, J. P. (2012). Complementarity in root architecture for nutrient uptake in ancient maize/bean and maize/bean/squash polycultures. *Ann Bot*, 110(2):521–34.
- Power, A. G. (2010). Ecosystem services and agriculture: tradeoffs and synergies. *Philosophical transactions of the Royal Society of London. Series B, Biological sciences*, 365(1554):2959–2971.

- Rewald, B. and Ephrath, J. (2013). *Minirhizotron Techniques*, pages 1–15.
- Rich, S. M. and Watt, M. (2013). Soil conditions and cereal root system architecture: review and considerations for linking Darwin and Weaver. *Journal of Experimental Botany*, 64(5):1193–1208.
- Robert, C. and Casella, G. (2013). *Monte Carlo Statistical Methods*. Springer Texts in Statistics. Springer New York.
- Roser, M., Ritchie, H., and Ortiz-Ospina, E. (2019). World Population Growth. *Our World in Data*.
- Ruano, M. V., Ribes, J., Seco, A., and Ferrer, J. (2012). An improved sampling strategy based on trajectory design for application of the Morris method to systems with many input factors. *Environmental Modelling & Software*, 37(Supplement C):103–109.
- Samson, B. K. and Sinclair, T. R. (1994). Soil core and minirhizotron comparison for the determination of root length density. *Plant and Soil*, 161(2):225–232.
- Sattelmacher, B., Marschner, H., and Kühne, R. (1990). Effects of the Temperature of the Rooting Zone on the Growth and Development of Roots of Potato (*Solanum tuberosum*). *Annals of Botany*, 65(1):27–36.
- Schnepf, A., Leitner, D., Landl, M., Lobet, G., Mai, T. H., Morandage, S., Sheng, C., Zörner, M., Vanderborght, J., and Vereecken, H. (2018). CRootBox: a structural–functional modelling framework for root systems. *Annals of Botany*, 121(5):1033–1053.
- Schroth, G. and Kolbe, D. (1994). A method of processing soil core samples for root studies by subsampling. *Biology and Fertility of Soils*, 18(1):60–62.
- Shierlaw, J. and Alston, A. M. (1984). Effect of soil compaction on root growth and uptake of phosphorus. *Plant and Soil*, 77(1):15–28.
- Slack, S., York, L. M., Roghazai, Y., Lynch, J., Bennett, M., and Foulkes, J. (2018). Wheat shovelomics II: Revealing relationships between root crown traits and crop growth. *bioRxiv*, page 280917.
- Smit, A. L., George, E., and Groenwold, J. (2000). *Root Observations and Measurements at (Transparent) Interfaces with Soil*, pages 235–271. Springer Berlin Heidelberg, Berlin, Heidelberg.

- Sánchez, B., Rasmussen, A., and Porter, J. R. (2014). Temperatures and the growth and development of maize and rice: a review. *Global Change Biology*, 20(2):408–417.
- Stadler, A., Rudolph, S., Kupisch, M., Langensiepen, M., van der Kruk, J., and Ewert, F. (2015). Quantifying the effects of soil variability on crop growth using apparent soil electrical conductivity measurements. *European Journal of Agronomy*, 64:8 – 20.
- Svane, S. F., Jensen, C. S., and Thorup-Kristensen, K. (2019). Construction of a large-scale semi-field facility to study genotypic differences in deep root growth and resources acquisition. *Plant Methods*, 15(1):15–26.
- Taiz, L. (2013). Agriculture, plant physiology, and human population growth: past, present, and future. *Theoretical and Experimental Plant Physiology*, 25:167–181.
- Tardieu, F. (1994). Growth and functioning of roots and of root systems subjected to soil compaction. Towards a system with multiple signalling? *Soil and Tillage Research*, 30(2):217–243.
- Taylor, H. M. and Brar, G. S. (1991). Effect of soil compaction on root development. *Soil and Tillage Research*, 19(2):111–119.
- ter Braak, C. J. F. and Vrugt, J. A. (2008). Differential Evolution Markov Chain with snooker updater and fewer chains. *Statistics and Computing*, 18(4):435–446.
- Topp, C. N., Iyer-Pascuzzi, A. S., Anderson, J. T., Lee, C. R., Zurek, P. R., Symonova, O., Zheng, Y., Bucksch, A., Mileyko, Y., Galkovskiy, T., Moore, B. T., Harer, J., Edelsbrunner, H., Mitchell-Olds, T., Weitz, J. S., and Benfey, P. N. (2013). 3D phenotyping and quantitative trait locus mapping identify core regions of the rice genome controlling root architecture. *Proc Natl Acad Sci U S A*, 110(18):E1695–1704.
- Tracy, S. R., Black, C. R., Roberts, J. A., Sturrock, C., Mairhofer, S., Craigon, J., and Mooney, S. J. (2012). Quantifying the impact of soil compaction on root system architecture in tomato (*Solanum lycopersicum*) by X-ray micro-computed tomography. *Annals of Botany*, 110(2):511–519.
- Tron, S., Bodner, G., Laio, F., Ridolfi, L., and Leitner, D. (2015). Can diversity in root architecture explain plant water use efficiency? A modeling study. *Ecological Modelling*, 312:200–210.
- Unger, P. W. and Kaspar, T. C. (1994). Soil Compaction and Root Growth: A Review. *Agronomy Journal*, 86(5):759–766.

- Valentine, T. A., Hallett, P. D., Binnie, K., Young, M. W., Squire, G. R., Hawes, C., and Bengough, A. G. (2012). Soil strength and macropore volume limit root elongation rates in many UK agricultural soils. *Annals of Botany*, 110(2):259–270.
- van de Schoot, R., Kaplan, D., Denissen, J., Asendorpf, J. B., Neyer, F. J., and van Aken, M. A. (2014). A Gentle Introduction to Bayesian Analysis: Applications to Developmental Research. *Child Development*, 85(3):842–860.
- van Dusschoten, D., Metzner, R., Kochs, J., Postma, J. A., Pflugfelder, D., Buhler, J., Schurr, U., and Jahnke, S. (2016). Quantitative 3D Analysis of Plant Roots Growing in Soil Using Magnetic Resonance Imaging. *Plant Physiol*, 170(3):1176–88.
- Vansteenkiste, J., Van Loon, J., Garré, S., Pagés, L., Schrevens, E., and Diels, J. (2014). Estimating the parameters of a 3-D root distribution function from root observations with the trench profile method: case study with simulated and field-observed root data. *Plant and Soil*, 375(1):75–88.
- Vaz, C. M., Manieri, J. M., de Maria, I. C., and Tuller, M. (2011). Modeling and correction of soil penetration resistance for varying soil water content. *Geoderma*, 166(1):92 – 101.
- Vaz, C. M. P., Manieri, J. M., de Maria, I. C., and Th. van Genuchten, M. (2013). Scaling the Dependency of Soil Penetration Resistance on Water Content and Bulk Density of Different Soils. *Soil Science Society of America Journal*, 77:1488–1495.
- Vincent, C. D. and Gregory, P. J. (1989). Effects of temperature on the development and growth of winter wheat roots. *Plant and Soil*, 119(1):87–97.
- Voss-Fels, K. P., Robinson, H., Mudge, S. R., Richard, C., Newman, S., Wittkop, B., Stahl, A., Friedt, W., Frisch, M., Gabur, I., Miller-Cooper, A., Campbell, B. C., Kelly, A., Fox, G., Christopher, J., Christopher, M., Chenu, K., Franckowiak, J., Mace, E. S., Borrell, A. K., Eagles, H., Jordan, D. R., Botella, J. R., Hammer, G., Godwin, I. D., Trevaskis, B., Snowdon, R. J., and Hickey, L. T. (2018). VERNALIZATION1 Modulates Root System Architecture in Wheat and Barley. *Molecular Plant*, 11(1):226–229.
- Vrugt, J. A. (2016). Markov chain Monte Carlo simulation using the DREAM software package: Theory, concepts, and MATLAB implementation. *Environmental Modelling & Software*, 75:273–316.
- Vrugt, J. A., ter Braak, C. J. F., Diks, C. G. H., Robinson, B. A., Hyman, J. M., and Higdon, D. (2009). Accelerating Markov Chain Monte Carlo Simulation by Differential Evolution with Self-Adaptive Randomized Subspace Sampling. *International Journal of Nonlinear Sciences and Numerical Simulation*, 10(3):273–290.

- Wasson, A. P., Chiu, G. S., Zwart, A. B., and Binns, T. R. (2017). Differentiating Wheat Genotypes by Bayesian Hierarchical Nonlinear Mixed Modeling of Wheat Root Density. *Frontiers in plant science*, 8:282–282.
- Wasson, A. P., Rebetzke, G. J., Kirkegaard, J. A., Christopher, J., Richards, R. A., and Watt, M. (2014). Soil coring at multiple field environments can directly quantify variation in deep root traits to select wheat genotypes for breeding. *Journal of Experimental Botany*, 65(21):6231–6249.
- Wasson, A. P., Richards, R. A., Chatrath, R., Misra, S. C., Prasad, S. V. S., Rebetzke, G. J., Kirkegaard, J. A., Christopher, J., and Watt, M. (2012). Traits and selection strategies to improve root systems and water uptake in water-limited wheat crops. *Journal of Experimental Botany*, 63(9):3485–3498.
- Weaver, J. E., Kramer, J., and Reed, M. (1924). Development of Root and Shoot of Winter Wheat Under Field Environment. *Ecology*, 5(1):26–50.
- Weihermüller, L., Huisman, J. A., Lambot, S., Herbst, M., and Vereecken, H. (2007). Mapping the spatial variation of soil water content at the field scale with different ground penetrating radar techniques. *Journal of Hydrology*, 340(3):205–216.
- Wendell, D., Luginbuhl, K., Guerrero, J., and Hosoi, A. (2011). Experimental Investigation of Plant Root Growth Through Granular Substrates. *Experimental Mechanics*, 52(7).
- Whalley, W., To, J., Kay, B., and Whitmore, A. (2007). Prediction of the penetrometer resistance of soils with models with few parameters. *Geoderma*, 137(3):370 – 377.
- White, R. G. and Kirkegaard, J. A. (2010). The distribution and abundance of wheat roots in a dense, structured subsoil—implications for water uptake. *Plant Cell Environ*, 33(2):133–48.
- Whiteley, G. M. and Dexter, A. R. (1984). The behaviour of roots encountering cracks in soil. *Plant and Soil*, 77(2):141–149.
- Wu, J. and Guo, Y. (2014). An integrated method for quantifying root architecture of field-grown maize. *Ann Bot*, 114(4):841–51.
- Wu, L., McGechan, M. B., McRoberts, N., Baddeley, J. A., and Watson, C. A. (2007). SPACSYS: Integration of a 3D root architecture component to carbon, nitrogen and water cycling—Model description. *Ecological Modelling*, 200(3):343–359.

- Wuest, S. B. (2001). Soil biopore estimation: effects of tillage, nitrogen, and photographic resolution. *Soil and Tillage Research*, 62(3):111–116.
- Xiyang, Chen, S., Sun, H., Wang, Y., and Shao, L. (2009). Root size, distribution and soil water depletion as affected by cultivars and environmental factors. *Field Crops Research*, 114:75–83.
- Xu, C., Tao, H., Tian, B., Gao, Y., Ren, J., and Wang, P. (2016). Limited-irrigation improves water use efficiency and soil reservoir capacity through regulating root and canopy growth of winter wheat. *Field Crops Research*, 196:268 – 275.
- Zeng, G., Birchfield, S. T., and Wells, C. E. (2008). Automatic discrimination of fine roots in minirhizotron images. *New Phytologist*, 177(2):549–557.
- Zhan, A. and P Lynch, J. (2015). Reduced frequency of lateral root branching improves N capture from low-N soils in maize. *Journal of Experimental Botany*, 66.
- Zhao, J., Bodner, G., Rewald, B., Leitner, D., Nagel, K. A., and Nakhforoosh, A. (2017). Root architecture simulation improves the inference from seedling root phenotyping towards mature root systems. *J Exp Bot*, 68(5):965–982.
- Zhuang, J., Yu, G., and Nakayama, K. (2001). Scaling of root length density of maize in the field profile. *Plant and Soil*, 235:135–142.
- Ziegler, C., Dyson, R., and Johnston, I. (2019). Model selection and parameter estimation for root architecture models using likelihood-free inference. *Journal of The Royal Society Interface*, 16:20190293.
- Zuo, Q., Shi, J., Li, Y., and Zhang, R. (2006). Root length density and water uptake distributions of winter wheat under sub-irrigation. *Plant and Soil*, 285(1):45–55.



Band / Volume 507

**Integration of Renewable Energy Sources into the Future European Power System Using a Verified Dispatch Model with High Spatiotemporal Resolution**

C. Syranidou (2020), VIII, 242 pp  
ISBN: 978-3-95806-494-2

Band / Volume 508

**Solar driven water electrolysis based on silicon solar cells and earth-abundant catalysts**

K. Welter (2020), iv, 165 pp  
ISBN: 978-3-95806-495-9

Band / Volume 509

**Electric Field Assisted Sintering of Gadolinium-doped Ceria**

T. P. Mishra (2020), x, 195 pp  
ISBN: 978-3-95806-496-6

Band / Volume 510

**Effect of electric field on the sintering of ceria**

C. Cao (2020), xix, 143 pp  
ISBN: 978-3-95806-497-3

Band / Volume 511

**Techno-ökonomische Bewertung von Verfahren zur Herstellung von Kraftstoffen aus H<sub>2</sub> und CO<sub>2</sub>**

S. Schemme (2020), 360 pp  
ISBN: 978-3-95806-499-7

Band / Volume 512

**Enhanced crosshole GPR full-waveform inversion to improve aquifer characterization**

Z. Zhou (2020), VIII, 136 pp  
ISBN: 978-3-95806-500-0

Band / Volume 513

**Time-Resolved Photoluminescence on Perovskite Absorber Materials for Photovoltaic Applications**

F. Staub (2020), viii, 198 pp  
ISBN: 978-3-95806-503-1

Band / Volume 514

**Crystallisation of Oxidic Gasifier Slags**

J. P. Schupsky (2020), III, 127, XXII pp  
ISBN: 978-3-95806-506-2

Band / Volume 515

**Modeling and validation of chemical vapor deposition for tungsten fiber reinforced tungsten**

L. Raumann (2020), X, 98, XXXVIII pp

ISBN: 978-3-95806-507-9

Band / Volume 516

**Zinc Oxide / Nanocrystalline Silicon Contacts for Silicon Heterojunction Solar Cells**

H. Li (2020), VIII, 135 pp

ISBN: 978-3-95806-508-6

Band / Volume 517

**Iron isotope fractionation in arable soil and graminaceous crops**

Y. Xing (2020), X, 111 pp

ISBN: 978-3-95806-509-3

Band / Volume 518

**Geophysics-based soil mapping for improved modelling of spatial variability in crop growth and yield**

C. Brogi (2020), xxi, 127 pp

ISBN: 978-3-95806-510-9

Band / Volume 519

**Measuring and modelling spatiotemporal changes in hydrological response after partial deforestation**

I. Wiekenkamp (2020), xxxvii, 276 pp

ISBN: 978-3-95806-512-3

Band / Volume 520

**Characterization of Root System Architectures from Field Root Sampling Methods**

S. Morandage (2020), xxii, 157 pp

ISBN: 978-3-95806-511-6

Weitere **Schriften des Verlags im Forschungszentrum Jülich** unter  
<http://wwwzb1.fz-juelich.de/verlagextern1/index.asp>



Energie & Umwelt / Energy & Environment  
Band / Volume 520  
ISBN 978-3-95806-511-6